

KUCP-0104
 KUNS 1435
 HE(TH)97/02
 OHU-PH 9702
 YITP-97-12
 hep-th/9704025

Recent Developments of the Theory of Tunneling

Hideaki AOYAMA,^{*)} Toshiyuki HARANO[†], Hisashi KIKUCHI^{††},
 Ikuo OKOUCHI[‡], Masatoshi SATO^{‡‡**)} and Shinya WADA[‡]

*Faculty of Integrated Human Studies, Kyoto University, Kyoto 606-01,
 Japan*

[†]*Department of Physics, Kyoto University, Kyoto 606-01, Japan*

^{††}*Ohu University, Koriyama 963, Japan*

[‡]*Graduate School of Human and Environmental Studies,
 Kyoto University, Kyoto 606-01, Japan*

^{‡‡}*Yukawa Institute for Theoretical Physics, Kyoto University, Kyoto
 606-01, Japan*

Abstract

Path-integral approach in imaginary and complex time has been proven successful in treating the tunneling phenomena in quantum mechanics and quantum field theories. Latest developments in this field, the proper valley method in imaginary time, its application to various quantum systems, complex time formalism, asymptotic theory for the large order analysis of the perturbation theory, are reviewed in a self-contained manner.

^{*)} The email addresses of the authors are; aoyama@phys.h.kyoto-u.ac.jp, harano@gauge.scphys.kyoto-u.ac.jp, kikuchi@yukawa.kyoto-u.ac.jp, dai@phys.h.kyoto-u.ac.jp, msato@yukawa.kyoto-u.ac.jp, and shinya@phys.h.kyoto-u.ac.jp, respectively.

^{**)} Address after April 1, 1997: *Physics Department, University of Tokyo, Tokyo 113, Japan*

Contents

1	Introduction	3
2	Interacting instantons in the anomalous B and L violation	5
3	Proper valley method	15
4	Application of the proper valley method	25
4.1	Valley instanton in the asymmetric double-well potential	25
4.2	Valley bubble	35
4.3	Valley instanton in the scalar ϕ^4 field theory	41
4.3.1	Valley instanton	43
4.3.2	Constrained instanton	46
4.3.3	Numerical analysis	48
4.4	Valley instanton in the gauge-Higgs system	50
4.4.1	Valley instanton	50
4.4.2	Constrained instanton	56
4.4.3	Numerical analysis	57
4.5	Valley calculation of the B and L violation	61
4.5.1	Valley instanton in the electroweak theory	62
4.5.2	Calculation of the cross section	64
5	Complex-time methods	68
5.1	Saddle-point method	71
5.2	Green function and the WKB wavefunctions	73
5.3	Reduction formula and its expansion	77
6	Asymptotic analysis of the perturbation theory	84
6.1	Borel function in the valley method	85
6.2	Asymptons	89
6.2.1	General formalism for the asympton analysis	89
6.2.2	Asympton for the double-well quantum mechanics	91
6.2.3	Asympton in the SU(2) gauge field theory	93
6.2.4	Asympton on the Valley	95
6.2.5	Discussion	98
	References	100

§1. Introduction

Tunneling phenomena are unique to quantum systems and play important roles in various fields. To name a few of them, B+L violation of the standard electroweak model, inflation in the early universe, nuclear fission and fusion reactions, spontaneous nucleation in He^3/He^4 systems, and chemical reactions are the area of immediate influence. Although it can be readily understood in Schrödinger formalism in simple quantum mechanical systems, once the degree of freedom increases the calculation becomes a challenge. This situation is quite serious in field theories, which have infinite degree of freedom. Since the tunneling phenomena is essentially non-perturbative one, extracting relevant degree of freedom and doing reliable calculation requires new formalism.

The imaginary time path-integral method has been known to be effective in dealing with such a situation for some time. This is mainly because of the existence of the classical configurations, instantons and bounces, around which the path-integral may be evaluated.^{*)} In theories with degenerate classical vacua, one often has instanton solutions, which connects the different (perturbative) vacua. When the coupling is small enough, the dilute-gas approximation for multi-instanton configurations yields the energy splitting of the ground states by the tunneling. Bounces are configurations that starts from the ground state and “bounces back” at the escape point and then comes back to the original ground state. A relevant analytical continuation of the Gaussian integral around bounce solution yields the decay rate of the unstable states. The power of the instanton method and the bounce method described so far are actually quite limited. Here we will point out three of the problems encountered by these methods.

The most obvious one is the fact that those calculations are limited only to the ground state. In quantum mechanical context, if one wishes to obtain the energy splitting of the excited states in the symmetric double-well, or if one wants the decay rate from higher excited states, one realizes the current methods are not enough. In field theoretical context, this difficulty became most apparent and serious in the late 80's, when the baryon number and lepton number violation processes in the electroweak standard model caught attention of some of the particle physicists, in relation of the anticipated PP collider in TeV region at that time. The tunneling process induced by the colliding quarks results in the B+L violation through the anomaly of the model. Since the potential height is of order $M_W/\alpha \sim$ few TeV, this process is highly suppressed in the low energy region. However when the initial

^{*)} In some literature, the word “instanton” is used for any the imaginary time classical configurations. This, however, is avoided in this paper for the sake of clarity; “instanton” and “bounce” are distinguished as will be seen in the rest of this paper.

energy of order TeV is available, this process may occur at observable rate. However, it was soon noticed that the usual instanton calculation is not only invalid, but yields inconsistent result at higher energies, violating unitarity. Thus the necessity of the further development of the formalism became apparent.

Another difficulty is a subtle one. There are theories in which tunneling is physically possible, but no classical solution exists. This happens for a specific potential in the scalar field theories and in the gauge-Higgs system. An elementary scaling argument shows that the action of any finite action configuration can be lowered by shrinking it. In other words, any configuration that is the stationary point of the action functional is point-like, which denies any hope of naive application of the instanton formalism.

The third problem is actually a paradox. In the quantum mechanics with asymmetric double-well potential, the ordinary bounce method yields a decay rate. This is due to the fact that the Gaussian integration of the fluctuations is concerned only with the neighborhood of the bounce solution. On the other hand, there is no decay, since Hamiltonian is hermitian; the energy spectrum is certainly affected by the tunneling, but does remain real and discrete. Thus this instability is a “fake”.

Motivated by these problems at various stages, we have developed several formalisms in the recent years. The aim of the paper then is to present these developments in a self-contained manner, together with several new results. We believe that the power of these formalisms is not limited to the original contexts and thus hope to make these widely available to researchers in other fields as well.

The organization of this paper is as follows. In section 2, we briefly review the B+L violation problem in the standard model, which was the starting point of these works. The use of the dilute instanton-gas approximation, its infamous “unitarity problem”, its solution by the “interacting instanton method”, the need for further developments are explained in a concise manner. The ultimate method in this line is “the proper valley method”, described in section 3. The presentation here is in a general model, not limited to any particular quantum mechanical or quantum field theoretical model. Its advantage over the pre-existing methods, the streamline method and the constrained instanton method are explained in detail. A numerical analysis that demonstrates the power of the proper valley method is also presented.

The application of the proper valley method to various models are presented in section 4. The asymmetric double-well potential, the “Fake instability” problem is treated and solved in the proper valley method in subsection 4.1. False vacuum problem in the scalar field theory is analyzed in subsection 4.2. Unstable scalar field theory that does not possess any finite-size instanton is studied in subsection 4.3, where we also compare our results with

the one from the constrained instanton method. Similar analysis is done for the gauge-Higgs system in subsection 4.4. Subsection 4.5 gives the application of the valley instanton configuration obtained in subsection 4.4 to the actual calculation of the cross section in the standard model.

In section 5 we describe a completely different approach, the complex time method. The big advantage of this formalisms over the imaginary time formalism is that the configuration goes through not only the forbidden region (just like instanton/bounce), but also the allowed region. This implies the solution of the fake instability problem, and calculation of the excited states, among others. However, the difficulty lies in the fact that the exact formulation is not clear at all. It is easy to construct complex-time configuration by patching up the instanton and the real-time solutions and then use those for evaluation by hand-waving argument. However, just how exactly these configuration should contribute to the path-integral remains a mystery, even in a simple one-dimensional quantum mechanics. What we present in this section is an analysis of the WKB calculation to show that there is at least one formalism that works in the one-dimensional quantum mechanical system.

In section 6, we discuss the problems of the perturbation theories that arise due to the existence of the tunneling phenomena. In models whose the perturbative series is not a Borel-summable series, we expect that it is due to the fact that physical observables are well defined only after the non-perturbative terms are added. This interplay between the perturbative effects at large orders and the non-perturbative effects has been a subject of the investigation for some time. In this section we give some of the new insights obtained recently. In subsection 6.1 we give a Borel analysis of this phenomenon using the idea of valley. And then in subsection 6.2 we present the theory of the asympton, which is the configuration that fictitiously dominates the perturbative functional at large orders. This provides us with an insight as to the original of the non Borel-summability and the possible direction for the converging calculations.

§2. Interacting instantons in the anomalous B and L violation

The anomalous baryon number (B) and lepton number (L) violation is one of the most fascinating processes predicted in the electroweak standard model. The prediction is based on the chiral anomaly and topological transition. In the electroweak model the apparent conservation of baryon number current j_B^μ and the lepton number current j_L^μ is, in fact, no longer valid due to the anomaly. Their divergence is deduced from the representation of the quarks or leptons under $SU_L(2)$ and $U_Y(1)$ group. Since we have, in each generation, three

SU(2) doublets that has $Y = 1/3$ for the left-handed quarks and six singlets with $Y = 4/3$ or $-2/3$ for the right-handed ones, the divergence of j_B^μ is

$$\partial_\mu j_B^\mu = \frac{N_f}{32\pi^2} [g^2 W_{\mu\nu}^a \tilde{W}^{a\mu\nu} - g'^2 B_{\mu\nu} \tilde{B}^{\mu\nu}], \quad (2.1)$$

where

$$W_{\mu\nu}^a = \partial_\mu W_\nu^a - \partial_\nu W_\mu^a - g\epsilon^{abc} W_\mu^b W_\nu^c, \quad (2.2)$$

$$B_{\mu\nu} = \partial_\mu B_\nu - \partial_\nu B_\mu, \quad (2.3)$$

are the field strength of the SU(2) W_μ^a and U(1) B_μ gauge fields, respectively; g and g' are their coupling constants; $\tilde{W}^{a\mu\nu} \equiv (1/2)\epsilon^{\mu\nu\lambda\sigma} W_{\lambda\sigma}^a$, and the N_f is the number of the generation. Interestingly the divergence of j_L^μ is exactly the same. Therefore the (B–L) current stays conserved.

The topological transition resides in the SU(2) sector in the model. Consider a trajectory in the finite energy configuration space made of $W_\mu^a(x)$ and the doublet Higgs $\Phi(x)$ that starts from and ends up with the vacuum. We parametrize this as

$$W_\mu^a(0, \mathbf{x}) = W_\mu^a(T, \mathbf{x}) = 0, \quad \Phi(0, \mathbf{x}) = \Phi(T, \mathbf{x}) = \begin{pmatrix} 0 \\ v \end{pmatrix},$$

using a parameter $t \in [0, T]$, where v is the vacuum expectation value. All the trajectories of this type are divided into topological classes that are labeled by the winding number of the homotopy $\Pi_3(S^3)$. The integral along the trajectory,

$$N_w \equiv \frac{g^2}{32\pi^2} \int dt d^3x W_{\mu\nu}^a \tilde{W}^{a\mu\nu}, \quad (2.4)$$

gives its winding number. Combined with Eq. (2.1), this relation indicates that the transition along the trajectory causes the B and L violation by $N_f N_w$ units.

The height of the potential barrier that the topological transition with $N_w = \pm 1$ need to go over is of the order of $(4\pi/g^2)m_W$. This is the static energy E_{sp} of the sphaleron, a static but unstable solution of the equations of motion.¹⁾ This large energy causes a strong suppression if the transition takes place through quantum tunneling starting from the low-lying states near the vacuum. Actually the WKB suppression factor in the amplitude is estimated²⁾ to be $e^{-8\pi^2/g^2} \simeq e^{-180}$.

A naive expectation, however, leads us to the interesting possibility that this strong suppression may be weakened if the energy of the transition becomes comparable to E_{sp} . Along this line, two issues have been discussed in literature; the effect of the B and L

violation on the baryogenesis of the Universe³⁾ and the direct detection of the violation at a high energy collision.⁴⁾

Only reliable estimates of the transition amplitudes in high energy processes can answer the question about these issues. This is not, however, a simple task. The difficulty lies in the fact that it is non-perturbative: the process

$$q + q \rightarrow 7\bar{q} + 3\bar{l}, \quad (2.5)$$

or, more generally, the one accompanied by the simultaneous production of n_W W bosons and n_H Higgs bosons,

$$q + q \rightarrow 7\bar{q} + 3\bar{l} + n_W W + n_H \phi, \quad (2.6)$$

is the specific example of the transition, but we cannot write down the relevant diagrams for this process by using the Feynman rules in the electroweak standard model.

't Hooft is the first person to have estimated the amplitude.²⁾ His tool was the imaginary time formalism of the path-integral; it can incorporate the topological transition as the background in the path-integral. Ringwald and Espinosa pushed the idea further; they applied the path-integral to the evaluation of Green functions appropriate for the scattering process (2.6).^{5),6)} Aoyama and Kikuchi improved their analysis by taking into account multi-transitions;⁷⁾ this can resolve the unitarity problem pointed out in their single transition calculation. The following of this section is a review of this non-perturbative calculation according to the line mentioned above. We are still at the middle of the way to the final answer and a lot of related works have been published. We are not going to look back all of these works here. (For the other related works, see, for example, Ref. 8.)

Let us start with Ringwald and Espinosa calculation. For simplicity, we take the SU(2)-Yang-Mills-Higgs-model with a single generation of massless quarks and leptons. All the essence of the calculation can be seen in this simple version. We intend to evaluate the B and L violating Green functions of the Heisenberg operator,

$$G(x_1, \dots, x_4; y_1, \dots, y_{n_W}; z_1, \dots, z_{n_H}) = \frac{\langle \text{vac} | q_1(x_1) q_2(x_2) q_3(x_3) l(x_4) W(y_1) \dots W(y_{n_W}) \phi(z_1) \dots \phi(z_{n_H}) | \text{vac} \rangle}{\langle \text{vac} | \text{vac} \rangle}, \quad (2.7)$$

where $q_1(x)$, $q_2(x)$, and $q_3(x)$ are SU(2) doublet quarks distinguished by their color, $l(x)$ the doublet lepton, $\phi(x)$ the physical Higgs boson. We have suppressed the Lorentz and the SU(2) indices in Eq. (2.7). We use the imaginary time formalism for the calculation, i.e. the time evolution operator is $e^{-\tau H}$ (H is the Hamiltonian) instead of e^{-itH} . This Green function can be evaluated also in the path-integral

$$G(x_1, \dots, x_4; y_1, \dots, y_{n_W}; z_1, \dots, z_{n_H})$$

$$= \frac{1}{Z} \int \prod_{f=q_1, q_2, q_3, l} [df d\bar{f}][dW][d\Phi] \exp \{-S[W, \Phi, q, l]\} \\ \times q_1(x_1)q_2(x_2)q_3(x_3)l(x_4)W(y_1)\dots W(y_{n_W})\phi(z_1)\dots\phi(z_{n_H}), \quad (2.8)$$

$$Z = \int \prod_{f=q_1, q_2, q_3, l} [df d\bar{f}][dW][d\Phi] \exp \{-S[W, \Phi, q, l]\}, \quad (2.9)$$

where S is the sum of the terms S_W , S_ϕ , and S_f , evaluated respectively from the Lagrangians,

$$\mathcal{L}_W = \frac{1}{4} (W_{\mu\nu}^a)^2, \quad (2.10)$$

$$\mathcal{L}_\phi = |D_\mu \Phi|^2 + \lambda (|\Phi|^2 - v^2), \quad (2.11)$$

$$\mathcal{L}_f = \sum_c \bar{q}_c D_\mu \bar{\sigma}_\mu q_c + \bar{l} D_\mu \bar{\sigma}_\mu l. \quad (2.12)$$

In these equations, D_μ is the covariant derivative;

$$D_\mu = \partial_\mu + ig \left(\frac{\tau^a}{2} \right) W_\mu^a, \quad (2.13)$$

and $\bar{\sigma}_\mu \equiv (\vec{\sigma}, -i)$ is the two component Pauli matrices for the left-handed spinors^{*)}. Hereafter, the Greek indices are understood as being summed up in the Euclidean metric.

The usual perturbative calculation of the function (2.8) around the vacuum is trivially zero. We instead evaluate it in the background of the topological transition. The anomaly equation (2.1) indicates it should have $|N_W| = 1$. In the standard model, we do not have a stationary configuration of the action around which we construct an systematic expansion of the Green function in powers of g : any finite size configuration tends to shrink toward zero size. To circumvent this, we use the constrained instanton method.¹⁰⁾ We first restrict the functional space by imposing the constraint on the size ρ and evaluate the path-integral over all fluctuations around the stationary configuration in this restricted functional space. At the end of the calculation, we integrate over ρ to recover the whole functional space. The constrained instanton is the name for the topological transition stationary in the restricted functional space. Hereafter in this section we simply call it instanton. The bosonic component of the instanton in the singular unitary gauge has the following form

$$W_{in\mu}^a \simeq \frac{1}{g} \eta_{a\mu\nu} \partial_\nu \ln \left(1 + \frac{\rho^2}{x^2} \right), \quad (2.14)$$

$$\Phi_{in} \simeq \left(\frac{x^2}{x^2 + \rho^2} \right)^{1/2} \begin{pmatrix} 0 \\ v \end{pmatrix}, \quad (2.15)$$

^{*)} We use the relation $t = -i\tau$ of the imaginary time τ and the real time t when we need to go back to Minkowski expression. Using the other one $t = i\tau$ as in Refs. 7), 9) is just the matter of convention.

in the central region $x \ll m_W^{-1}, m_H^{-1}$, and

$$W_{\text{in}\mu}^a \simeq \frac{4\pi^2 \rho^2}{g} \eta_{a\mu\nu} \partial_\nu G_{m_W}(x), \quad (2.16)$$

$$\Phi_{\text{in}} \simeq \left(1 - 2\pi^2 \rho^2 G_{m_H}(x)\right) \begin{pmatrix} 0 \\ v \end{pmatrix}, \quad (2.17)$$

in the asymptotic region $x \gg \rho$, where we have used G_m for the four dimensional massive propagator,

$$(-\partial^2 + m^2)G_m(x) = \delta^4(x), \quad (2.18)$$

and the 't Hooft symbol $\eta_{a\mu\nu}$,

$$\eta_{a\mu\nu} = \begin{cases} \delta_{a\nu} & \text{if } \mu = 4; \\ -\delta_{a\mu} & \text{if } \nu = 4; \\ \epsilon_{a\mu\nu} & \text{otherwise.} \end{cases} \quad (2.19)$$

Its action is approximately

$$S_{\text{in}} \simeq \frac{8\pi^2}{g^2} + \pi^2 \rho^2 v^2. \quad (2.20)$$

In this background, the operator $D\bar{\sigma}$ has a zero mode $\psi^{(0)}$;

$$D_\mu \bar{\sigma}_\mu \psi^{(0)}(x) = 0. \quad (2.21)$$

In the explicit notation with α for the Lorentz index and a for the SU(2) index, it behaves as

$$\psi_{\alpha a}^{(0)}(x) \simeq \frac{\rho}{\pi} \frac{x_\mu (\sigma_\mu)_{\alpha\beta} \epsilon_{a\beta}}{|x|(x^2 + \rho^2)^{3/2}} \quad (2.22)$$

at the central region and

$$\psi_{\alpha a}^{(0)}(x) \simeq (2\pi\rho) G_{F\alpha\beta}(x) \epsilon_{\beta a} \quad (2.23)$$

at the asymptotic region, where $\sigma_\mu = (\vec{\sigma}, i)$,

$$G_{F\alpha\beta}(x) \equiv \partial_\mu (\sigma_\mu)_{\alpha\beta} G_{m=0}(x) \quad (2.24)$$

is the fermionic massless propagator, and $\epsilon_{\beta a}$ is the two dimensional anti-symmetric matrix. For the path-integral of the fermionic degrees of freedom, we expand the fermion fields, collectively denoting them by f , as

$$f(x) = \sum_n \psi^{(n)}(x) a_n^f, \quad (2.25)$$

$$\bar{f}(x) = \sum_n \varphi^{(n)\dagger}(x) \bar{a}_n^f, \quad (2.26)$$

with Grassmann coefficients a_n and \bar{a}_n and eigenfunctions $\psi^{(n)}$ and $\varphi^{(n)}$; they obey eigenvalue equations

$$-D_\mu \sigma_\mu D_\nu \bar{\sigma}_\nu \psi^{(n)} = \lambda_n^2 \psi^{(n)}, \quad (2.27)$$

$$-D_\mu \bar{\sigma}_\mu D_\nu \sigma_\nu \varphi^{(n)} = \lambda_n^2 \varphi^{(n)}, \quad (2.28)$$

and are normalized as follows;

$$\int d^4x \psi^{(n)\dagger}(x) \psi^{(m)}(x) = \delta_{mn}, \quad \int d^4x \varphi^{(n)\dagger}(x) \varphi^{(m)}(x) = \delta_{mn}. \quad (2.29)$$

Note $\psi^{(0)}$ is the one with $\lambda = 0$. The fermionic action S_f becomes diagonalized,

$$S_f = \sum_{n \neq 0, f} \lambda_n \bar{a}_n^f a_n^f, \quad (2.30)$$

because the nonzero modes of $\varphi^{(n)}$ and $\psi^{(n)}$ are related one-to-one,

$$\varphi^{(n)} = \frac{1}{\lambda_n} (\bar{\sigma}_\mu D_\mu) \psi^{(n)}. \quad (2.31)$$

The zero mode $\psi^{(0)}$ does not have the partner and its coefficients a_0^f do not appear in Eq. (2.30). The fields q_1, \dots, l put in the integrand of Eq. (2.8) provide a proper number of a_0^f for the non-vanishing Green function against the path-integral measure;

$$[df d\bar{f}] \propto da_0^{q_1} da_0^{q_2} da_0^{q_3} da_0^l. \quad (2.32)$$

We now have all the necessary ingredients to evaluate the Green function (2.8). The fermion fields in the integrand are now replaced with the zero mode. For the bosonic fields, we can just put the background instanton, Eqs. (2.14–2.17), to the leading order in g : the nonzero mode fluctuation around the background will give smaller contribution as long as n_W or n_H is not so large^{*)} and zero mode fluctuations, corresponding to the translation and the SU(2) isospin rotation, can be taken care of collective coordinate integral as usually done (see the Eq. (2.33) below.) The path-integral is carried out by the Gaussian approximation and results in the determinants from the bosonic and fermionic nonzero mode fluctuations. We then perform the Fourier transformation on the resulting Green function G to use the LSZ procedure to extract the proper vertex. The external momenta have the magnitude of the particles masses and are smaller than the dominant instanton size $\rho \sim 1/v$. Noticing

^{*)} The nonzero mode fluctuations of W and ϕ are of the order of g compared with the background. The next leading correction is obtained by replacing any two of the background with a propagator in the background; there are about n_W^2 ways to pick up the two of W and n_H^2 ways for ϕ . It is thus of the order of $n_W^2 g^2$ or $n_H^2 g^2$ compared with the leading term.

that both the fermionic zero mode and the bosonic configuration of the instanton have the form of the propagator at the asymptotic region, we obtain

$$\Gamma = \int \frac{d\rho}{\rho^5} e^{-S_{\text{in}}(\rho)} \int dR \rho^2 D(\rho) \left[\prod_f \chi_{\alpha_f a_f} \right] \left[\prod_{j=1}^{n_W} (\beta_{\mu_j \nu}^{a_j} i p_{j\nu}) \right] (-2\pi^2 \rho^2 v)^{n_H} \quad (2.33)$$

for the vertex, where

$$\beta_{\mu\nu}^a \equiv \frac{4\pi^2 \rho^2}{g} R^{ab} \eta_{b\mu\nu}, \quad (2.34)$$

$$\chi_{\alpha a} \equiv 2\pi \rho U_{ab} \epsilon_{\alpha b}, \quad (2.35)$$

and p_j is the momentum of the j -th external W boson. The integral measure dR represents the functional integral over the zero mode of the isospin rotation; the corresponding variables R^{ab} and U_{ab} are related by $U\tau^b U^\dagger = \tau^a R^{ab}$. The integral over the translational zero mode has been done already when we Fourier-transformed the Green function to arrive at Eq. (2.33), and it provides the momentum conservation at the vertex. The factor $\rho^{2-5} D(\rho)$ is the product of the Jacobians for the bosonic collective coordinates and the determinants of the bosonic and fermionic nonzero modes.

The main outcome of the above Ringwald and Espinosa analysis is that the so-obtained vertex (2.33) is point-like independently of the momenta of external particles. Thus the cross section increases monotonically as $\sim E^{(2+2n_W+2n_H)}$ as the energy E of the process increases. It would eventually violate the unitarity bound if one naively extrapolate the result to high energy. One may think that we could predict nothing about the high energy behavior of the amplitude from the calculation we have done above: We have just used the asymptotic form of the instanton, while it is the form at the central region that determines the behavior at $E > 1/\rho \sim v$. This very plausible argument, however, is false. As we have seen, the Green function to the leading order in g is basically the product of the instanton configurations. The Lorentz invariance then forces its Fourier transform to depend on the simple momentum squares p_i^2 of the external particle, not on $p_i \cdot p_j$ for example. Then we can use the asymptotic forms since we will put the on-shell condition $p_i^2 = m^2$ after all when we apply the LSZ procedure.

The single instanton never disappears from the functional space no matter how large we take the energy in the calculation. Therefore, there must be other configurations that cancel it, becoming also the same order of magnitude at the energy of the unitarity violation. Aoyama and Kikuchi have shown that the multi-instanton configurations take this task.⁷⁾ The interaction between the instantons plays the important role in this cancelation. With the interactions the instantons construct ‘‘connected diagrams’’ for the scattering amplitude

and in fact they have the property that is required to recover the unitarity. Let us now turn to this part.

We investigate the contribution of the n -instanton– \bar{n} -anti-instanton configuration,

$$W(x) = \sum_{i=1}^n W_{\text{in}}(x - w_i, R_i) + \sum_{j=n+1}^{\bar{n}+n} \bar{W}_{\text{in}}(x - w_j, R_j), \quad (2.36)$$

$$\phi(x) = \sum_{k=1}^{\bar{n}+n} \phi_{\text{in}}(x - w_k), \quad (2.37)$$

to the Green function. In Eq. (2.36), \bar{W}_{in} represents the anti-instanton, whose form is given by replacing $\eta_{\alpha\mu\nu}$ in Eqs. (2.14) and (2.16) with $\bar{\eta}_{\alpha\mu\nu}$ ($\bar{\eta}_{\alpha\mu\nu}$ is minus of $\eta_{\alpha\mu\nu}$ for $\mu = 4$ or $\nu = 4$, otherwise the same.) The parameters w_i and R_i are the location and isospin-orientation of the i -th (anti-)instanton. We intend to treat the parameters w_i , R_i , and ρ_i as the collective coordinates for the path-integral. In the strict sense, we should extract out the canonical variables for the fluctuations at each values of the collective coordinates and carry out first the functional integral over the fluctuations, and then integrate the resulting effective action over them. This is, however, impossible in practice. We adopt two approximations. First, we approximate the functional integral over the fluctuations to the simple product of the determinants of each (anti-)instanton. Although the configuration is not stationary in any sense, we do not expect this will cause a large error since the fluctuations are suppressed by g (the coupling constant) compared with the collective coordinates. Second, we approximate the action to the sum of the instanton action S_{in} of each (anti-)instanton and two-body interaction of each pair evaluated at large separation. These approximations are quite adequate if the relative distances $|w_i - w_j|$ are larger than m_{W}^{-1} or m_{H}^{-1} , but if some of them become smaller, we will miss some part of the exact contribution. It will turn out that the contribution taken into account by the above procedure is sufficient to show the cancelation of the single instanton contribution at the energy of unitarity violation.

The bosonic part of the interaction between the i -th instanton and j -th anti-instanton is defined by

$$S_{\text{b:int}}(i, j) \equiv S[W(i) + \bar{W}(j), \phi(i) + \phi(j)] - 2S_{\text{in}} \quad (2.38)$$

and readily evaluated by using the fact that the each background configuration satisfies the equation of motion in the asymptotic region (see Ref. 7) for detail);

$$\begin{aligned} S_{\text{b:int}}(i, j) = & -\beta_{\nu\lambda}^a(\rho_i, R_i) \frac{\partial}{\partial w_{i\lambda}} \bar{\beta}_{\nu\sigma}^a(\rho_j, R_j) \frac{\partial}{\partial w_{j\sigma}} G_{m_{\text{W}}}(w_i - w_j) \\ & - (2\pi^2 \rho_i^2 v)(2\pi^2 \rho_j^2 v) G_{m_{\text{H}}}(w_i - w_j), \end{aligned} \quad (2.39)$$

where $\bar{\beta}$ is defined by (2.34) with $\bar{\eta}$ substituting η . The interaction term for a pair of instantons or anti-instantons is written in a similar equation in which β or $\bar{\beta}$ are replaced

correspondingly. Regarding the fermionic part, the zero mode located at each instanton has now overlap with the other, which also generates the interaction. Starting from the expansion (we suppress the suffix 0 for the zero-modes hereafter),

$$f(x) = \sum_i a^{f_i} \psi(x - w_i) + (\text{nonzero modes}) \quad (2.40)$$

$$\bar{f}(x) = \sum_j \bar{a}^{f_j} \varphi^\dagger(x - w_j) + (\text{nonzero modes}), \quad (2.41)$$

we obtain

$$\begin{aligned} S_{\text{f:int}}(i, j) &\equiv \bar{a}^{f_j} a^{f_i} \int dx \varphi^\dagger(j) \bar{\sigma}_\mu (\partial_\mu + igW_\mu(i) + ig\bar{W}_\mu(j)) \psi(i) \\ &= \bar{a}^{f_j} a^{f_i} \int dx \varphi^\dagger(j) (-\partial_\mu) \bar{\sigma}_\mu \psi(i) \\ &= -\bar{a}^{f_j} a^{f_i} \bar{\chi}_{\alpha\alpha} G_{\text{F}\alpha\beta}(w_j - w_i) \chi_{\beta\alpha}, \end{aligned} \quad (2.42)$$

where $\bar{\chi}_{\alpha\alpha} \equiv 2\pi\rho U_{ba}^\dagger \epsilon_{ba}^\dagger$ comes from the fermionic zero mode φ at the anti-instanton (its form is Eq. (2.22) with $\bar{\sigma}$ for σ .) We have also used the fact that the zero modes satisfy Eq. (2.21) to go from the first to the second line. Note that the interactions (2.39) and (2.42) have the one-particle exchange type with the vertex exactly the same as the single instanton one for the relevant particle production.

These interacting multi-instantons contributes to the B and L violating Green function. As an example let us see the contribution of two instantons, labeled 1 and 3, and one anti-instanton, 2, to the process $\bar{q}_1 \bar{q}_2 \rightarrow q_3 l$ (See Fig. 1 (b).)

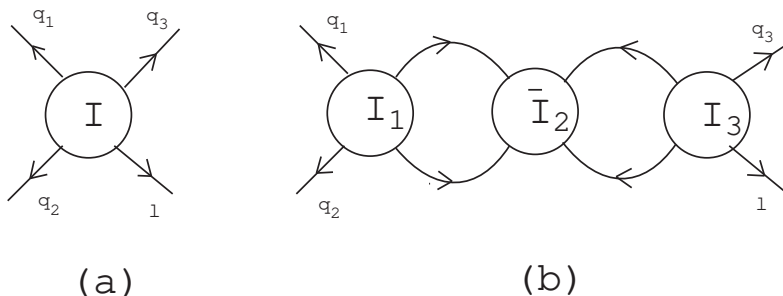


Fig. 1. The diagrams in the instanton expansion of the process $\bar{q}_1 \bar{q}_2 \rightarrow q_3 l$.

The corresponding Green function is

$$\begin{aligned} G^{(3)}(x_1, \dots, x_4) \\ = \frac{1}{Z} \int [\prod_f df d\bar{f}] [dW] [d\phi] q_1(x_1) \dots l(x_4) \exp \left\{ -3S_{\text{in}} - \sum S_{\text{b:int}}(i, j) - \sum S_{\text{f:int}}(i, j) \right\}. \end{aligned} \quad (2.43)$$

To evaluate this, we expand the factor $e^{-S_{\text{int}}}$ in powers of S_{int} and pick up nonzero terms. The simplest one in $G^{(3)}$ is

$$\begin{aligned}
G^{(3)} &\simeq \left[\prod_{i=1}^3 \int \frac{d\rho_i dR_i dw_i}{\rho_i^{5-2}} D(\rho_i) e^{-S_{\text{in}}(i)} \right] \left[\prod_f \int da^{f1} d\bar{a}^{f2} da^{f3} \right] \\
&\times a^{q11} \psi(x_1 - w_1) a^{q21} \psi(x_2 - w_1) a^{q33} \psi(x_3 - w_3) a^{l3} \psi(x_4 - w_3) \\
&\times \bar{a}^{q32} a^{q31} \bar{\chi}(2) G_{\text{F}}(w_2 - w_1) \chi(1) \bar{a}^{l2} a^{l1} \bar{\chi}(2) G_{\text{F}}(w_2 - w_1) \chi(1) \\
&\times \bar{a}^{q12} a^{q13} \bar{\chi}(2) G_{\text{F}}(w_2 - w_3) \chi(3) \bar{a}^{q22} a^{q23} \bar{\chi}(2) S_{\text{F}}(w_2 - w_3) \chi(3) \\
&\simeq \left[\prod_{i=1}^3 \int \frac{d\rho_i dR_i dw_i}{\rho_i^{5-2}} D(\rho_i) e^{-S_{\text{in}}(i)} \right] \\
&\times (G_{\text{F}}(x_1 - w_1) \chi(1)) (G_{\text{F}}(x_2 - w_1) \chi(1)) (G_{\text{F}}(x_3 - w_3) \chi(3)) (G_{\text{F}}(x_4 - w_3) \chi(3)) \\
&\times (\bar{\chi}(2) G_{\text{F}}(w_2 - w_1) \chi(1)) (\bar{\chi}(2) G_{\text{F}}(w_2 - w_1) \chi(1)) \\
&\times (\bar{\chi}(2) G_{\text{F}}(w_2 - w_3) \chi(3)) (\bar{\chi}(2) G_{\text{F}}(w_2 - w_3) \chi(3)). \tag{2.44}
\end{aligned}$$

This function has the same structure as the one obtained from the diagram (b) in Fig. 1 with the ‘‘Feynman rule’’, the vertices are understood as Γ in (2.33) or $\bar{\Gamma}$ defined for the anti-instanton with the proper replacements of β and χ , and the lines are the free propagators. The similar analysis can be extended for the other terms that contain any powers of S_{int} . This way we will get the instanton expansion for the Green function. The Green function of a given process gets the contribution from all possible multi-instanton sectors in which $n - \bar{n}$ is fixed by the degree of B and L violation. Each term in the given sector is obtained by expanding $e^{-S_{\text{int}}}$ in S_{int} .

We can show the terms generated by the instanton expansion is exactly the same as those generated by the following effective Lagrangian;⁷⁾

$$\begin{aligned}
L &= \sum_f \bar{f} \partial_\mu \bar{\sigma}_\mu f + \frac{1}{2} [(\partial_\mu \phi)^2 + m_{\text{H}}^2 \phi^2] \\
&+ \frac{1}{4} (\partial_\mu W_\nu^a - \partial_\nu W_\mu^a)^2 + \frac{1}{2} m_{\text{W}}^2 W_\mu^a{}^2 + V + \bar{V}, \tag{2.45}
\end{aligned}$$

where

$$\begin{aligned}
V &= \int \frac{d\rho dR D(\rho)}{\rho^{5-2}} \left[\prod_f \bar{f}(x) \chi \right] \exp[-S_{\text{in}} + (-2\pi^2 \rho^2 v) \phi(x) + \beta_{\mu\nu}^a \partial_\mu W_\nu^a], \\
\bar{V} &= \int \frac{d\rho dR D(\rho)}{\rho^{5-2}} \left[\prod_f \bar{\chi} f(x) \right] \exp[-S_{\text{in}} + (-2\pi^2 \rho^2 v) \phi(x) + \bar{\beta}_{\mu\nu}^a \partial_\mu W_\nu^a]. \tag{2.46}
\end{aligned}$$

The single instanton amplitude now turns out to be the leading term of this expansion. If one moves back to the Minkowski metric, this Lagrangian becomes hermitian. This indicates the

non-leading terms in this expansion give the contribution that cancel exactly the unitarity violating high energy behavior of the single instanton amplitude. We can use for example the K-matrix method to show this cancelation.⁷⁾ [The K-matrix method provides us with a systematic way to pick up the diagrams in different orders of the instanton expansion so that their sum holds the unitarity. In the leading order of the K-matrix method, the internal momenta of loop diagrams are set on-shell and we can see the cancelation without suffering from the ultra-violet divergence that the instanton expansion has in the non-leading terms.] In this respect, the unitarity problem that exists in the single instanton sector is resolved.

When returning back to the initial problem, the reliable estimate of the B and L violating amplitude, we note that the instanton expansion constructed so far is not sufficient. Once one wants to evaluate the amplitude to the non-leading orders, he encounters pathological ultra-violet divergences coming from the loop integrals of internal particles that connect the instanton vertices. The cure must come from the more rigid evaluation of the action of the multi-instanton configuration. Remember the approximation we adopt for the calculation of the interaction is adequate only for well-separated instantons, not for those with small separations. The interaction in the latter configuration must be important for the loop integrals of large momenta. We believe the proper valley method that is introduced and explained in the following sections is the most promising to this end. To choose the proper collective coordinates for the functional integral is indispensable in the multi-instanton calculation of the path-integral. The proper valley method has the potential to tell us the way even for those configurations in which a small-separated instanton–anti-instanton pair is merging into the vacuum.

§3. Proper valley method

In order to describe the proper valley method in the most general context, we will discretize all the bosonic degrees of freedom and denote then by ϕ_i . The subscript i stands for coordinate labels in quantum mechanics, particle species, vector and tensor indices and any internal quantum numbers, as well as the space-time coordinates x_μ . Translation to the continuum indices is trivial; sums over indices should be understood as integrals with suitable measure, the derivatives as functional derivatives.^{*)} These variables ϕ_i are the “coordinates” of the functional space, which allows some intuitive understanding of the equations. The bosonic action is written as a function of these variables; $S = S(\phi_i)$. In this notation, the equation of motion is written as $\partial_i S = 0$, where $\partial_j \equiv \partial/\partial\phi_j$. We assume that the metric of

^{*)} Inclusion of fermionic degree of freedom is done in the background of the valley configurations, as will be seen later in Section 4.

the functional space is trivial in these variables. Otherwise, the metric should be inserted in the following equations in a straightforward manner.

The proper valley equation^{*)} is the following;

$$D_{ij}\partial_j S = \lambda\partial_i S, \quad (3.1)$$

where summation over the repeated indices are assumed and

$$D_{ij} \equiv \partial_i \partial_j S. \quad (3.2)$$

Since (3.1) has a parameter λ , it defines a one-dimensional trajectory in the ϕ -space. (The cases when we have a finite region with $\lambda = 0$ can be treated without any problems. This will be explained later in this section. For the moment, we assume $\lambda \neq 0$.) The solution of the equation of motion apparently satisfies the proper valley equation (3.1). In this sense the proper valley equation is an extension of the (field) equation of motion.

According to the proper valley equation (3.1), the parameter λ in the right-hand side of (3.1) is one of the eigenvalues of the matrix D_{ij} . Therefore the proper valley equation requires that the “gradient vector” $\partial_j S$ be parallel to the eigenvector of D_{ij} with the eigenvalue λ . A question arises which eigenvalue of D_{ij} we should choose for (3.1). As we will show later, the proper valley method converts the eigenvalue λ to a collective coordinate, by completely removing λ from the Gaussian integration and introducing the valley trajectory parameter instead. Thus the question is which eigenvalue ought to be converted to a collective coordinate for the given theory. This really depends on the theory in question. Therefore we will address this issue later as we investigate various models. Here we will simply mention that the general guideline is to choose λ to be the eigenvalue with the smallest absolute value, *i.e.*, the pseudo-zero mode, or the negative eigenvalue, for which the Gaussian integration converges badly or diverges. In some models, the eigenvalue changes from a negative value to (still negative and) pseudo-zero value along the valley. In such a case, proper valley equation will be shown to be able to deal with both types of eigenvalues.

The proper valley equation (3.1) can be interpreted within a framework of the variational method: Let us rewrite it as the following;

$$\partial_i \left(\frac{1}{2} (\partial_j S)^2 - \lambda S \right) = 0. \quad (3.3)$$

^{*)} This method in the manner described here was proposed by two of the current authors, H. Aoyama and K. Kikuchi in Ref. 11). Later they found that the same equation had been written down by P. G. Silvestrov in Ref. 12), and well before that (in different contexts) in Ref. 13). (Some very early literatures of general discussion of the contour-lines in geological context are found in Ref. 14).) Furthermore, this method is apparently useful in the theoretical chemistry.¹⁵⁾ The authors thank Dr. Silvestrov, Dr. Quapp and S. Takagi at Tohoku University for letting us know of these references.

This allows an interpretation that the norm of the gradient vector is extremized under the constraint $S = \text{const}$, where λ plays the role of the Lagrange multiplier. Since such a point is found at each hypersurface of constant action, the solutions of the proper valley equation form a line in the functional space. This is an alternative explanation for the existence of the valley line. In addition, we require that the norm be *minimized*. Since the valley with maximum norm is disjoint from the one with minimum norm, this can be easily done by choosing the appropriate valley line. We are therefore defining the valley to be the trajectory that is tangent to the most gentle direction. This is a plausible definition, suitable for the word “valley”.

What is important, however, is not its intuitive interpretation, but the evaluation of the relevant functional integral. It is carried out along the valley line in the following manner: Let us parametrize the valley line by a parameter α and denote the solutions of (3.1) as $\phi(\alpha)$. The integration over α is to be carried out exactly, while for other directions the one-loop (or higher order) approximation is applied. We are to change the integration variables (ϕ_i) to α and a subspace of (ϕ_i) , which is determined uniquely by the following argument: We first expand the action in terms of the fluctuation $\tilde{\phi} = \phi - \phi(\alpha)$,

$$S(\phi) = S(\phi(\alpha)) + \partial_i S(\phi(\alpha)) \tilde{\phi}_i + \frac{1}{2} D_{ij}(\phi(\alpha)) \tilde{\phi}_i \tilde{\phi}_j + \dots \quad (3.4)$$

The first order derivative term in the above is *not* equal to zero, for $\phi(\alpha)$ is *not* a solution of the equation of motion. In such a case, the \hbar -expansion is no longer the loop expansion, as the tree contribution floods the expansion. In order to avoid this, we force this term to vanish by the choice of the subspace. It is most conveniently done by the Faddeev-Popov technique. We introduce the FP determinant $\Delta(\phi(\alpha))$ by the following identity;

$$\int d\alpha \delta(\tilde{\phi}_i R_i) \Delta(\phi(\alpha)) = 1, \quad (3.5)$$

where $R_i(\phi(\alpha)) \equiv \partial_i S / \sqrt{(\partial S)^2}$ is the normalized gradient vector. From the above definitions, we find the FP determinant to be the following;

$$\Delta(\phi(\alpha)) = \left| \frac{d\phi_i(\alpha)}{d\alpha} \{R_i - \partial_i R_j \tilde{\phi}_j\} \right|. \quad (3.6)$$

In the one-loop approximation, the second term in the curly bracket can be neglected and the remaining term is simply the cosine of the angle between the gradient vector and the vector tangent to the trajectory. This is simply a Jacobian factor, because the trajectory is not necessarily orthogonal to the chosen subspace. This situation is illustrated in Fig. 2.

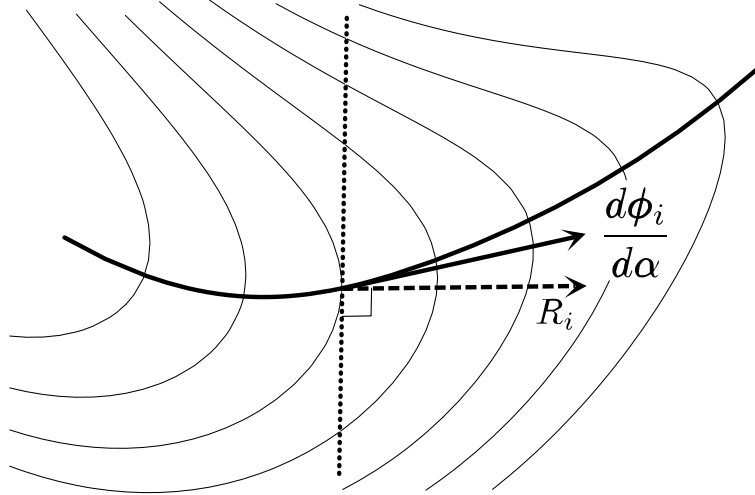


Fig. 2. A two-dimensional model of the functional space. The thin solid lines denote the contours of the action S . The thick solid line is the valley line. The gradient vector R_i and the tangent vector $d\phi_i/d\alpha$ are denoted by the broken and solid arrows, respectively. The vertical dotted line is the subspace chosen for the one-loop integral.

Let us evaluate the the path-integral for the vacuum-to-vacuum transition amplitude,

$$Z = \mathcal{N} \int \prod_j \frac{d\phi_j}{\sqrt{2\pi}} e^{-S}, \quad (3.7)$$

using the valley trajectory, where \mathcal{N} is a suitable normalization factor. The evaluation for observables is essentially the same.^{*)} Substituting (3.5) into (3.7), we obtain

$$Z = \mathcal{N} \int d\alpha \int \prod_j \frac{d\phi_j}{\sqrt{2\pi}} \delta(\tilde{\phi}_i R_i) \left| \frac{d\phi_i}{d\alpha} R_i \right| e^{-S(\phi)}, \quad (3.8)$$

where we have already used the one-loop expression for the FD determinant (the Jacobian) $\Delta(\phi(\alpha))$. We note that the above expression is apparently invariant under the general coordinate transformation of α . The second (functional) integration, $\int \prod_j d\phi_j \delta(\tilde{\phi}_i R_i)$, is the integration over the subspace denoted by the dotted line in Fig. 2. At the one-loop order, the ϕ_i integration yields \det' , the determinant of D_{ij} restricted to the subspace. This subspace is orthogonal to the gradient vector, which is the eigenvector with the eigenvalue λ according to the proper valley equation (3.1). Therefore this subspace is the whole space less the direction of the eigenvalue λ of D_{ij} . Therefore the resulting determinant is simply the ordinary determinant less the eigenvalue λ ;

$$\det' D = \frac{\det D}{\lambda}, \quad (3.9)$$

^{*)} The only possible exceptions are the cases then we have “large observables”; if for example we have a large number of fields, which contributions could override the dominations by the exponentiated action. This requires further development of the theory at hand.

This can be shown by evaluating (3.8) by exponentiating the delta-function and integrating over the fluctuations $\tilde{\phi}$ as follows;

$$\begin{aligned}
Z &= \mathcal{N} \int d\alpha \int \prod_j \frac{d\tilde{\phi}_j}{\sqrt{2\pi}} \int_{-\infty}^{\infty} \frac{dk}{2\pi} e^{ik\tilde{\phi}_i R_i} \left| \frac{d\phi_i}{d\alpha} R_i \right| e^{-S(\phi)} \\
&= \mathcal{N} \int d\alpha \int_{-\infty}^{\infty} \frac{dk}{2\pi} \frac{1}{\sqrt{\det D}} \exp\left(-\frac{1}{2} R D^{-1} R k^2\right) \\
&= \mathcal{N} \int d\alpha \left| \frac{d\phi_i}{d\alpha} R_i \right| \frac{1}{\sqrt{2\pi(RD^{-1}R) \det D}} e^{-S(\phi(\alpha))}. \tag{3.10}
\end{aligned}$$

Since the proper valley equation (3.1) yields $D^{-1}R = R/\lambda$ and the vector R is normalized, we obtain

$$(RD^{-1}R) \det D = \frac{1}{\lambda} \det D (= \det' D), \tag{3.11}$$

as in (3.9). We thus obtain the following expression at the one-loop order;

$$Z = \mathcal{N} \int d\alpha \left| \frac{d\phi_i}{d\alpha} R_i \right| \frac{1}{\sqrt{2\pi \det' D}} e^{-S(\phi(\alpha))}. \tag{3.12}$$

In this sense, the proper valley method converts the eigenvalue to the collective coordinate, *exactly*. As we briefly mentioned at the beginning of this section, this exact conversion is quite ideal for the actual calculations: In physical situation one often suffers from a negative, zero, or positive but very small eigenvalue, which renders the ordinary Gaussian integration meaningless or unreliable. The proper valley method saves this situation by converting the unwanted eigenvalue to the collective coordinate, for the factor $\det' D$ is exactly free from this eigenvalue.

When there are solutions of the equation of motion with a zero mode, as in the models with ordinary instantons, the proper valley method reduces to the usual collective coordinate method. This is seen as follows. Let us denote the solution of the equation of motion by ϕ_{sol} ;

$$\partial_i S(\phi_{\text{sol}}) = 0. \tag{3.13}$$

This satisfies the proper valley equation (3.1) at the same time. The normalized gradient vector R_i is apparently singular due to (3.13). However, R_i is well-defined by a limiting procedure $\lambda \rightarrow 0$. In order to show this, we denote the original action by $S^{(0)}$ and we add a term $\lambda S^{(1)}$ to the original action, so that ϕ_{sol} is no longer a solution of equation of motion for the theory defined by the total action $S = S^{(0)} + \lambda S^{(1)}$. (The parameter λ is an arbitrary small quantity and $S^{(1)}$ can be any function of ϕ that satisfy the above requirement.) The solution of the proper valley equation for S can be expanded in terms of λ around ϕ_{sol} .

For this purpose, We introduce a set of auxiliary variables F_i and rewrite the proper valley equation (3.1) as follows;

$$D_{ij}F_j = \lambda F_i, \quad (3.14)$$

$$\partial_i S = F_i. \quad (3.15)$$

The equation (3.13) guarantees that at $\lambda = 0$, $F_i = 0$. Thus we use the following expansion;

$$\phi = \phi_{\text{sol}} + \lambda \phi^{(1)} + \dots,$$

$$F = \lambda F^{(1)} + \dots.$$

Substituting the above expansion to (3.14) and (3.15), we find that the zeroth order equation in λ is simply (3.13), and that the first order equations are as the follows;

$$D_{ij}^{(0)} F_j^{(1)} = 0, \quad (3.16)$$

$$\partial_i S^{(1)}(\phi_{\text{sol}}) + D_{ij}^{(0)} \phi_j^{(1)} = F_i^{(1)}, \quad (3.17)$$

where $D_{ij}^{(0)} \equiv \partial_i \partial_j S^{(0)}(\phi_{\text{sol}})$. From the equation (3.16), we find that $F^{(1)}$ is proportional to the zero-mode of the original solution ϕ_{sol} . The proportionality constant is determined by multiplying $F_i^{(1)}$ on (3.17);

$$F_i^{(1)} \partial_i S^{(1)}(\phi_{\text{sol}}) = F_i^{(1)} F_i^{(1)}, \quad (3.18)$$

where we have used the fact that D_{ij} is symmetric and (3.16). The quantity $\phi_j^{(1)}$ is determined by (3.17) under the above condition. Since the normalized gradient vector R_i in question is the normalized F vector, *i.e.*, $R_i = F_i/|F|$, it is, in the limit $\lambda = 0$, simply the the normalized zero-mode of the solution of the equation of motion. Therefore, we conclude that the FP procedure (3.6) is equivalent to the usual collective coordinate method, as promised.

The above analysis shows that the proper valley method can be considered as an generalization of the usual collective coordinate method. An added bonus of this property is that the resulting $\det' D$ is quite easy to calculate; we simply calculate the whole determinant and divide it by the smallest eigenvalue. If several unwanted eigenvalues exist, the proper valley method can be extended straightforwardly. The equation should then specify that the gradient vector $\partial_i S$ lie in the subspace spanned by the unwanted eigenvalues. This leads to a multi-dimensional valley with the advantages noted above.

There is another valley method, called ‘‘streamline method’’¹⁶⁾, which has been extensively used in the literatures. It proposes to trace the steepest descent line starting from a region of larger action. Namely, it uses the equation

$$\frac{d\phi_i}{d\alpha} = f(\alpha) \partial_i S, \quad (3.19)$$

where $f(\alpha)$ is an arbitrary function of α (there is a general reparametrization invariance of α in this formalism). This valley line coordinate can be introduced in the same manner as before using the FP technique. This makes the Jacobian trivial at the one-loop order. This streamline method, however, suffers from many difficulties unknown to the proper valley method: The most serious one is the fact that its subspace for the Gaussian integration has no relation to the eigenvalues of D_{ij} whatsoever. The relation (3-11) does not hold; the determinant is not guaranteed to be free from the unwanted eigenvalue. Another problem is that it is a flow equation in the functional space: Once given a point in the functional space, it defines other valley configurations in the infinitesimally small neighborhood of that point. In other words, it is not a local definition in the functional space. As such, it does not define a solution by itself. One has to define the starting point to start the valley. Therefore the construction of the configurations on the valley trajectory is quite difficult. When the starting configuration is known (like a pair of instanton and anti-instanton separated by infinite distance), this might be said to be a technical difficulty. In this method, however, the valley can be traced only from the above; it suffers from instability if the valley is traced from the *bottom* of the valley. An elementary analysis shows that the streamline most often climbs up the side-walls of the valley, not the bottom line. This problem becomes fatal when one is dealing with the theories with zero-size instantons, like the standard model noted in the previous section, in which the higher starting point is not known at all. For more detailed comparison of these methods and other features of the proper valley method, we refer the readers to Ref. 11).

There is yet one another formalism that deals with this kind of situation. It is the “constrained (instanton) method”,¹⁰⁾ explained briefly in the context of the standard model in Section 2. This method is actually a valley method, in the sense that we obtain a line of configuration parametrized by the constraint parameter. In the case mentioned above, this method allows the definition of configurations, are very close to the zero-size instanton. It has a problem that there is no prescription for the choice of the constraint that guarantees the effective evaluation of the path-integral. In general one knows some way to choose the constraint so that it allows desirable configurations. But this is only a prescription for the constraint not to be meaningless. Among all the meaningful constraints which allows effective evaluation is the question unanswered.

Actually there is a subtle relation between the proper valley method and the constraint method. Let us elaborate upon this point for clarification. The equation (3-3) can be interpreted as a constrained equation in a different manner: By dividing with λ , it can be

viewed as extremizing the action S under the constraint functional;

$$S_{\text{const.}} = -\frac{1}{2\lambda}(\partial_i S)^2. \quad (3\cdot20)$$

Therefore, the proper valley method can be interpreted as a constraint method, but *with the specific choice of the constraint* (3·20). However, with all the geometrical properties and the special features, especially in relation with the Gaussian integrations, which are all unique to the proper valley method, we consider it is best to distinguish it from the generic constraint method without any special consideration to the constraint. Hereafter in this paper we simply call the latter the constraint method.

While the detailed comparison of the configurations obtained by the constraint method and the ones by the proper valley method in specific field theoretical models are done in Section 4, here we discuss a toy two-dimensional functional space to demonstrate the power of the proper valley method. The two degrees of freedom in the model is denoted as ϕ_i ($i = 1, 2$), and the action is given by the following,

$$S(\phi_1, \phi_2) = \frac{1}{g^2} \left((\phi_1^2 + \phi_2)^2 + 5(\phi_1^2 - \phi_2)^2 \right). \quad (3\cdot21)$$

This is constructed by distorting a simple parabolic potential so that the valley trajectory is not trivial. Its contours ($S = \text{constant}$ lines) are plotted as thin lines in Fig. 3.

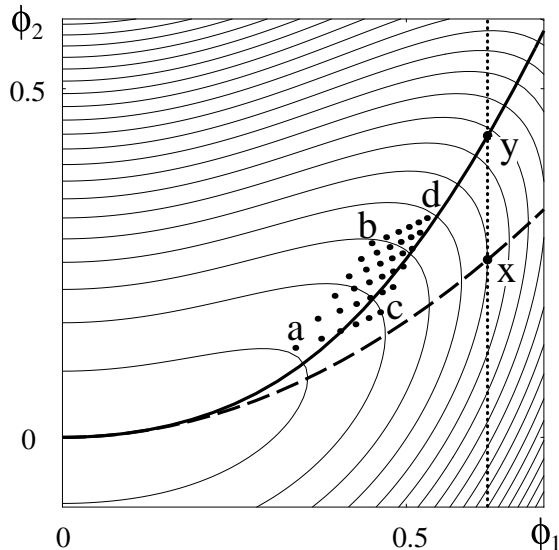


Fig. 3. The valley instanton and the constrained instanton in the toy model. The solid line denotes the valley instanton and the dashed line shows the constrained instanton. The dots show the positions of the saddle points of the integrand of $O(p, q)$.

The proper valley equation is now a simple algebraic equation, which can be solved numerically. Alternatively, we could reparametrize the functional space by (r, θ) defined by

the following;

$$\phi_1^2 + \phi_2 = r \cos \theta, \quad \phi_1^2 - \phi_2 = \frac{1}{\sqrt{5}} r \sin \theta. \quad (3.22)$$

Under this parametrization $S = r^2/g^2$. Therefore following the variational interpretation of the proper valley equation, we can minimize the square of the norm of the gradient vector, $(\partial_i S)^2$, as a function of θ . In Fig. 3, the thick solid line denotes the proper valley trajectory.

As an analogue of the constrained instanton formalism in this toy model, we introduce a simple constraint. Near the origin the valley trajectory extends to the ϕ_1 direction. Any reasonable constraint has to reproduce this property. Therefore, as a simple example for the constraint, we choose the following;

$$\phi_1 = \text{const.} \quad (3.23)$$

The solution of the constraint method is plotted in Fig. 3 by the dashed line.

In Fig. 3, it is apparent that the proper valley trajectory goes through the region of importance, while the constrained trajectory does not. This property can be displayed more explicitly by considering the analogue of the physical observables $O(p, q)$ defined by the following;

$$O(p, q) = \int_0^\infty d\phi_1 \int_{-\infty}^\infty d\phi_2 \phi_1^p \phi_2^q e^{-S(\phi_1, \phi_2)}. \quad (3.24)$$

Following the prescription given above, we have carried out the numerical evaluation of $O(p, q)$ exactly and by the Gaussian (“one-loop”) approximation around the proper valley trajectory and the constrained trajectory. Table.I gives the ratio of the one-loop values over the exact value.

As is seen in the table, the proper valley method gives a better approximation than the constraint method in this range of (p, q) consistently. This could be explained in the following manner; one could calculate the position of the maximum of the integrand in (3.24), or the following “effective action”;

$$\tilde{S}^{(p,q)}(\phi) = S(\phi) - p \log \phi_1 - q \log \phi_2. \quad (3.25)$$

The peak positions calculated in this manner are denoted in Fig. 3 by dots. The point a in the left bottom is for $(p, q) = (2, 2)$, b for $(2, 12)$, c for $(12, 2)$, and d for $(12, 12)$. The dots are distributed around the proper valley trajectory. This explains the fact that the proper valley trajectory gives the better approximation over the constrained trajectory. Only when the power of one of the observable gets high enough as in the point c , the constraint method starts to give a little better values. However, this is exactly the range in which the

ordinary instanton calculation starts to fail; For the n -point function with $n > O(1/g^2)$, it is well known that one needs to take into account the effect of the external particles on the instanton itself. The power of the valley method lies in the fact that even in this range the calculation is done with good accuracy for generic type of observables, like the (12,12) case. Only when the observable is very special, like the (12,2) case, the constraint method tuned to that operator may give reasonable estimates.

$p \backslash q$	2	4	6	8	10	12
2	0.827	0.679	0.585	0.520	0.474	0.439
	0.545	0.248	0.110	0.049	0.022	0.010
4	0.997	0.870	0.767	0.689	0.629	0.581
	0.667	0.324	0.149	0.068	0.030	0.014
6	1.061	0.986	0.900	0.826	0.764	0.712
	0.737	0.384	0.185	0.086	0.040	0.018
8	1.064	1.046	0.991	0.931	0.876	0.826
	0.783	0.432	0.218	0.105	0.050	0.023
10	1.029	1.063	1.041	1.003	0.960	0.918
	0.815	0.473	0.248	0.123	0.060	0.028
12	0.971	1.046	1.058	1.043	1.017	0.985
	0.839	0.508	0.276	0.141	0.070	0.034

Table I. The ratio of the $O(p, q)$ estimated by proper valley method (the upper column) and the constraint method (the lower column) over the exact value for $g = 0.2$.

Let us note a tricky point in comparing the valley instanton and the constrained instanton. If we compare them with the same parameter values, the constrained instanton has smaller action than the valley instanton. This is not a contradiction, nor it means the constrained instanton has a larger contribution: This becomes clear by considering the dotted vertical line in Fig. 3. The point x and y are the valley and the constrained configurations, respectively, which have the same value of ϕ_1 . The configuration y has a larger action than x , by the definition of the constraint method. However, as we have seen above, this does not mean that the constrained trajectory gives a better approximation. (One way to illustrate this

point is that if we compare the configurations at the same distance, $\int d\alpha |(d\phi_i/d\alpha)R_i|$, from the origin, the valley configuration has the smaller action.) The same situation will be seen in the results of the following sections; when we compare the instantons at the same value of the constraint parameter, the constrained instanton has a smaller action than that of the valley instanton. This is a red herring and has nothing to do with the relevancy of the valley instanton.

In this analysis we took a very simple constraint (3.23). Alternatively we could take some ad-hoc constraint as long as any of these yield “finite-size” instantons, *i.e.*, points away from the origin. Most of these constraints yield essentially similar results. Only when the trajectory goes through the dotted area in the Fig. 2, one can obtain good quantitative results. Such a trajectory, however, is destined to be very close to the proper valley trajectory. Therefore the proper valley method, defined without any room for adjustment and guaranteed to give good results is superior to the constrained method.

Finally, we note that in the actual calculation of the solutions in the continuum space-time the proper valley equation with auxiliary variable F , the equations (3.14) and (3.15), is most convenient. Let us denote all the real bosonic fields in the theory by $\phi_\alpha(x)$, where we denote all the space-time coordinates by x and the rest of the indices by α . The proper valley equation is as follows;

$$\sum_{\beta} \int d^4y \frac{\delta^2 S}{\delta\phi_{\alpha}(x)\delta\phi_{\beta}(y)} F_{\beta}(y) = \lambda F_{\alpha}(x), \quad (3.26)$$

$$F_{\alpha}(x) = \frac{\delta S}{\delta\phi_{\alpha}(x)}.$$

This is a set of second-order differential equation, which can be analyzed by the conventional methods. The solution of the ordinary field equation of motion is a solution of the above equation with $F_{\alpha}(x) = 0$. In other words, $F_{\alpha}(x)$ specifies where and how much the valley configuration deviates from the solution of equation of motion. This property is useful for the qualitative discussion of the properties of the valley configurations. The analysis in the following sections will be carried out in this auxiliary field formalism.

§4. Application of the proper valley method

4.1. Valley instanton in the asymmetric double-well potential

In this subsection we apply the proper valley method to an one-dimensional quantum mechanical model. Our aim is to resolve a paradox¹⁷⁾ that arises if we naively apply the semi-classical approximation to the potentials, $V(\phi)$, depicted in Fig. 4 and 5. Let us start

with reviewing the path-integral formalism in the quantum mechanics and then clarify what is the paradox we are concerned with.

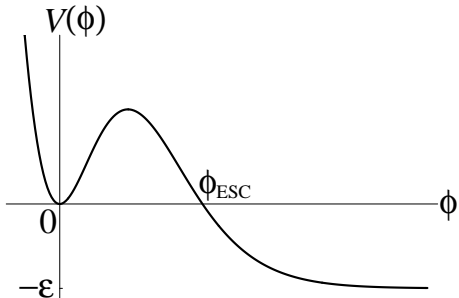


Fig. 4. A potential that is flat in the asymptotic direction, $V(\infty) = -\epsilon$.

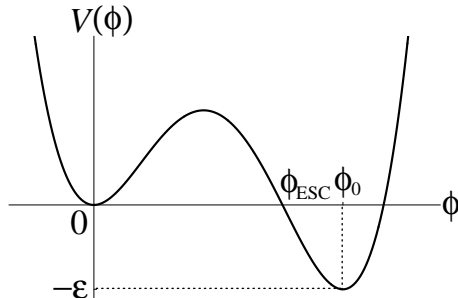


Fig. 5. An asymmetric double-well potential, in which $\phi = 0$ is only metastable.

For a given Hamiltonian with the dynamical variable ϕ and its conjugate momentum p ,

$$H = \frac{1}{2} p^2 + V(\phi), \quad (4.1)$$

the transition amplitude from the initial value $\phi = q_1$ at $\tau = 0$ to the final one q_2 at T in imaginary time formalism is evaluated by the path-integral

$$\langle q_2 | e^{-HT/\hbar} | q_1 \rangle = \mathcal{N} \int \mathcal{D}\phi e^{-S[\phi]/\hbar} \quad (4.2)$$

where

$$S[\phi] = \int_0^T d\tau \left[\frac{1}{2} \left(\frac{d\phi}{d\tau} \right)^2 + V(\phi) \right]. \quad (4.3)$$

In Eq. (4.2), $\phi(\tau)$ is parameterized as

$$\phi(\tau) = \phi_B(\tau) + \sum_n a_n \varphi^{(n)}(\tau), \quad (4.4)$$

where ϕ_B is a background that satisfies

$$\phi_B(0) = q_1, \quad \phi_B(T) = q_2, \quad (4.5)$$

and $\varphi^{(n)}$ are elements of a normalized complete set in the functional space for the interval $[0, T]$; they satisfy

$$\left(\varphi^{(n)} \cdot \varphi^{(m)} \right) \equiv \int_0^T d\tau \varphi^{(n)}(\tau) \varphi^{(m)}(\tau) = \delta_{nm} \quad (4.6)$$

and

$$\varphi^{(n)}(0) = \varphi^{(n)}(T) = 0. \quad (4.7)$$

The integral measure is then defined in terms of the coefficients a_n by

$$\mathcal{D}\phi = \prod_n \frac{da_n}{\sqrt{2\pi\hbar}}, \quad \mathcal{N} = \left[\frac{1}{2\pi\hbar T} \prod_{m=1}^{\infty} \left(\frac{\pi m}{T} \right)^2 \right]^{1/2}. \quad (4.8)$$

The infinite products over m and n are understood to be combined properly in actual calculations so that the final expression becomes a convergent product. The information on the model will be given by calculating Eq. (4.2) for the various values of q_1 , q_2 , and T . We are interested in the energy eigenvalues E of the lowest-lying states; we calculate Eq. (4.2) with the boundary condition $\phi(0) = \phi(T) = 0$ and with sufficiently large T (compared with the inverse of the excitation energies of the other states.) The energy eigenvalues are extracted from the T dependence of the transition amplitude, $\langle 0|e^{-HT/\hbar}|0\rangle \sim e^{-ET/\hbar}$.

The semi-classical approximation for the path-integral Eq. (4.2) is carried out by the following: use the classical solutions ϕ_{cl}

$$\frac{\delta S}{\delta \phi_{\text{cl}}} = 0 \quad (4.9)$$

as ϕ_{B} and expand the action around it,

$$S[\phi] = S[\phi_{\text{cl}}] + \frac{1}{2} \int \int d\tau d\tau' D(\tau, \tau') \varphi(\tau) \varphi(\tau'), \quad (4.10)$$

where $D(\tau, \tau') \equiv \delta^2 S / \delta \phi(\tau) \delta \phi(\tau')$ and $\varphi \equiv \phi - \phi_{\text{cl}}$; use the eigenfunctions of D for the complete set $\{\varphi^{(n)}\}$ and approximate the functional integral by Gaussian,

$$\langle 0|e^{-HT}|0\rangle \simeq \sum_{\phi_{\text{cl}}} e^{-S[\phi_{\text{cl}}]} \frac{\mathcal{N}}{\sqrt{\det D[\phi_{\text{cl}}]}} \quad (4.11)$$

where “det” denote the product of all the eigenvalues of D (we will set $\hbar = 1$ hereafter.) The zero modes will be treated by the collective coordinate method (see for example Ref. 9)) if D has some.

For the potentials in Fig. 4 and 5 we have the bounce solution, that starts at $\phi = 0$ and bounce at ϕ_{ESC} back to $\phi = 0$ for the large time interval, $T \gg \omega_+^{-1}$ (ω_+ is the frequency at $\phi = 0$.) There is a subtlety in the semi-classical approximation at the bounce: it has one negative eigenvalue mode and the Gaussian integral along this direction becomes ill-defined. The way we usually adopt to circumvent this is to assume an appropriate analytic continuation of the contour for the ill-defined Gaussian integral; The bounce then gives an imaginary part for the energy eigenvalues^{9), 18), 19)} for both potentials in Fig. 4 and 5.

Although the exact form of the analytic continuation is not so clear, the complex energy for the potential in Fig. 4 has a sound interpretation: if one restricts the wave functions to have only the outgoing component at $\phi \gg \phi_{\text{ESC}}$, the hermiticity of the Hamiltonian

is violated and the energy eigenvalues become complex. This imaginary part reflects the instability of the localized wave packet at $\phi \sim 0$.

For the potential in Fig. 5, however, the imaginary part is obviously a wrong answer.¹⁷⁾ We can only take wave functions with decaying exponential at $\phi \gg \phi_0$ and the hermiticity of the Hamiltonian cannot be violated. There is no room for the energy eigenvalue to be complex. This is the paradox we intend to solve.

We use the proper valley method to see how the action behaves for the path-integral related to the negative mode at the bounce and to make the corresponding path-integral well-defined. We construct “valley instanton”, which should replace the bounce solution. Interestingly, it has a zero mode and this expedites the calculation of its determinant and Jacobian as was the case of the instanton. It is a well-localized configuration with respect to the imaginary time and their dilute-gas sum generates the reasonable energy shift instead of the decay rate. We will also show that it converges analytically to the instanton in the limit of $\epsilon \rightarrow 0$ and all the results reproduce the well-known instanton results.

Specifically we parameterize the potential in Fig. 5 as

$$V(\phi) = \frac{1}{2}\phi^2(1 - g\phi)^2 - \epsilon(4g^3\phi^3 - 3g^4\phi^4), \quad (4.12)$$

where the coupling constants g and ϵ are positive. The potential (4.12) has a local minimum, $V(0) = 0$ and a global minimum at $\phi_0 = 1/g$, where $V(1/g) = -\epsilon$. (Fig. 5 is plotted for $g = 0.3$ and $\epsilon = 0.25$.) The potential $V(\phi)$ in Eq. (4.12) is a canonical form of quartic potentials with two minima, since any such potential can be cast into this form by suitable linear transformations on ϕ and τ . In this sense the following analysis is quite a general one. (Especially, the above form is related to that of Ref. 20) by a simple reparametrization.) In the following, we consider the cases with small coupling $g \ll 1$, but not necessarily small ϵ .

The proper valley configurations are given by the equations

$$-\partial_\tau^2\phi + V'(\phi) = F, \quad (4.13)$$

$$\left(-\partial_\tau^2 + V''(\phi)\right)F = \lambda F. \quad (4.14)$$

as has been explained in the section 3. The bounce satisfies this equation trivially since it has $F = 0$. We take λ in the infinitesimal neighborhood of the bounce as its negative eigenvalue. Then the valley trajectory extends to the direction of the negative mode from the bounce. By changing the parameter λ , we will obtain a trajectory in the functional space. The general solutions can be parameterized by the eigenvalue λ , or any arbitrary function α of λ . We denote the valley trajectory by $\phi(\alpha)$. We consider the contribution of such a configuration to the transition amplitude $\langle 0|e^{-HT}|0\rangle$. By the result of Eq. (3.12), this

amplitude is given as

$$\langle 0|e^{-HT}|0\rangle = \mathcal{N} \int d\alpha \frac{1}{\sqrt{2\pi \det' D}} J_\alpha e^{-S[\phi(\alpha)]}, \quad (4.15)$$

to the leading order in g , where $\det' D$ is the usual determinant less the eigenvalue λ in the proper valley equation (4.14) and

$$J_\alpha \equiv \frac{\int d\tau \frac{d\phi(\alpha)}{d\alpha} F}{\sqrt{\int d\tau F^2}} = \frac{\frac{dS[\phi(\alpha)]}{d\alpha}}{\sqrt{\int d\tau F^2}}. \quad (4.16)$$

The factor J_α is the Jacobian for this change of the integration variable which is explained at the previous section.

We have carried out the numerical analysis and obtained the solutions of the proper valley equation plotted in Fig. 6. The solid line, a , is the bounce solution of the equation of

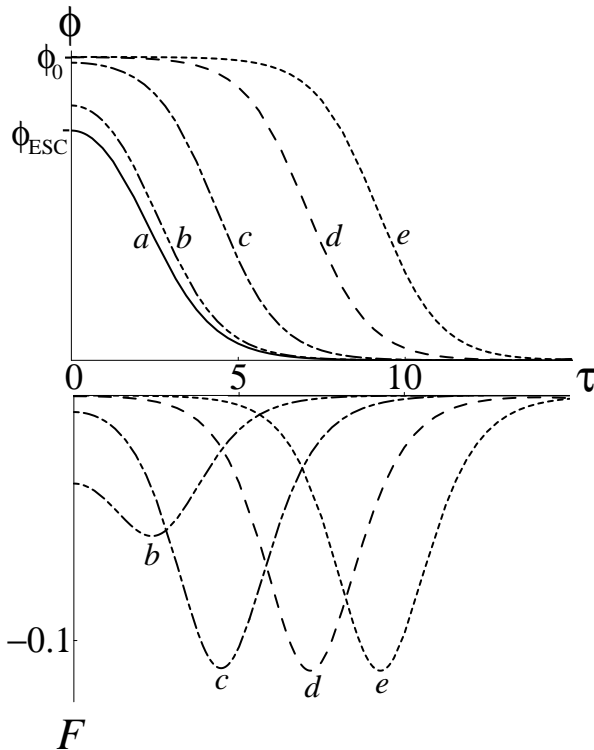


Fig. 6. Valley bounce solutions $(\phi(\tau), F(\tau))$ of the proper valley equations. Center of all of the configurations are chosen to be at the origin, $\tau = 0$, around which the solutions are symmetric. The solid line a in the upper figure is the usual bounce solution, which has $F(\tau) = 0$. The other lines, $b-e$, are unique to the proper valley equations.

motion. The rest do not satisfy the equation of motion. We call these solutions (including

the bounce solution) “valley bounce”. The values of the action, S , and the eigenvalue, λ , for the valley bounces are plotted in Fig. 7. The bounce solution lies at the top of the line of the

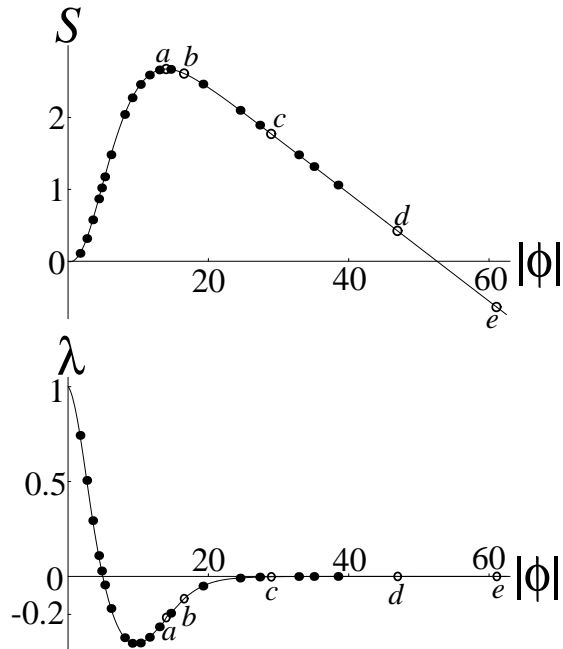


Fig. 7. The values of the action, S , and the eigenvalue, λ , of the valley bounces. The peak of the action is given by the bounce solution, the line a in Fig. 6. The points corresponding to the valley bounces in Fig. 6 are plotted with circle. The solid lines are drawn as the guide for eyes. The valley parameter is chosen to be $|\phi| \equiv \int d\tau \phi$.

action in Fig. 7, corresponding to the fact that it has a negative eigenvalue. This negative eigenvalue can be read from the corresponding point of the plot of λ in the lower half of Fig. 7. The most notable feature is that the large size valley bounces have a clean interior, where $\phi = \phi_0$ and $F = 0$. (This property is shared by the higher dimensional configurations, *i.e.*, the valley bubbles.) The effect of this is apparent in the behavior of the action in Fig. 7; the action decreases linearly with large $|\phi|$, which is proportional to the size of the valley bounce.

In the large valley bounces, c , d , and e in Fig. 6, we notice that the shape of the wall, *i.e.*, the transition region from $\phi \sim \phi_0$ to $\phi \sim 0$, is almost identical to each other. That is, they overlap with each other very well when translated in τ . Thus these large valley bounces can be approximated by simply connecting the walls by a flat region, $\phi = \phi_0$, at various separation. The shape of the wall can be most readily identified when the size ($|\phi| \equiv \int d\tau \phi$) of the valley bounce becomes ∞ . In this limit, the wall is simply a localized transition from $\phi = 0$ to $\phi = \phi_0$ (or vice-versa). Such a solution is an analogue of the instanton (or

anti-instanton). The difference is that now it is not a solution of equation of motion, but is a solution of the proper valley equation. This kind of configuration is called the “valley (anti-)instanton.”²¹⁾

The notable information from this numerical analysis is that the path-integral for the negative mode direction at the bounce can be translated eventually into the collective coordinate integral with respect to the relative distance between the valley instanton and the valley anti-instanton. This integral indeed gets the large contribution from the large separation and is divergent for $T \rightarrow \infty$, but we can handle it anyway; we will be even able to carry out the dilute-gas summation for the multi valley instantons. Before doing so, we look into the details of the valley instanton which is needed for the summation.

Since we define the valley instantons at the large-size limit, $|\phi| \rightarrow \infty$, of the valley bounce, the plot of the eigenvalue in Fig. 6 implies that the eigenvalue λ of the valley instanton is exactly zero. This is not a trivial property. A solution of equation of motion is guaranteed to have zero modes corresponding to its symmetry transformation, such as a time translation. Arbitrary background configurations do not have this property in general. However, we can prove the existence of the zero mode as follows: Take a derivative of Eq. (4.13) with respect to τ , multiply F , and integrate over τ . After partial integrations (which surface terms vanish), we then find that

$$\lambda \int_{-\infty}^{\infty} F \dot{\phi} d\tau = \int_{-\infty}^{\infty} F \dot{F} d\tau . \quad (4.17)$$

The integral in the left-hand side is generally non-zero due to the boundary conditions of the valley instantons. This can be seen from the behavior of ϕ and F in the walls in Fig. 6. Since the right-hand side is zero, we find that $\lambda = 0$. (For the valley bounces, the integral in the left-hand side is zero since $\phi(\tau)$ and $F(\tau)$ are even functions. Therefore, $\lambda \neq 0$ is allowed.)

We have carried out the numerical investigation of the valley instanton with $\lambda = 0$ and have successfully obtained the solutions, which have turned out to be almost identical to the wall regions in Fig. 6.

Although we know of no exact analytical expression of the valley instanton, it can be constructed analytically for small g^2 in a manner used in the construction of the constrained instanton¹⁰⁾ as well as other types of the valley instantons.²¹⁾ Consider the valley instanton in $\tau \in [-T/2, T/2]$ ($T \gg 1$). We define its central coordinate to be at the origin, $\tau = 0$, by $\phi(0) = 1/2g$. The naive perturbation in ϵg^2 yields the following perturbative valley instanton solution;

$$\phi = \phi_0^I + 3\epsilon g^2 \tau \dot{\phi}_0^I + O((\epsilon g^2)^2),$$

(4.18)

$$F = -6\epsilon g^2 \dot{\phi}_0^I + 36\epsilon^2 g^5 \tau \phi_0^I \dot{\phi}_0^I + O((\epsilon g^2)^3),$$

where ϕ_0^I is the instanton solution for $\epsilon = 0$;

$$\phi_0^I = \frac{1}{g} \frac{1}{1 + e^{-\tau}}. \quad (4.19)$$

From Eq.(4.18), it is apparent that this naive perturbation is valid only in the region close to the instanton center, $|\tau| \ll 1/(\epsilon g^2)$. On the other hand, in the asymptotic regions, $\tau \rightarrow \pm\infty$, we linearize the proper valley equation and find the general solutions valid for $|\tau| \gg 1$. Coefficients of the general solutions are fixed by matching it with the inner solution Eq.(4.18) in the intermediate region, $1 \ll |\tau| \ll 1/(\epsilon g^2)$. We have found that this procedure can be done consistently. The resulting asymptotic behaviors are for $\tau \rightarrow +\infty$;

$$\phi \simeq \frac{1}{g} \left(1 - \left(1 + \frac{3\epsilon g^2}{\omega_-} \tau \right) e^{-\omega_- \tau} \right), \quad (4.20)$$

$$F \simeq -6\epsilon g e^{-\omega_- \tau},$$

where $\omega_-^2 \equiv V''(\phi_0) = 1 + 12\epsilon g^2$, and for $\tau \rightarrow -\infty$;

$$\phi \simeq \frac{1}{g} \left(1 + 3\epsilon g^2 \tau \right) e^{\tau}, \quad (4.21)$$

$$F \simeq -6\epsilon g e^{\tau}.$$

This way, the valley instanton is constructed in all regions of τ for small ϵ .

The action of the valley instanton is given by $S^I = 1/6g^2 + \epsilon(-T/2 + 1/2) + O(\epsilon^2)$. This action is divided to the volume part and the remaining (proper) part as $S^I = -\epsilon T/2 + \tilde{S}^I$. From the construction above, we find that $\tilde{S}^I = 1/6g^2 + \epsilon/2 + \dots$. However, there is a subtlety on this point: In the following we integrate over the position coordinate of the instantons and anti-instantons in the dilute-gas approximation. These coordinates are originally the valley parameters (α s) of the valley bounces (and their central coordinates). The $O(\epsilon)$ term in \tilde{S}^I depends on the definition of these valley parameters, since the definition of the volume (T) is affected by it. Therefore, careful study of the small valley bounces is needed to fix this term. This term, however, has only the non-leading contribution. Therefore, we will not pursue this problem any further here.

The Jacobian for the instanton position is given by,

$$J^I = \frac{\epsilon}{\sqrt{\int d\tau F^2}}. \quad (4.22)$$

Since the contribution to the integration is dominated by the central region, the leading term of Eq.(4.22) for small ϵ is evaluated by the use of Eq.(4.18). The result is that $J^I = 1/\sqrt{6g^2}(1 + O(\epsilon g^2))$. The first term is the instanton action for $\epsilon = 0$. Therefore, in the limit $\epsilon \rightarrow 0$, the Jacobian of the valley instanton reduces to that of the ordinary instanton.

The determinant, $\det' D$, can be calculated by extending the Coleman's method,⁹⁾ in spite of the fact that the valley instanton is not the solution of the equation of motion. This is due to the fact that the valley instanton possesses the exact zero mode $F(\tau)$. We define the asymptotic coefficients F_{\pm} by $F(\tau) \simeq F_{\pm} e^{\mp\omega_{\pm}\tau}$, where for the sake of notation we introduced $\omega_{\pm}^2 = V''(0) = 1$. After some calculation, we find that the ratio of the determinants for the valley instanton located at $\tau_0 (\in [-T/2, T/2])$ is given by the following;

$$\frac{\det'(-\partial_{\tau}^2 + V''(\phi^I))}{\det(-\partial_{\tau}^2 + \omega_{\pm}^2)} = \kappa e^{(\omega_- - \omega_+)(T/2 - \tau_0)}, \quad \kappa \equiv \frac{1}{2\omega_+ \omega_- F_+ F_-} \int_{-\infty}^{\infty} F^2. \quad (4.23)$$

The exponential factor represents the contribution of the difference between the zero point energies at the two local minima. The factor κ is the ‘proper’ instanton contribution. From Eq.(4.20) and Eq.(4.21), we find that κ reduces to the ordinary instanton determinant for $\epsilon \rightarrow 0$.

We combine all factors and calculate the amplitude using the ‘dilute-gas’ valley instanton approximation. We find the transition amplitude to be the following;

$$Z(T) \equiv \frac{\langle 0 | e^{-HT} | 0 \rangle}{\langle 0 | e^{-H_0 T} | 0 \rangle} = \sum_{n=0}^{\infty} \alpha^{2n} I_n, \quad (4.24)$$

where we have normalized the amplitude to that of the free Hamiltonian $H_0 = (1/2)[p^2 + \omega_{\pm}^2 \phi^2]$; n is the number of the valley instanton pairs, and the factor α is the product of the proper contributions of the action, the determinant ratio and the Jacobian; $\alpha = (J^I / \sqrt{2\pi\kappa}) e^{-\tilde{S}^I}$. The actual integrations over the positions of the valley instantons are in the factors I_n ;

$$I_n(T) \equiv \begin{cases} 1, & \text{for } n = 0, \\ \int_0^T d\tau_{2n} \int_0^{\tau_{2n}} d\tau_{2n-1} \dots \int_0^{\tau_2} d\tau_1 e^{\tilde{\epsilon}(\tau_{2n} - \tau_{2n-1} + \dots + \tau_2 - \tau_1)}, & \text{for } n \geq 1, \end{cases} \quad (4.25)$$

where zero-energy contributions of the determinants are absorbed in ϵ by $\tilde{\epsilon} \equiv \epsilon - (\omega_- - \omega_+)/2$.

The infinite series can be summed by the use of the generating function method:²²⁾ From Eq.(4.25), we find that the following differential equation is satisfied by $Z(T)$;

$$Z(T)'' - \tilde{\epsilon} Z(T)' - \alpha^2 Z(T) = 0. \quad (4.26)$$

Also, $Z(0) = 1$, and $Z'(0) = 0$. Therefore, we find that

$$Z(T) = \frac{k_+ e^{-k_- T} - k_- e^{-k_+ T}}{k_+ - k_-}, \quad (4.27)$$

where,

$$k_{\pm} \equiv -\frac{\tilde{\epsilon}}{2} \pm \sqrt{\frac{\tilde{\epsilon}^2}{4} + \alpha^2}. \quad (4.28)$$

Thus we find that the energies of the two lowest states, E_{\pm} is given by

$$E_{\pm} = \frac{\omega_+}{2} + k_{\pm} = \frac{\omega_+}{2} - \frac{\tilde{\epsilon}}{2} \pm \sqrt{\frac{\tilde{\epsilon}^2}{4} + \alpha^2}. \quad (4.29)$$

Furthermore, from the coefficients of the respective exponents of Eq.(4.27), we find that $|\langle \phi = 0 | E_{\pm} \rangle|^2 = \pm k_{\pm} / (k_+ - k_-)$. Note that there appear no fake imaginary parts in the energy spectrum.

We also examine the validity of the dilute-gas approximation. The mean size of the bounce, which is the mean distance, R , between the instanton and the anti-instanton located at the right of the instanton, can be obtained as the expectation value, $\langle \tau_2 - \tau_1 \rangle$ in the amplitude, Eq.(4.24) and Eq.(4.25). (Any other $\langle \tau_{2m} - \tau_{2m-1} \rangle$ with integer m would yield the same result for $T \rightarrow \infty$.) Using the same generating function method as above, we obtain the following;

$$R = \frac{1}{\alpha^2} \left(\frac{\tilde{\epsilon}}{2} + \sqrt{\frac{\tilde{\epsilon}^2}{4} + \alpha^2} \right). \quad (4.30)$$

Similarly, the mean distance, d , between the anti-instanton and the instanton located at the right of the anti-instanton $\langle \tau_3 - \tau_2 \rangle$ is given by,

$$d = \frac{1}{\alpha^2} \left(-\frac{\tilde{\epsilon}}{2} + \sqrt{\frac{\tilde{\epsilon}^2}{4} + \alpha^2} \right). \quad (4.31)$$

For $\epsilon \gg \alpha$, $d \sim 1/\tilde{\epsilon}$. On the other hand, the thickness of the instanton is $O(1/\sqrt{\epsilon})$ for $\epsilon \gg 1$, which can be seen by a simple scaling argument on the proper valley equations, Eq.(4.13) and Eq.(4.14). This means that the dilute-gas approximation is valid for $\tilde{\epsilon} < 1$.

The result (4.29) has now a simple explanation. We observe that E_{\pm} are equal to the eigenvalues of the following matrix;

$$H = \begin{pmatrix} \frac{\omega_+}{2} & \alpha \\ \alpha & -\epsilon + \frac{\omega_-}{2} \end{pmatrix}. \quad (4.32)$$

Furthermore, the weights of the state localized in the left well agree with Eq.(4.27): Denoting the eigenvectors of Eq.(4.32) V_{\pm} with eigenvalues E_{\pm} ,

$$\begin{pmatrix} 1 \\ 0 \end{pmatrix} = \sqrt{\frac{k_+}{k_+ - k_-}} V_+ + \sqrt{\frac{-k_-}{k_+ - k_-}} V_-. \quad (4.33)$$

The energy spectrum we obtain is the same as the two-level system made of the perturbative ground state at $\phi = 0$ and $\phi = \phi_0$, with the tunneling matrix element α . This simple picture is correct if the higher excited states have large energy gap from the two, and the condition is exactly the one obtained from the validity of the dilute-gas summation, $\tilde{\epsilon} < 1$.

Finally let us check the result (4.29) for a few cases. For $\epsilon \ll \alpha$, the energy spectrum Eq.(4.29) gives the following;

$$E_{\pm} = \frac{\omega_+ + \omega_-}{4} \pm \alpha - \frac{\epsilon}{2} + O\left(\frac{\epsilon^2}{\alpha}\right). \quad (4.34)$$

In the limit $\epsilon \rightarrow 0$, this result reduces to the well-known instanton result for the degenerate case. In addition, we have the average of the perturbative zero-point energies of the left-well $\omega_+/2$ and the right-well $\omega_-/2 - \epsilon$. Since the wave function is distributed evenly at the zeroth order of the ϵ expansion, this is the correct formula for the two lowest energy eigenvalues. Since the perturbative contribution to the energy splitting, $\delta E = E_+ - E_-$, is of order ϵg^4 , even a purist⁹⁾ would retain our result, $\delta E = 2\alpha$. For $\alpha \ll \epsilon < 1$, Eq.(4.29) leads to,

$$E_+ = \frac{\omega_+}{2} + \frac{\alpha^2}{\tilde{\epsilon}} + O\left(\frac{\alpha^4}{\epsilon^3}\right), \quad E_- = -\epsilon + \frac{\omega_-}{2} - \frac{\alpha^2}{\tilde{\epsilon}} + O\left(\frac{\alpha^4}{\epsilon^3}\right). \quad (4.35)$$

The lower energy, E_- corresponds to the state almost localized in the right well; this is also an expected result since the tunneling transition is small compared with the energy difference.

In summary, we have developed the method to obtain the correct energy shift in the asymmetric double-well potential by applying the proper valley method. In view of this development, the ordinary calculation of the imaginary part of the energy in the unstable cases (Fig. 4) needs to be examined under the new light.

4.2. Valley bubble

In this subsection, we study another example of quantum metastability problem, the false vacuum decay. It also can be treated in the imaginary-time path-integral formalism using the bounce solution.^{18), 19)}

Due to the existence of a negative-eigenvalue fluctuation-mode around the bounce solution, the contour of the Gaussian integration through the bounce has to be deformed to yield the imaginary part of the energy level. Thus the decay rate of the false vacuum is obtained.

This bounce belongs to a valley of the action in the whole functional space.²³⁾ This situation is analogous to that of the tunneling processes via instanton, such as the baryon number violation process in the standard model explained in section 2.

In either case, when the initial condition is such that the state is the local minimum, the solutions of the equations of motion (bounce or instanton) dominate the relevant imaginary-time path-integral. However, when the initial state is of higher energy, different configurations could dominate. For the quantum tunneling between degenerate vacua, the deformed instanton and anti-instanton pair is known to play that role.²⁴⁾ These configurations generally belong to the valley of action, since they form a line of relatively small actions.¹¹⁾ This is obtained by separation of a collective coordinate that corresponds to small, zero or negative eigenvalue, which is dangerous for the Gaussian integration. On the other hand, not much is known for quantum decay of metastable states: In the false vacuum, decay occurs through a vacuum bubble.¹⁸⁾ When the energy is high, we expect that modified vacuum bubbles dominate the path-integral, just like instanton anti-instanton with shorter separation dominates as energy increases. In fact, one may estimate the n -point Green function in a thin-wall bubble background as follows; Far from the bubble at the origin, the scalar field $\phi(x)$ behaves as $\sim e^{R-\rho}$ for $\rho \equiv |x| \rightarrow \infty$, where we denote the radius of the bubble by R . Thus the n -point function has the integrand, e^{nR-S} . Minimizing this expression with respect to R , we find that the radius shifts by $-O(\epsilon n/S_1^2)$, where S_1 is the surface energy, and ϵ is the energy density difference. This leads to a smaller bubble, whose mid-section is a three-dimensional bubble with energy of $O(n)$. This argument demonstrates that in fact the induced decay of the false vacuum is mediated by smaller bubbles under the presence of low energy incoming particles. However, this is quite a crude estimate. Accurate analysis should be carried out on the basis of the imaginary-time path-integral formalism. The starting point is then to clarify the structure of those modified bubbles. This series of bubbles forms a valley, on which the bounce is the saddle point. In this subsection, we carry out the analysis of this valley, employing the proper valley method. We consider a quantum field theory of a scalar field $\phi(x)$ in 3+1 dimensional space-time with an action S , which we shall specify later. The proper valley equation (3-26) can be obtained by varying the following total action, S_{tot} ,

$$S_{\text{tot}} = S_{\text{pv}} + S_{\text{F}}, \quad (4.36)$$

where

$$S_{\text{pv}} = S + S_{\lambda}, \quad S_{\lambda} = -\frac{1}{2\lambda} \int d^4x \left(\frac{\delta S}{\delta \phi(x)} \right)^2, \quad (4.37)$$

$$S_{\text{F}} = \frac{1}{2\lambda} \int d^4x \left(F(x) - \frac{\delta S}{\delta \phi(x)} \right)^2. \quad (4.38)$$

We consider the following action,

$$S = \int d^4x \left[\frac{1}{2} (\partial_{\mu} \phi)^2 + V(\phi) \right], \quad V(\phi) = \frac{1}{2} \phi^2 (1 - \phi)^2 - \epsilon (4\phi^3 - 3\phi^4). \quad (4.39)$$

Since the above potential is same as Eq.(4.12) of $g = 1$, it has the false minima at $\phi = 0$ and the true minima at $\phi = 1$, regardless of the value of the parameter $\epsilon(\geq 0)$. The energy density of the true vacuum is $-\epsilon$, even for large ϵ . In this sense, this action defines a convenient model for study of thick-wall bubbles as well as thin-wall ones.

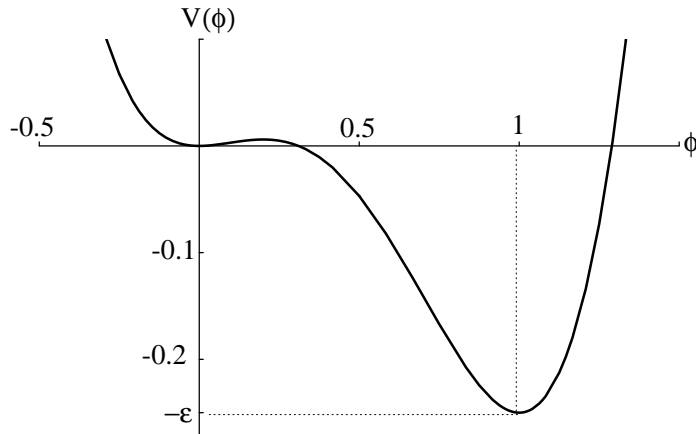


Fig. 8. Potential $V(\phi)$ for $\epsilon = 0.25$.

As the bounce solution is spherically symmetric, we shall confine ourselves to the study of spherically symmetric configurations, $\phi(x) = \phi(\rho)$ and $F(x) = F(\rho)$, where $\rho = \sqrt{x_\mu^2}$. The proper valley equations lead to the following;

$$\phi'' + \frac{3}{\rho}\phi' - \frac{dV}{d\phi} + F = 0, \quad (4.40)$$

$$F'' + \frac{3}{\rho}F' - \frac{d^2V}{d\phi^2}F + \lambda F = 0, \quad (4.41)$$

where we denote the derivatives with respect to ρ by primes. Just as in Coleman's treatise of the bounce equation, the above equations can be thought as the set of Minkowskian equations of motion of a particle in two dimensional space (ϕ, F) at "time" ρ . The linear differential terms of ϕ and F act as friction terms. (Note that there are no friction term in Eq.(4.13) and Eq.(4.14).) The other terms are space-dependent forces. The big difference is that now this force is not conservative. Therefore, no simple energy argument is possible.

The proper valley equations Eq.(4.40) and Eq.(4.41) require four boundary conditions. They are as follows: For the solution to be regular at the origin $\rho = 0$, we require boundary conditions $\phi'(0) = F'(0) = 0$. The outside of the bubble has to be the false vacuum, so $\phi(\infty) = F(\infty) = 0$ have to be satisfied.

In solving Eq.(4.40) and Eq.(4.41) numerically, we have chosen to start at the origin with the boundary conditions $\phi'(0) = F'(0) = 0$ and adjust $\phi(0)$ and $F(0)$ so that $\phi(\infty) =$

$F(\infty) = 0$ are (approximately) satisfied. We have done this calculation for $\epsilon = 0.25$. The potential for this value of ϵ is given in Fig. 8. Since the depth of the true vacuum is much more than the height of the potential barrier, we expect that the bounce solution is a bubble with a thick wall.

In Fig. 9, we show the numerical solutions and Fig. 10 is the relation between smallest eigenvalue λ of D and the starting point $\phi(0)$. We observe the following in these figures:

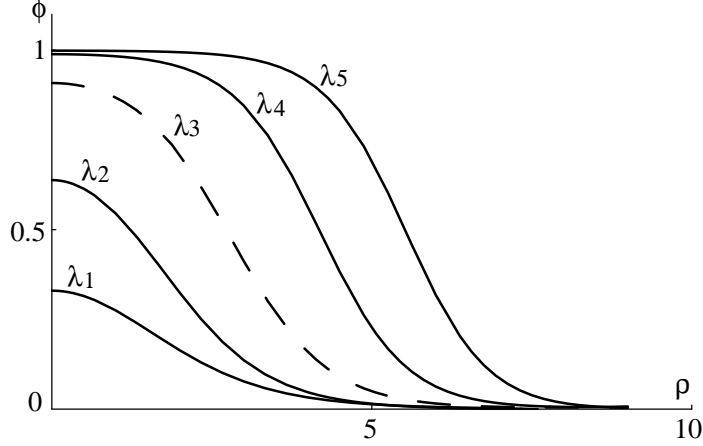


Fig. 9. Shapes of the solutions of the proper valley equation Eq.(4.40) and Eq.(4.41). The eigenvalues $\lambda_{1\sim 5}$ of each lines are $\lambda_1 = 0.3$, $\lambda_2 = -0.2$, $\lambda_3 = -0.34$, $\lambda_4 = -0.25$, $\lambda_5 = -0.2$. The broken line shows the bounce solution.

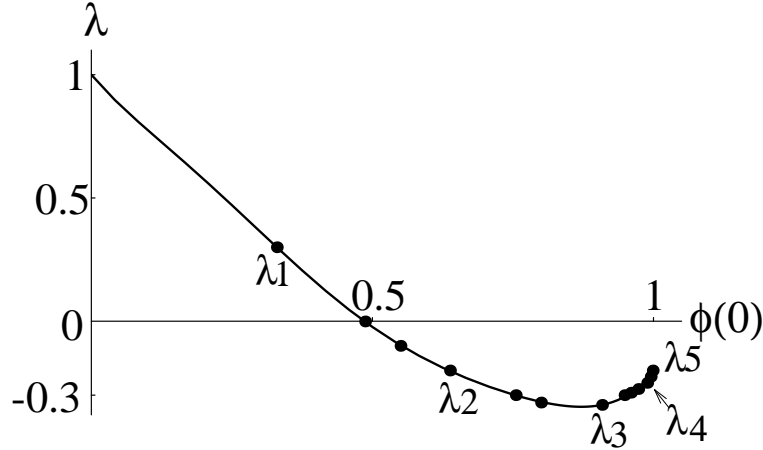


Fig. 10. The value of the smallest eigenvalue λ of D as a function of $\phi(0)$.

- (1) The proper valley contains the bounce solution (broken line in Fig. 9). This solution

has a thick wall, as expected. It has a negative eigenvalue λ_3 , which causes the instability. Another solutions that construct the valley are not the classical solutions. We call these series of the thick-wall (including the bounce) to the thin-wall bubbles "valley bubbles". (2) In Fig. 10, when $\phi(0)$ goes to zero, λ goes to one, because the minimum eigenvalue in the false vacuum is equal to the mass, which is equal to one. The eigenvalue λ_3 of the bounce solution does not occupy any particular position in Fig. 10. As $\phi(0)$ approaches to one, λ approaches to zero. This is the region where we have large thin-wall bubbles, as can be seen in the λ_5 -line of Fig. 9. (There is another zero point near $\phi(0) \sim 0.5$, but this point does not play any special role.) The interior of these bubbles is the true vacuum, $\phi = 1$. The latter property is especially notable: Even though the bounce solution is a thick-wall bubble, we find that the valley contains large, thin-wall, clean bubbles in the outskirts.

These thin-wall bubbles can be analyzed by extending the original Coleman's argument: The solution of the proper valley equation Eq.(4.40) and Eq.(4.41) extremizes the action $S_{\text{PV}} + S_{\text{F}}$. Using the valley equation Eq.(3.26), we rewrite it as follows for negative λ ;

$$S_{\text{PV}} + S_{\text{F}} = S + S_{\lambda}, \quad S_{\lambda} = \frac{1}{2|\lambda|} \int d^4x F^2. \quad (4.42)$$

Now consider a fictitious particle in a one-dimensional space ϕ at time ρ . In the equation Eq.(4.40), the auxiliary field $-F(\rho)$ acts as an "external force" for this particle. If the initial value $\phi(0)$ is sufficiently close to 1 and F is sufficiently small, ϕ remains close to 1 for a long time, until the friction term dies away. When it finally rolls down the hill, it does so under the external force $-F(\rho)$. If $-F(\rho)$ is just right, the particle approaches to the top of the lesser hill $\phi = 0$ asymptotically. Note that there is a major difference with Coleman's argument here: When the roll-down occurs, it does so under the external force, which is the sole source of the energy reduction, while in the bounce solution the timing of the roll-down has to be such that the friction term is just right to take care of the extra energy. [This does not prove the existence of the thin-wall solution, but Fig. 9 shows that this in fact happens.] Since $-F(\rho)$ is the stopping force, it deviates from zero only at the wall. Therefore the second term in Eq.(4.42) contributes positively *only* at the wall. The actions S and S_{λ} can be approximately written in terms of the radius of the bubble R as the following;

$$S = -\epsilon \frac{\pi^2}{2} R^4 + S_1 2\pi^2 R^3, \quad (4.43)$$

$$S_{\lambda} = \frac{W_F}{2|\lambda|} 2\pi^2 R^3, \quad (4.44)$$

where S_1 and W_F are the numbers of $O(1)$. Taking the derivative of $S + S_{\lambda}$ in the above

with respect to R , we find the radius of the solution of the proper valley equation to be

$$R_{\text{PV}} = \frac{3}{\epsilon} \left(S_1 + \frac{W_F}{2|\lambda|} \right). \quad (4.45)$$

Therefore, even when ϵ is not small enough to guarantee the large radius, $|\lambda|$ can be small enough to do so. This is what is causing the thin-wall bubble to be a solution of the proper valley equation.

The shape of the large bubble and its thin wall can be examined in detail by looking at the 0+1 dimensional model, since the friction term can be neglected. We have thus also analyzed the 0+1 dimensional model. (See the previous subsection.) We have obtained the numerical value $W_F \simeq 0.2104$ from this analysis. The radius seen in Fig. 9 for $\lambda_{4,5}$ is in agreement with Eq.(4.45) for this value of W_F .

Numerical values of the action S are plotted in Fig. 11, where the horizontal coordinate

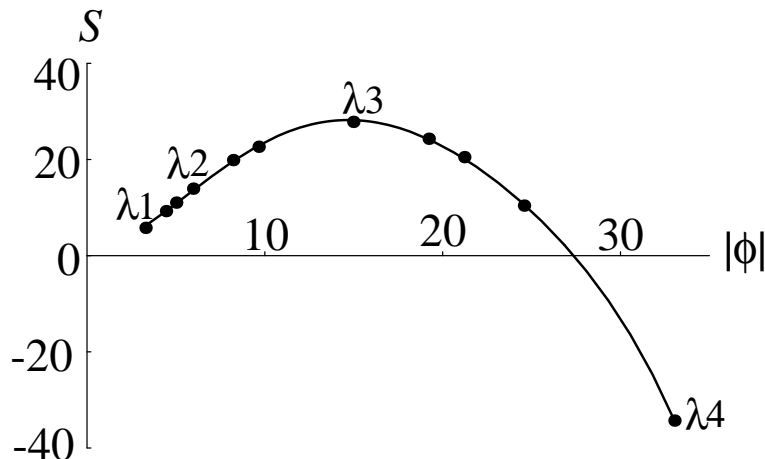


Fig. 11. The action of the solutions of the proper valley equation as a function of the norm $|\phi|$. The points with eigenvalues $\lambda_{1\sim 4}$ correspond to the lines in Fig. 9.

is the “norm” of the solution, $|\phi| \equiv \sqrt{\int d^4x \phi(x)^2}$, which for large R should be $\sim \sqrt{\pi^2/2R^2}$. We see in this figure that the bounce solution denoted by its smallest eigenvalue, λ_3 , is in fact at the maximum point of the valley. We have also compared the asymptotic expression of the action S in Eq.(4.44) with numerical value of S for large $|\phi|$ and have confirmed that the action is in fact dominated by the volume and the surface terms.

On the other side of the valley are small bubbles. In order to see their role, we have calculated the energy E of the mid-section of bubbles and plotted the result in Fig. 12. As

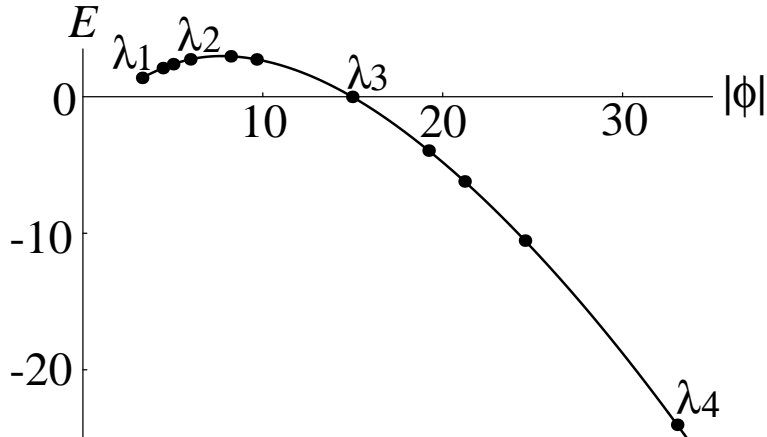


Fig. 12. The energy of the bubbles at the mid-section, where $\partial\phi/\partial\tau = 0$.

is well known, the bounce solution (λ_3) has $E = 0$, so that the energy conservation allows it to contribute to the tunneling from the false vacuum. We find that the bubbles smaller than the bounce have $E > 0$, while the larger ones have $E < 0$. This shows that the smaller bubble contribute to the tunneling from the states with higher energy than the false vacuum.

We have numerically examined the valley that contains the bounce solution. We have obtained a series of deformed bounce solutions, valley bubbles, on the valley. These configurations play the roles similar to instanton anti-instanton pairs with various distances. We have found that even when the bounce solution is a thick-wall bubble, the valley contains thin-wall large bubbles, whose interior is the true vacuum. Smaller bubbles are also identified. We expect them to contribute to the decay of the higher energy states. This is quite an interesting possibility, which should be explored further. We note that we confined ourselves to spherical configurations in this letter. However, non-spherical configurations may also be interesting, as they could also contribute to the induced decay.

4.3. Valley instanton in the scalar ϕ^4 field theory

In the following two subsections, using the proper valley method, we examine the instanton-like configurations in the unstable scalar field theory and the gauge-Higgs system.²¹⁾ In both systems, the instanton-like configuration has an important role in the quantum tunneling, but a simple scaling argument shows that no classical solution exists except a zero size one.

To construct finite size instanton-like configurations, it was often used the so-called the constrained instanton method,¹⁰⁾ which was explained briefly in section 2 and 3. In this method, one introduces a constraint to define a sub-functional space of finite radius configurations. The field equation is solved in this subspace and the finite-radius configuration similar to instantons is defined. After doing the one-loop (and possibly higher order) integral in this subspace, the constraint parameter is integrated over. The configuration constructed this way is called “constrained instanton”. One problem about this method is that its validity depends on the choice of the constraint: Since in practice one does the Gaussian integration around the solution under the constraint, the degree of approximation depends on the way constraint is introduced. Unfortunately, no known criterion guarantees the effectiveness of the approximation.

This situation could be remedied once one realizes that what we have near the point-like (true) instanton is the valley.²¹⁾ That is, although the zero-size instanton may be the dominating configurations, it is expected to be followed by a series of configurations that makes the valley of the action. Therefore, instead of trying to cover all the neighborhoods of the zero-radius instanton, one may cover the valley region, which is expected to dominate the path-integral. The trajectory along the valley bottom should correspond to the scaling parameter, or the radius parameter of the instanton. As such, the finite-size instanton can be defined as configurations along the valley trajectory. This is similar to a calculation in the electroweak theory in which one evaluates the contribution of the instanton-anti-instanton valley.^{16), 25), 26)} Thus treating a single instanton as a configuration on the valley provides a means of unifying the approximation schemes. These configurations are named “valley instanton”.

One convenient way to define the valley trajectory is to use the proper valley method. Since the constrained instanton has been used extensively in the existing literature, our main purpose here is to establish the existence of the valley instanton on a firm basis and compare its properties with that of the constrained instanton. This should serve as a starting point for the reanalysis of the existing theories and results under the new light.

First, in this subsection, we consider the scalar ϕ^4 theory in the 4 dimensional space-time with Euclidean Lagrangian,

$$\mathcal{L} = \frac{1}{g^2} \left[\frac{1}{2} (\partial_\mu \phi)^2 + \frac{1}{2} \mu^2 \phi^2 - \frac{1}{4!} \phi^4 \right]. \quad (4.46)$$

The negative sign for the ϕ^4 term is useful for estimating the asymptotic behavior of the perturbative expansion in the theory with a positive ϕ^4 term.^{10), 27), 28), 29), 30)} Namely, the instanton-like configurations in the negative ϕ^4 theory reveal the large order behavior of the positive ϕ^4 theory. This model allows finite-size instantons only for $\mu = 0$; otherwise, a

scaling argument shows that the action of any finite-size configuration can be reduced by reducing its size. As is shown in the following, when the size of the configuration is small, the valley instanton can be constructed analytically. The differences from the constrained instanton are rather small in this case. For a configuration with a large radius, we construct both instanton numerically. It will be found that remarkable differences between them appear in this case. While the action of the valley instanton increases monotonously and remains positive, the one of the constrained instanton becomes negative when the radius becomes large.

4.3.1. Valley instanton

For this model, the proper valley equation introduced in the previous section is

$$\begin{aligned} -\partial_\mu\partial_\mu\phi + \mu^2\phi - \frac{1}{3!}\phi^3 &= F, \\ \left(-\partial_\mu\partial_\mu + \mu^2 - \frac{1}{2}\phi^2\right)F &= \lambda F. \end{aligned} \tag{4.47}$$

Now we introduce the scale parameter ρ defined by $\phi(0) \equiv 4\sqrt{3}/\rho$, in order to fix the radius of the instanton solution to be unity. We rescale fields and variables as in the following;

$$r = \frac{\sqrt{x^2}}{\rho}, \quad \lambda = \mu^2\nu, \quad \phi(x) = \frac{h(r)}{\rho}, \quad F(x) = \frac{\mu^2}{\rho}f(r). \tag{4.48}$$

The proper valley equation (4.47) is given by the following under this rescaling;

$$-\frac{1}{r^3}\frac{d}{dr}\left(r^3\frac{dh}{dr}\right) + (\rho\mu)^2h - \frac{1}{3!}h^3 = (\rho\mu)^2f, \tag{4.49}$$

$$-\frac{1}{r^3}\frac{d}{dr}\left(r^3\frac{df}{dr}\right) + (\rho\mu)^2f - \frac{1}{2}h^2f = (\rho\mu)^2\nu f. \tag{4.50}$$

This system has an instanton solution in the massless limit, $\rho\mu \rightarrow 0$.^{27), 28)} In this limit, (4.49) reduces to the equation of motion and (4.50) the equation for the zero-mode fluctuation, f , around the instanton solution. The solution is the following;

$$h_0 = \frac{4\sqrt{3}}{1+r^2}, \quad f_0 = C\left(\frac{4\sqrt{3}}{1+r^2} - \frac{8\sqrt{3}}{(1+r^2)^2}\right), \tag{4.51}$$

where C is an arbitrary constant. Note that solution f_0 is obtained from $\partial\phi_0(x)/\partial\rho$, $\phi_0 = h_0/\rho$.

Let us construct the valley instanton in the scalar ϕ^4 theory analytically. When $\rho\mu$ is very small but finite, the valley instanton is expected to have $\rho\mu$ corrections to (4.51). On the other hand, at large distance from the core region of the valley instanton, since the term

of $O(h^2)$ is negligible, the valley equation can be linearized. This linearized equation can be solved easily. By matching the solution near the core and the solution in the asymptotic region in the overlapping intermediate region, we can construct approximate solution analytically. We will carry out this procedure in the following.

In the asymptotic region, $(\rho\mu)^2 \gg h^2$, the linearized valley equation is the following;

$$\begin{aligned} -\frac{1}{r^3} \frac{d}{dr} \left(r^3 \frac{dh}{dr} \right) + (\rho\mu)^2 h &= (\rho\mu)^2 f, \\ -\frac{1}{r^3} \frac{d}{dr} \left(r^3 \frac{df}{dr} \right) + (\rho\mu)^2 f &= (\rho\mu)^2 \nu f. \end{aligned} \quad (4.52)$$

The solution of these equations is

$$h(r) = C_1 G_{\rho\mu}(r) + \frac{f}{\nu}, \quad f(r) = C_2 G_{\rho\mu\sqrt{1-\nu}}(r), \quad (4.53)$$

where C_1 and C_2 are arbitrary functions of $\rho\mu$. The function $G_m(r)$ is

$$G_m(r) = \frac{mK_1(mr)}{(2\pi)^2 r}, \quad (4.54)$$

where K_1 is a modified Bessel function. The functions f and h decay exponentially at large r . In the region of $r \ll (\rho\mu)^{-1}$, $r \ll (\rho\mu\sqrt{1-\nu})^{-1}$, f and h can be expanded in series as the following;

$$\begin{aligned} h &= \frac{C_1}{(2\pi)^2} \left[\frac{1}{r^2} + \frac{1}{2}(\rho\mu)^2 \ln(\rho\mu r c) + \dots \right] \\ &+ \frac{C_2}{(2\pi)^2 \nu} \left[\frac{1}{r^2} + \frac{1}{2}(\rho\mu)^2 (1-\nu) \ln(\rho\mu\sqrt{1-\nu} r c) + \dots \right], \\ f &= \frac{C_2}{(2\pi)^2} \left[\frac{1}{r^2} + \frac{1}{2}(\rho\mu)^2 (1-\nu) \ln(\rho\mu\sqrt{1-\nu} r c) + \dots \right]. \end{aligned} \quad (4.55)$$

In the above, $c = e^{\gamma-1/2}/2$, where γ is the Euler's constant.

Near the origin, we expect that the valley instanton is similar to the ordinary instanton. It is convenient to define \hat{h} and \hat{f} as the following;

$$h = h_0 + (\rho\mu)^2 \hat{h}, \quad f = f_0 + (\rho\mu)^2 \hat{f}, \quad (4.56)$$

where C in f_0 is the function of $\rho\mu$ and is decided in the following. The ‘‘core region’’ is defined as

$$h_0 \gg (\rho\mu)^2 \hat{h}, \quad f_0 \gg (\rho\mu)^2 \hat{f}. \quad (4.57)$$

The valley equation for perturbation field \hat{h} , \hat{f} becomes

$$\begin{aligned} -\frac{1}{r^3} \frac{d}{dr} \left(r^3 \frac{d\hat{h}}{dr} \right) - \frac{1}{2} h_0^2 \hat{h} &= f_0 - h_0, \\ -\frac{1}{r^3} \frac{d}{dr} \left(r^3 \frac{d\hat{f}}{dr} \right) - \frac{1}{2} h_0^2 \hat{f} &= (\nu - 1) f_0 + h_0 f_0 \hat{h}. \end{aligned} \quad (4.58)$$

The left-hand side of (4.58) has a zero mode, φ . It satisfies the equation,

$$-\frac{1}{r^3} \frac{d}{dr} \left(r^3 \frac{d\varphi}{dr} \right) - \frac{1}{2} h_0^2 \varphi = 0, \quad (4.59)$$

and is given by the following;

$$\varphi = \frac{4\sqrt{3}}{1+r^2} - \frac{8\sqrt{3}}{(1+r^2)^2}. \quad (4.60)$$

We multiply $r^3\varphi$ to both sides of (4.58), and integrate them from 0 to r . The existence of zero mode φ makes it possible to integrate the left-hand side of (4.58). As a result of the integration by parts, only the surface terms remain and we obtain,

$$-r^3\varphi \frac{d\hat{h}}{dr} + r^3 \frac{d\varphi}{dr} \hat{h} = \int_0^r dr' r'^3 \varphi [f_0 - h_0], \quad (4.61)$$

$$-r^3\varphi \frac{d\hat{f}}{dr} + r^3 \frac{d\varphi}{dr} \hat{f} = \int_0^r dr' r'^3 \varphi [(\nu - 1) f_0 + h_0 f_0 \hat{h}]. \quad (4.62)$$

First, using (4.51) and (4.60), we can find that the right-hand side of (4.61) is proportional to $\ln r$ at $r \gg 1$. Thus (4.61) becomes

$$r \frac{d\hat{h}}{dr} + 2\hat{h} = 4\sqrt{3}(1-C) \ln r. \quad (4.63)$$

This equation can be solved easily at $r \gg 1$. Using the solution of (4.63), we can find the right-hand side of (4.61) also proportional to $\ln r$ as the following;

$$r \frac{d\hat{f}}{dr} + 2\hat{f} = 4\sqrt{3}C(1-\nu) \ln r. \quad (4.64)$$

Finally, we obtain \hat{h} and \hat{f} at $r \gg 1$,

$$\hat{h} = 2\sqrt{3}(1-C) \ln r + \dots, \quad \hat{f} = (1-\nu)2\sqrt{3}C \ln r + \dots. \quad (4.65)$$

For these solutions to meet to (4.55), the parameters need to be the following;

$$C_1 = 0, \quad C_2 = 4\sqrt{3}(2\pi)^2, \quad \nu = 1, \quad C = 1, \quad (4.66)$$

as $\rho\mu = 0$. Now we have obtained the solution of the proper valley equation;

$$h(r) = \begin{cases} \frac{4\sqrt{3}}{1+r^2}, & \text{if } r \ll (\rho\mu)^{-1/2}; \\ \frac{4\sqrt{3}}{r^2} + o((\rho\mu)^2), & \text{if } (\rho\mu)^{-1/2} \ll r \ll (\rho\mu)^{-1}; \\ 4\sqrt{3} (2\pi^2) G_{\rho\mu\sqrt{1-\nu}}(r), & \text{if } (\rho\mu)^{-1/2} \ll r. \end{cases} \quad (4.67)$$

Let us discuss the consistency of our analysis. In the construction of the analytical solution, especially in the argument of the matching of the core and asymptotic region solution, we have implicitly assumed that there exists an overlapping region where both (4.52) and (4.58) are valid. Using the solution (4.67), it is found that (4.52) is valid in the region of $r \gg (\rho\mu)^{-1/2}$, and (4.58) is valid in the region of $r \ll (\rho\mu)^{-1}$. Therefore in the above analysis we have limited our calculation in the overlapping region $(\rho\mu)^{-1/2} \ll r \ll (\rho\mu)^{-1}$.

We calculate the action of the valley instanton using the above solution. Rewriting the action in terms of $h(r)$, we find

$$S = \frac{\pi^2}{g^2} \int_0^\infty dr r^3 \left[\left(\frac{dh}{dr} \right)^2 + (\rho\mu)^2 h^2 - \frac{1}{12} h^4 \right]. \quad (4.68)$$

Substituting the analytic solution for S , we obtain

$$S = \frac{16\pi^2}{g^2} + O((\rho\mu)^2). \quad (4.69)$$

The leading contribution term comes from the ordinary instanton solution, and the correction term comes from the distortion of the instanton solution.

4.3.2. *Constrained instanton*

Here, we consider the constrained instanton in the scalar ϕ^4 theory, following the construction in Ref. 10). We require the constraint in the path-integral. The field equation under the constraint is

$$\frac{\delta S}{\delta \phi} + \sigma \frac{\delta O}{\delta \phi} = 0, \quad (4.70)$$

where σ is a Lagrange multiplier. The functional O had to satisfy the certain scaling properties that guarantee the existence of the solution.¹⁰⁾ We choose it as follows;

$$O = \int d^4x \frac{\phi^6}{6}. \quad (4.71)$$

This choice is one of the simplest for constructing the constrained instanton in the scalar ϕ^4 theory. Again, adopting the rescaling (4.48), the equation of motion under this constraint becomes

$$-\frac{1}{r^3} \frac{d}{dr} \left(r^3 \frac{dh}{dr} \right) + (\rho\mu)^2 h - \frac{1}{3!} h^3 + (\rho\mu)^2 \tilde{\sigma} h^5 = 0, \quad (4.72)$$

where we rescale the parameter σ as $\sigma = (\rho\mu)^2 \tilde{\sigma}$. The solution of this equation can be constructed in a manner similar to the previous subsection. To carry out the perturbation calculation in the core region, we replace the field variable as $h = h_0 + (\rho\mu)^2 \hat{h}$, where $h_0 \gg (\rho\mu)^2 \hat{h}$. The field equation of \hat{h} becomes

$$-\frac{1}{r^3} \frac{d}{dr} \left(r^3 \frac{d\hat{h}}{dr} \right) - \frac{1}{2} h_0^2 \hat{h} = -h_0 - \tilde{\sigma} h_0^5. \quad (4.73)$$

We multiply this equation by the zero mode (4.60) and integrate this from 0 to r . Then we obtain

$$-r^3 \varphi \frac{d\hat{h}}{dr} + r^3 \frac{d\varphi}{dr} \hat{h} = -\int_0^r dr' r'^3 \varphi [h_0 + \tilde{\sigma} h_0^5]. \quad (4.74)$$

The solution of this equation in the region where $r \gg 1$ is

$$\hat{h} = 2\sqrt{3} \ln r - \frac{192\sqrt{3}}{7} \tilde{\sigma} + \dots \quad (4.75)$$

In the asymptotic region, we consider the field variable and the parameter as $h^2 \ll (\rho\mu)^2$, $\tilde{\sigma} h^4 \ll 1$. Under this condition, the field equation of the asymptotic region becomes

$$-\frac{1}{r^3} \frac{d}{dr} \left(r^3 \frac{dh}{dr} \right) + (\rho\mu)^2 h = 0. \quad (4.76)$$

The solution is

$$h(r) = C_1 G_{\rho\mu}(r), \quad (4.77)$$

where C_1 is arbitrary constant. In the region of $r \ll (\rho\mu)^{-1}$, this solution can be expanded as the following;

$$h = \frac{C_1}{(2\pi)^2} \left[\frac{1}{r^2} + \frac{1}{2} (\rho\mu)^2 \ln(\rho\mu r) + \dots \right]. \quad (4.78)$$

Matching this solution and the core region solution (4.75), parameters are determined as the following;

$$C_1 = 4\sqrt{3}(2\pi)^2, \quad \tilde{\sigma} = -\frac{7}{96} \ln(\rho\mu). \quad (4.79)$$

To summarize, the analytical solution of the constrained instanton we have obtained is the following,

$$h(r) = \begin{cases} \frac{4\sqrt{3}}{1+r^2}, & \text{if } r \ll (\rho\mu)^{-1/2}; \\ \frac{4\sqrt{3}}{r^2} + 2\sqrt{3}(\rho\mu)^2 \ln(\rho\mu rc) + o((\rho\mu)^2), & \text{if } (\rho\mu)^{-1/2} \ll r \ll (\rho\mu)^{-1}; \\ 4\sqrt{3}(2\pi^2) G_{\rho\mu}(r), & \text{if } (\rho\mu)^{-1/2} \ll r. \end{cases} \quad (4.80)$$

The action of the constrained instanton is given by the following;

$$S = \frac{16\pi^2}{g^2} - 96\pi^2(\rho\mu)^2 \ln(\rho\mu) + O((\rho\mu)^2). \quad (4.81)$$

This differs from the action of the valley instanton at the next-to-leading order. This correction term shows that the constrained instanton is more distorted from the ordinary instanton than the valley instanton.

4.3.3. Numerical analysis

In this subsection, we calculate the valley equation (4.49), (4.50) and the constrained equation (4.72) numerically. Then we compare the valley and the constrained instanton.

Each of the equations is the second order differential equation, so we require two boundary conditions for each field variable to decide the solution. We require all the field variables are regular at the origin. The finiteness of the action requires $h, f \rightarrow 0$ faster than $1/r^2$ at infinity. In solving (4.49) and (4.50), we adjust the parameter ν and $f(0)$ so that $h, f \rightarrow 0$ at infinity for the fixed $\rho\mu$. In the similar way, in case of the constrained instanton, the parameter σ is determined so that $h \rightarrow 0$ at infinity.

Numerical solutions of the valley equation near the origin are plotted in Fig. 13 (a) for $\rho\mu = 0.1, 1.0$. The solid line shows the instanton solutions (4.51), which corresponds to $\rho\mu = 0$. The numerical solutions of the constrained instanton are also plotted in Fig. 13 (b) for $\rho\mu = 0.1, 0.5, 1.0$. Both the valley and the constrained solution for $\rho\mu = 0.1$ agree with the analytical result. As $\rho\mu$ becomes large, both solutions are deformed from the original instanton solution. We find that the distortion of the constrained instanton is much larger than that of the valley instanton. This also agrees with the analytic result. In the analytical solution (4.80), the correction term $2\sqrt{3}(\rho\mu)^2 \ln(\rho\mu rc)$ contributes to this distortion. On the other hand, the correction term of the valley instanton (4.80) is $o((\rho\mu)^2)$, which is smaller than the previous one. In addition, we find that the exponentially damping behavior of the analytical solution in the asymptotic region, where $r \gg (\rho\mu)^{-1}$ agrees with the result of numerical analysis.

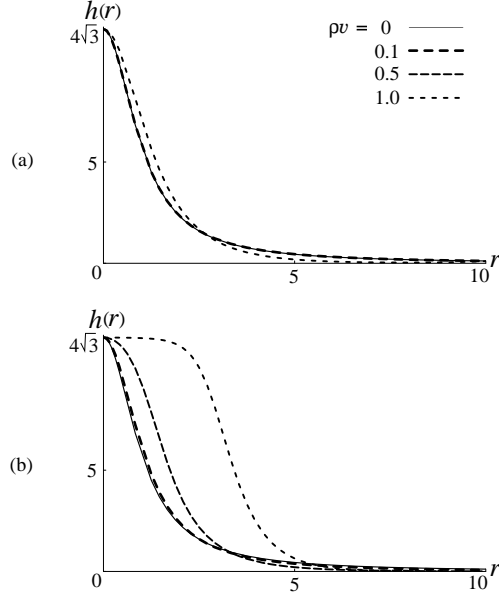


Fig. 13. (a) Shapes of the numerical solution of the valley instanton, $h(r)$, for $\rho\mu = 0, 0.1$, and 1.0 near the origin. The solid line denotes the original instanton, h_0 . (b) Shapes of the constrained instanton for $\rho\mu = 0, 0.1, 0.5$, and 1.0 .

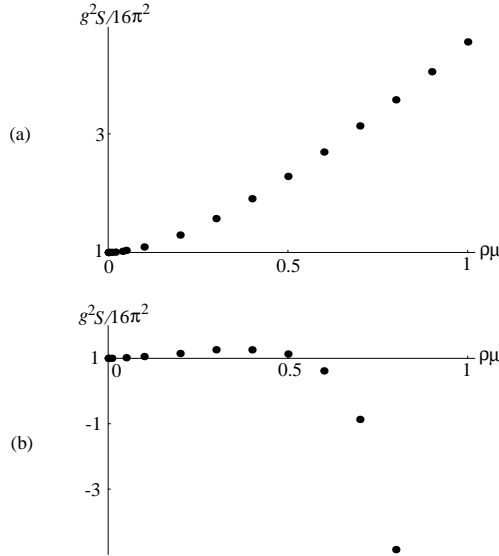


Fig. 14. (a) The action S (in units of $g^2/16\pi^2$) of the numerical solution of the valley equation as a function of the parameter $\rho\mu$. (b) The action S of the constrained instanton.

The values of the action of the valley instanton for $\rho\mu = 0.0001 \sim 1.0$ are plotted in Fig. 14 (a). If $\rho\mu$ is very small, this result is consistent with (4.69). The values of the action of the constrained instanton for $\rho\mu = 0.0001 \sim 0.8$ are plotted in Fig. 14 (b). This figure shows that the behavior of the action is similar to that of the valley instanton when $\rho\mu$ is very small. When $\rho\mu$ becomes large, the behavior of the action is different from the valley

instanton case.

4.4. Valley instanton in the gauge-Higgs system

In this subsection, we consider the SU(2) gauge theory with one scalar Higgs doublet, which has the following action $S = S_g + S_h$;

$$S_g = \frac{1}{2g^2} \int d^4x \operatorname{tr} F_{\mu\nu} F_{\mu\nu}, \quad (4.82)$$

$$S_h = \frac{1}{\lambda} \int d^4x \left\{ (D_\mu H)^\dagger (D_\mu H) + \frac{1}{8} (H^\dagger H - v^2)^2 \right\}, \quad (4.83)$$

where $F_{\mu\nu} = \partial_\mu A_\nu - \partial_\nu A_\mu - i[A_\mu, A_\nu]$ and $D_\mu = \partial_\mu - iA_\mu$. The masses of the gauge boson and the Higgs boson are given by,

$$m_w = \sqrt{\frac{g^2}{2\lambda}} v, \quad m_H = \frac{1}{\sqrt{2}} v. \quad (4.84)$$

When v is not zero, this theory is known not to have any finite-size instanton solutions, in spite of its importance. In the following, we will construct instanton-like configurations for this theory, relevant for tunneling phenomena, including the baryon and lepton number violation processes. As well as the unstable scalar theory, the valley instanton can be constructed analytically when the size of the configuration is small. For a configuration with a large radius, numerical constructions are done. There are differences between the valley instanton and the constrained instanton in this case. Therefore, when the large size configuration dominates the path integral, we must use the valley instanton instead of the constrained instanton.

4.4.1. Valley instanton

The valley equation for this system is given by,

$$\begin{aligned} \frac{\delta^2 S}{\delta A_\mu \delta A_\nu} F_\nu^A + \frac{\delta^2 S}{\delta A_\mu \delta H^\dagger} F^H + \frac{\delta^2 S}{\delta A_\mu \delta H} F^{H\dagger} &= \lambda_e F_\mu^A, \\ \frac{\delta^2 S}{\delta H^\dagger \delta A_\mu} F_\mu^A + \frac{\delta^2 S}{\delta H^\dagger \delta H} F^{H\dagger} + \frac{\delta^2 S}{\delta H \delta H^\dagger} F^H &= \lambda_e F^{H\dagger}, \\ F_\mu^A &= \frac{\delta S}{\delta A_\mu}, \quad F^H = \frac{\delta S}{\delta H}, \end{aligned} \quad (4.85)$$

where the integration over the space-time is implicitly assumed. The valley is parameterized by the eigenvalue λ_e that is identified with the zero mode corresponding to the scale invariance in the massless limit, $v \rightarrow 0$.

To simplify the equation, we adopt the following ansatz;

$$A_\mu(x) = \frac{x_\nu \bar{\sigma}_{\mu\nu}}{x^2} \cdot 2a(r), \quad H(x) = v(1 - h(r))\eta, \quad (4.86)$$

where η is a constant isospinor, and a and h are real dimensionless functions of dimensionless variable r , which is defined by $r = \sqrt{x^2}/\rho$. The matrix $\bar{\sigma}_{\mu\nu}$ is defined, according to the conventions of Ref. 6), as $\bar{\sigma}_{\mu\nu} = \bar{\eta}_{a\mu\nu}\sigma^a/2$. We have introduced the scaling parameter ρ so that we adjust the radius of valley instanton as we will see later in subsection 4.4.3. The tensor structure in (4.86) is the same as that of the instanton in the singular gauge.²⁾

Inserting this ansatz to (4.85), the structure of F_μ^A and $F^{H\dagger}$ is determined as the following;

$$F_\mu^A(x) = \frac{x_\nu \bar{\sigma}_{\mu\nu}}{x^2} \cdot \frac{2v^2}{\lambda} f^a(r), \quad F^{H\dagger}(x) = -\frac{v^3}{\lambda} f^h(r)\eta. \quad (4.87)$$

By using this ansatz, (4.86) and (4.87), the valley equation (4.85) is reduced to the following;

$$-\frac{1}{r} \frac{d}{dr} \left(r \frac{da}{dr} \right) + \frac{4}{r^2} a(a-1)(2a-1) + \frac{g^2}{2\lambda} (\rho v)^2 a(1-h)^2 = \frac{g^2}{\lambda} (\rho v)^2 f^a, \quad (4.88)$$

$$-\frac{1}{r^3} \frac{d}{dr} \left(r^3 \frac{dh}{dr} \right) + \frac{3}{r^2} (h-1)a^2 + \frac{1}{4} (\rho v)^2 h(h-1)(h-2) = (\rho v)^2 f^h, \quad (4.89)$$

$$-\frac{1}{r} \frac{d}{dr} \left(r \frac{df^a}{dr} \right) + \frac{4}{r^2} (6a^2 - 6a + 1)f^a + \frac{g^2}{2\lambda} (\rho v)^2 (h-1)^2 f^a + \frac{g^2}{\lambda} (\rho v)^2 a(h-1)f^h = \frac{g^2}{\lambda} (\rho v)^2 \nu f^a, \quad (4.90)$$

$$-\frac{1}{r^3} \frac{d}{dr} \left(r^3 \frac{df^h}{dr} \right) + \frac{3a^2}{r^2} f^h + \frac{1}{4} (\rho v)^2 (3h^2 - 6h + 2)f^h + \frac{6a}{r^2} (h-1)f^a = (\rho v)^2 \nu f^h, \quad (4.91)$$

where ν is defined as $\lambda_e = v^2\nu/\lambda$.

In the massless limit, $\rho v \rightarrow 0$, (4.88) and (4.89) reduce to the equation of motion and (4.90) and (4.91) to the equation for the zero-mode fluctuation around the instanton solution. The solution of this set of equations is the following;

$$a_0 = \frac{1}{1+r^2}, \quad h_0 = 1 - \left(\frac{r^2}{1+r^2} \right)^{1/2}, \quad (4.92)$$

$$f_0^a = \frac{2Cr^2}{(1+r^2)^2}, \quad f_0^h = \frac{Cr}{(1+r^2)^{3/2}},$$

where C is an arbitrary function of ρv . Note that a_0 is an instanton solution in the singular gauge and h_0 is a Higgs configuration in the instanton background.²⁾ We have adjusted the scaling parameter ρ so that the radius of the instanton solution is unity. The mode solutions f_0^a and f_0^h are obtained from $\partial a_0/\partial\rho$ and $\partial h_0/\partial\rho$, respectively.

Now we will construct the valley instanton analytically. When $\rho v = 0$, it is given by the ordinary instanton configuration a_0 , h_0 , f_0^a and f_0^h . When ρv is small but not zero, it is expected that small ρv corrections appear in the solution. On the other hand, at large distance from the core of the valley instanton, this solution is expected to decay exponentially, because gauge boson and Higgs boson are massive. Therefore, the solution is similar to the instanton near the origin and decays exponentially in the asymptotic region. In the following, we will solve the valley equation in both regions and analyze the connection in the intermediate region. In this manner we will find the solution.

In the asymptotic region, a , h , f^a and f^h become small and the valley equation can be linearized;

$$-\frac{1}{r} \frac{d}{dr} \left(r \frac{da}{dr} \right) + \frac{4}{r^2} a + \frac{g^2}{2\lambda} (\rho v)^2 a = \frac{g^2}{\lambda} (\rho v)^2 f^a, \quad (4.93)$$

$$-\frac{1}{r^3} \frac{d}{dr} \left(r^3 \frac{dh}{dr} \right) + \frac{1}{2} (\rho v)^2 h = (\rho v)^2 f^h, \quad (4.94)$$

$$-\frac{1}{r} \frac{d}{dr} \left(r \frac{df^a}{dr} \right) + \frac{4}{r^2} f^a + \frac{g^2}{2\lambda} (\rho v)^2 f^a = \frac{g^2}{\lambda} (\rho v)^2 \nu f^h, \quad (4.95)$$

$$-\frac{1}{r^3} \frac{d}{dr} \left(r^3 \frac{df^h}{dr} \right) + \frac{1}{2} (\rho v)^2 f^h = (\rho v)^2 \nu f^h. \quad (4.96)$$

The solution of this set of equations is

$$a(r) = C_1 r \frac{d}{dr} G_{\rho m_W}(r) + \frac{1}{\nu} f^a(r), \quad (4.97)$$

$$h(r) = C_2 G_{\rho m_H}(r) + \frac{1}{\nu} f^h(r), \quad (4.98)$$

$$f^a(r) = C_3 r \frac{d}{dr} G_{\rho \mu_W}(r), \quad (4.99)$$

$$f^h(r) = C_4 G_{\rho \mu_H}(r), \quad (4.100)$$

where C_i are arbitrary functions of ρv and $\mu_{W,H}$ are defined as $\mu_{W,H} = m_{W,H} \sqrt{1 - 2\nu}$. As was expected above, these solutions decay exponentially at infinity and when $r \ll (\rho v)^{-1}$ they have the series expansions;

$$a(r) = \frac{C_1}{(2\pi)^2} \left[-\frac{2}{r^2} + \frac{1}{2} (\rho m_W)^2 + \dots \right] + \frac{C_3}{\nu (2\pi)^2} \left[-\frac{2}{r^2} + \frac{1}{2} (\rho \mu_W)^2 + \dots \right], \quad (4.101)$$

$$h(r) = \frac{C_2}{(2\pi)^2} \left[\frac{1}{r^2} + \frac{1}{2} (\rho m_H)^2 \ln(\rho m_H r c) + \dots \right] + \frac{C_4}{\nu (2\pi)^2} \left[\frac{1}{r^2} + \frac{1}{2} (\rho \mu_H)^2 \ln(\rho \mu_H r c) + \dots \right], \quad (4.102)$$

$$f^a(r) = \frac{C_3}{(2\pi)^2} \left[-\frac{2}{r^2} + \frac{1}{2} (\rho \mu_W)^2 + \dots \right], \quad (4.103)$$

$$f^h(r) = \frac{C_4}{(2\pi)^2} \left[\frac{1}{r^2} + \frac{1}{2}(\rho\mu_H)^2 \ln(\rho\mu_H r c) + \dots \right], \quad (4.104)$$

c being a numerical constant $e^{\gamma-1/2}/2$, where γ is the Euler's constant.

Near the origin, we expect that the valley instanton is similar to the ordinary instanton. Then the following replacement of the field variables is convenient; $a = a_0 + (\rho v)^2 \hat{a}$, $h = h_0 + (\rho v)^2 \hat{h}$, $f^a = f_0^a + (\rho v)^2 \hat{f}^a$, $f^h = f_0^h + (\rho v)^2 \hat{f}^h$. If we assume $a_0 \gg (\rho v)^2 \hat{a}$, $h_0 \gg (\rho v)^2 \hat{h}$, $f_0^a \gg (\rho v)^2 \hat{f}^a$ and $f_0^h \gg (\rho v)^2 \hat{f}^h$, the valley equation becomes

$$-\frac{1}{r} \frac{d}{dr} \left(r \frac{d\hat{a}}{dr} \right) + \frac{4}{r^2} (6a_0^2 - 6a_0 + 1) \hat{a} + \frac{g^2}{2\lambda} a_0 (h_0 - 1)^2 = \frac{g^2}{\lambda} f_0^a, \quad (4.105)$$

$$-\frac{1}{r^3} \frac{d}{dr} \left(r^3 \frac{d\hat{h}}{dr} \right) + \frac{3}{r^2} a_0^2 \hat{h} + \frac{6}{r^2} (h_0 - 1) a_0 \hat{a} + \frac{1}{4} h_0 (h_0 - 1) (h_0 - 2) = f_0^h, \quad (4.106)$$

$$-\frac{1}{r} \frac{d}{dr} \left(r \frac{d\hat{f}^a}{dr} \right) + \frac{4}{r^2} (6a_0^2 - 6a_0 + 1) \hat{f}^a + \frac{24}{r^2} (2a_0 - 1) f_0^a \hat{a} + \frac{g^2}{2\lambda} (h_0 - 1)^2 f_0^a + \frac{g^2}{\lambda} a_0 (h_0 - 1) f_0^h = \frac{g^2}{\lambda} \nu f_0^a, \quad (4.107)$$

$$-\frac{1}{r^3} \frac{d}{dr} \left(r^3 \frac{d\hat{f}^h}{dr} \right) + \frac{3}{r^2} a_0^2 \hat{f}^h + \frac{6}{r^2} a_0 f_0^h \hat{a} + \frac{1}{4} (3h_0^2 - 6h_0 + 2) f_0^h + \frac{6}{r^2} a_0 (h_0 - 1) \hat{f}^a + \frac{6}{r^2} (h_0 - 1) f_0^a \hat{a} + \frac{6}{r^2} a_0 f_0^h \hat{h} = \nu f_0^h. \quad (4.108)$$

To solve this equation, we introduce solutions of the following equations;

$$-\frac{1}{r} \frac{d}{dr} \left(r \frac{d\varphi_a}{dr} \right) + \frac{4}{r^2} (6a_0^2 - 6a_0 + 1) \varphi_a = 0, \quad (4.109)$$

$$-\frac{1}{r^3} \frac{d}{dr} \left(r^3 \frac{d\varphi_h}{dr} \right) + \frac{3}{r^2} a_0^2 \varphi_h = 0.$$

They are given as,

$$\varphi_a = \frac{r^2}{(1+r^2)^2}, \quad \varphi_h = \left(\frac{r^2}{1+r^2} \right)^{1/2}. \quad (4.110)$$

Using these solutions, we will integrate the valley equation. We multiply (4.105) and (4.107) by $r\varphi_a$, and multiply (4.106) and (4.108) by $r^3\varphi_h$ then integrate them from 0 to r . Integrating by parts and using (4.109), we obtain

$$-\varphi_a r \frac{d\hat{a}}{dr} + \frac{d\varphi_a}{dr} r \hat{a} = \frac{g^2}{\lambda} \int_0^r dr' r' \varphi_a \left[f_0^a - \frac{1}{2} a_0 (h_0 - 1)^2 \right], \quad (4.111)$$

$$-\varphi_h r^3 \frac{d\hat{h}}{dr} + \hat{h} r^3 \frac{d\varphi_h}{dr} = \int_0^r dr' r'^3 \varphi_h \left[f_0^h - \frac{1}{4} h_0 (h_0 - 1) (h_0 - 2) - \frac{6}{r'^2} (h_0 - 1) a_0 \hat{a} \right], \quad (4.112)$$

$$\begin{aligned}
& -\varphi_a r \frac{d\hat{f}^a}{dr} + \frac{d\varphi_a}{dr} r \hat{f}^a \\
& = \int_0^r dr' r' \varphi_a \left[\frac{g^2}{\lambda} \nu f_0^a - \frac{24}{r'^2} (2a_0 - 1) f_0^a \hat{a} - \frac{g^2}{2\lambda} (h_0 - 1)^2 f_0^a - \frac{g^2}{\lambda} a_0 (h_0 - 1) f_0^h \right],
\end{aligned} \tag{4.113}$$

$$\begin{aligned}
& -\varphi_h r^3 \frac{d\hat{f}^h}{dr} + \hat{h} r^3 \frac{d\varphi_h}{dr} \\
& = \int_0^r dr' r'^3 \varphi_h \left[\nu f_0^h - \frac{6}{r'^2} a_0 f_0^a \hat{a} - \frac{1}{4} (3h_0^2 - 6h_0 + 2) f_0^h \right. \\
& \quad \left. - \frac{6}{r'^2} a_0 (h_0 - 1) \hat{f}^a - \frac{6}{r'^2} (h_0 - 1) f_0^a \hat{a} - \frac{6}{r'^2} a_0 f_0^a \hat{h} \right]
\end{aligned} \tag{4.114}$$

First we will find \hat{a} . The right-hand side of (4.111) is proportional to $(C - 1/4)$ and when r goes to infinity this approaches a constant. At $r \gg 1$, (4.111) becomes

$$-\frac{1}{r} \frac{d\hat{a}}{dr} - \frac{2}{r^2} \hat{a} = \frac{1}{3} \frac{g^2}{\lambda} \left(C - \frac{1}{4} \right). \tag{4.115}$$

Then at $r \gg 1$, $\hat{a}(r)$ is proportional to $(C - 1/4)r^2$ and $a(r)$ becomes

$$a = \frac{1}{r^2} - \frac{(\rho\nu)^2 g^2}{12\lambda} \left(C - \frac{1}{4} \right) r^2 + \dots \tag{4.116}$$

To match this with (4.101), it must be hold that $C = 1/4$ when $\rho\nu = 0$. When $C = 1/4$, the right-hand sides of (4.111) vanishes and \hat{a} satisfy $-\varphi_a d\hat{a}/dr + \hat{a} d\varphi_a/dr = 0$. Hence $\hat{a} = D \varphi_a$, where D is a constant. Identifying $a_0 + (\rho\nu)^2 \hat{a}$ with (4.101) again at $r \gg 1$, we find that $C_1 + C_3/\nu = -2\pi^2$ and $C_3 = -\pi^2$ at $\rho\nu = 0$. In the same manner, \hat{h} , \hat{f}^a and \hat{f}^h are obtained. At $r \gg 1$, we find

$$\begin{aligned}
& \hat{h} = \text{const.} + \dots, \\
& \hat{f}^a = \frac{g^2}{48\lambda} \left(\frac{1}{4} - \nu \right) r^2 - \frac{g^2}{16\lambda} (1 - 2\nu) + \dots, \\
& \hat{f}^h = \frac{1}{16} (1 - 2\nu) \ln r + \dots.
\end{aligned} \tag{4.117}$$

Here const. is a constant of integration. Comparing (4.102)-(4.104) with them, we find that $C_2 + C_4/\nu = 2\pi^2$, $C_4 = \pi^2$ and $\nu = 1/4$ at $\rho\nu = 0$.

Now we have obtained the solution of the proper valley equation. Near the origin of the valley instanton, $r \ll (\rho m_{w,H})^{-1/2}$, it is given by,

$$\begin{aligned}
a(r) &= \frac{1}{1+r^2}, & h(r) &= 1 - \left(\frac{r^2}{1+r^2} \right)^{1/2}, \\
f^a(r) &= \frac{r^2}{2(1+r^2)^2}, & f^h(r) &= \frac{r}{4(1+r^2)^{3/2}},
\end{aligned} \tag{4.118}$$

where we ignore the correction terms that go to zero as $\rho v \rightarrow 0$, since they are too small comparing with the leading terms. As r becomes larger, the leading terms are getting smaller and so the correction terms become more important;

$$\begin{aligned} a(r) &= \frac{1}{r^2} + o((\rho v)^2), & h(r) &= \frac{1}{2r^2} - \frac{(\rho v)^2}{16} \ln 2 + \dots, \\ f^a(r) &= \frac{1}{2r^2} - \frac{g^2(\rho v)^2}{32\lambda} + \dots, & f^h(r) &= \frac{1}{4r^2} - \frac{(\rho v)^2}{32} \ln r + \dots, \end{aligned} \quad (4.119)$$

for $(\rho m_{w,H})^{-1/2} \ll r \ll (\rho m_{w,H})^{-1}$. Finally, far from the origin, $r \gg (\rho m_{w,H})^{-1/2}$, the solution is given by the following:

$$\begin{aligned} a(r) &= 2\pi^2 r \frac{d}{dr} G_{\rho m_w}(r) + \frac{1}{\nu} f^a(r), \\ h(r) &= -2\pi^2 G_{\rho m_H}(r) + \frac{1}{\nu} f^h(r), \\ f^a(r) &= -\pi^2 r \frac{d}{dr} G_{\rho \mu_w}(r), \\ f^h(r) &= \pi^2 G_{\rho \mu_H}(r), \end{aligned} \quad (4.120)$$

where $\nu = 1/4$ for $\rho v = 0$. In (4.120), we ignore correction terms, since they are too small.

Let us make a brief comment about the consistency of our analysis. Until now, we have implicitly assumed that there exists an overlapping region where both (4.93)-(4.96) and (4.105)-(4.108) are valid. Using the above solution, it is found that (4.93)-(4.96) are valid when $r \gg (\rho m_{w,H})^{-1/2}$ and (4.105)-(4.108) are valid when $r \ll (\rho m_{w,H})^{-1}$. If $\rho m_{w,H}$ is small enough, there exists the overlapping region $(\rho m_{w,H})^{-1/2} \ll r \ll (\rho m_{w,H})^{-1}$. Then our analysis is consistent.

The action of the valley instanton can be calculated using the above solution. Rewriting the action in terms of a and h , we find

$$S_g = \frac{12\pi^2}{g^2} \int_0^\infty \frac{dr}{r} \left\{ \left(r \frac{da}{dr} \right)^2 + 4a^2(a-1)^2 \right\}, \quad (4.121)$$

$$S_h = \frac{2\pi^2}{\lambda} (\rho v)^2 \int_0^\infty r^3 dr \left\{ \left(\frac{dh}{dr} \right)^3 + \frac{3}{r^2} (h-1)^2 a^2 + \frac{1}{8} (\rho v)^2 h^2 (h-2)^2 \right\}. \quad (4.122)$$

Substituting the above solution for S , we obtain

$$S = \frac{8\pi^2}{g^2} + \frac{2\pi^2}{\lambda} (\rho v)^2 - \frac{\pi^2}{4\lambda} (\rho v)^4 \ln(\rho v) + O((\rho v)^4). \quad (4.123)$$

The leading contribution $8\pi^2/g^2$ comes from S_g for a_0 , which is the action of the instanton, and the next-to-leading and the third contributions come from S_h for a_0 and h_0 .

4.4.2. Constrained instanton

Here, we consider the constrained instanton. According to Affleck's analysis,¹⁰⁾ the constrained instanton satisfies the following equation:

$$\frac{\delta S}{\delta A_\mu} + \sigma \frac{\delta O_A}{\delta A_\mu} = 0, \quad (4.124)$$

$$\frac{\delta S}{\delta H} + \sigma \frac{\delta O_H}{\delta H} = 0, \quad (4.125)$$

where σ is a Lagrange multiplier and depends on the constraint. Both O_A and O_H are functionals of A_μ and H respectively that give a solution of the constrained equation, as the scalar theory in the subsection 4.3.2. Here we adopt the ansatz (4.86) again. By the similar analysis as the valley instanton, it turns out that the behavior of the constrained instanton is the following. Near the origin of the instanton, the solution is given by a_0, h_0 in (4.92) as well as the valley instanton. In the region where $(\rho m_{w,H})^{-1/2} \ll r \ll (\rho m_{w,H})^{-1}$, the solution is given by

$$a(r) = \frac{1}{r^2} - \frac{(\rho v)^2 g^2}{8} \frac{g^2}{\lambda} + \dots, \quad h(r) = \frac{1}{2r^2} + \frac{(\rho v)^2}{8} \ln(\rho v r c) + \dots \quad (4.126)$$

Let us compare (4.119) and (4.126). The correction term of the valley instanton is smaller than one of the constrained instanton. Finally, for $r \gg (\rho m_{w,H})^{-1/2}$, the constrained instanton is given by

$$a(r) = -2\pi^2 r \frac{d}{dr} G_{\rho m_w}(r), \quad h(r) = 2\pi^2 G_{\rho m_H}(r). \quad (4.127)$$

The action of the constrained instanton is the following:

$$S = \frac{8\pi^2}{g^2} + \frac{2\pi^2}{\lambda} (\rho v)^2 + O((\rho v)^4 \ln(\rho v)). \quad (4.128)$$

The leading contribution $8\pi^2/g^2$ comes from S_g for a_0 , which is the action of the instanton, and the next-to-leading contributions comes from S_h for a_0 and h_0 . The difference from the valley instanton is that we cannot determine the term of $O((\rho v)^4 \ln(\rho v))$ by the current analysis.

Now we choose a constraint and analyze the constrained instanton. We adopt the following functionals for the constraint: $O_A = ig^2 \int d^4x \text{tr} F_{\mu\nu} F_{\nu\rho} F_{\rho\mu}$, $O_H = 0$. This constraint is one of the simplest for giving the constrained instanton. Then the constrained equation of motion is given by,

$$-\frac{1}{r} \frac{d}{dr} \left(r \frac{da}{dr} \right) + \frac{4}{r^2} a(a-1)(2a-1) + \frac{g^2}{2\lambda} (\rho v)^2 a(1-h)^2$$

$$+6(\rho v)^2 \frac{\tilde{\sigma}}{r^2} \left\{ (2a-1) \left(\frac{da}{dr} \right)^2 + 2a(a-1) \frac{d^2a}{dr^2} - \frac{2}{r} a(a-1) \frac{da}{dr} \right. \quad (4.129)$$

$$\left. - \frac{4}{r^2} a^2 (a-1)^2 (2a-1) \right\} = 0,$$

$$- \frac{1}{r^3} \frac{d}{dr} \left(r^3 \frac{dh}{dr} \right) + \frac{3}{r^2} (h-1)a^2 + \frac{1}{4} (\rho v)^2 h(h-1)(h-2) = 0, \quad (4.130)$$

where $\sigma = \rho^4 v^2 \tilde{\sigma}$. By solving these equations approximately, in fact, we obtain the behavior of the solution that we have given previously, and the multiplier is determined by $\tilde{\sigma} = 5g^2/48\lambda$ as $\rho v \rightarrow 0$.

4.4.3. Numerical analysis

In this subsection, we solve the valley equation (4.88)-(4.91) and the constrained equation (4.129), (4.130) numerically, and compare the valley instanton and constrained instanton.

We need a careful discussion for solving the valley equation (4.88)-(4.91): Since the solution must be regular at the origin, we assume the following expansions for $r \ll 1$;

$$a(r) = \sum_{n=0}^{\infty} a_{(n)} r^n, \quad h(r) = \sum_{n=0}^{\infty} h_{(n)} r^n, \quad (4.131)$$

$$f^a(r) = \sum_{n=0}^{\infty} f_{(n)}^a r^n, \quad f^h(r) = \sum_{n=0}^{\infty} f_{(n)}^h r^n.$$

Inserting (4.131) to (4.88)-(4.91), we obtain

$$a_{(0)} = 1, h_{(0)} = 1, f_{(0)}^a = 0, f_{(0)}^h = 0,$$

$$a_{(1)} = 0, f_{(1)}^a = 0, \quad (4.132)$$

$$h_{(2)} = 0, f_{(2)}^h = 0.$$

The coefficients $a_{(2)}$, $h_{(1)}$, $f_{(2)}^a$ and $f_{(1)}^h$ are not determined and remain as free parameters. The higher-order coefficients ($n \geq 3$) are determined in terms of these parameters. Four free parameters are determined by boundary conditions at infinity. The finiteness of action requires $a, h \rightarrow 0$ faster than $1/r^2$ at infinity. This condition also requires $f_a, f_h \rightarrow 0$.

We have introduced ρ as a free scale parameter. We adjust this parameter ρ so that $a_{(2)} = -2$ to make the radius of the valley instanton unity. As a result we have four parameters $h_{(1)}$, $f_{(2)}^a$, $f_{(1)}^h$ and ρv for a given ν . These four parameters are determined so that a, h, f^a , and $f^h \rightarrow 0$ at infinity. In the case of the constrained instanton, the two parameters $h_{(1)}$ and $\tilde{\sigma}$ are determined under $a_{(2)} = -2$ so that $a, h \rightarrow 0$ at infinity.

A numerical solution of the valley equation near the origin is plotted in Fig. 15 for $\rho v = 0.1, 1.0$ at $\lambda/g^2 = 1$, when $m_w = m_H$. We plot the instanton solution (4.92) by the solid line, which corresponds to the valley instanton for $\rho v = 0$. This behavior of the numerical solution for $\rho v = 0.1$ agrees with the result of the previous subsection, (4.118). Moreover, even when $\rho v = 1.0$, the numerical solution is quite similar to the instanton solution. We find that the behavior of $f^a(r)$ and $f^h(r)$ also agrees with the analytical result (4.118) as well as $a(r)$ and $h(r)$. We also find that the numerical solution in the asymptotic region where $r \gg (\rho v)^{-1/2}$, is damping exponentially and agrees with the analytical result (4.120).

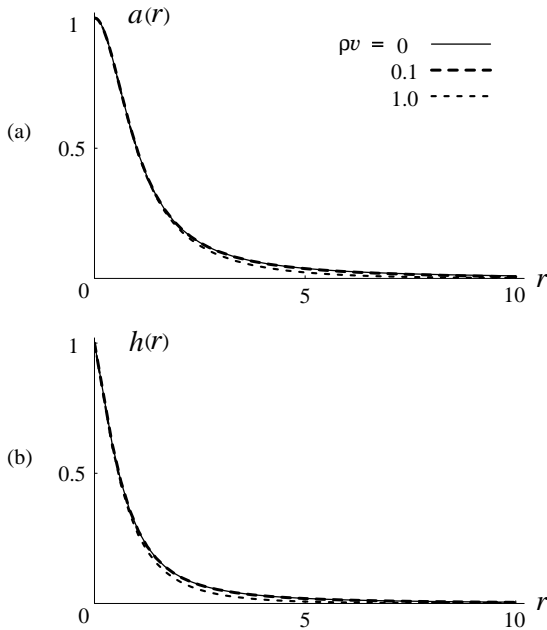


Fig. 15. Shapes of the numerical solution of the valley equation, $a(r)$ and $h(r)$ for $\rho v = 0.1, 1.0$ near the origin. The solid lines denote the original instanton solution, a_0 and h_0 .

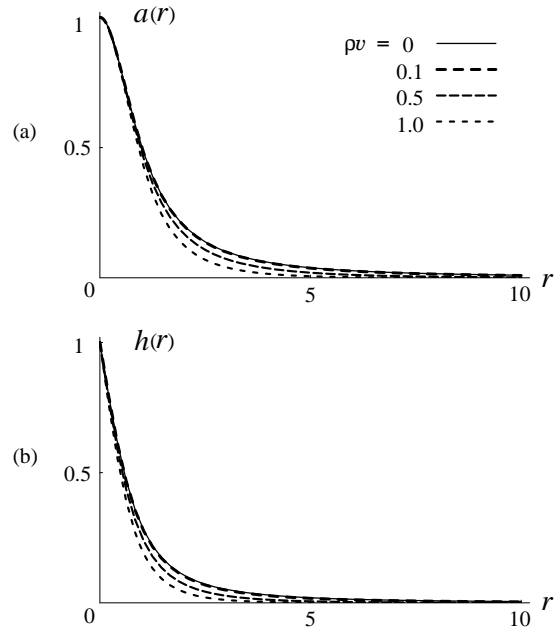


Fig. 16. Shapes of the numerical solution of the constrained instanton, $a(r)$ and $h(r)$ for $\rho v = 0.1, 0.5, 1.0$ near the origin. The solid lines denote the original instanton solution, a_0 and h_0 .

On the other hand, a solution of the constrained equation is plotted for $\rho v = 0.1, 0.5, 1.0$ at $\lambda/g^2 = 1$ in Fig. 16. The numerical solution for $\rho v = 0.1$ also agrees with the analytical result. As ρv is larger, both the valley instanton and the constrained instanton are more deformed from the original instanton solution. Nevertheless, the correction of the constrained instanton from the original instanton is much larger than one of the valley instanton, especially when $\rho v \gtrsim 0.5$.

The values of the action of the valley instanton for $\rho v = 0.001 \sim 1.0$ are plotted in Fig. 17: Fig. 17(a) depicts the behavior of the total action S , while the contribution from

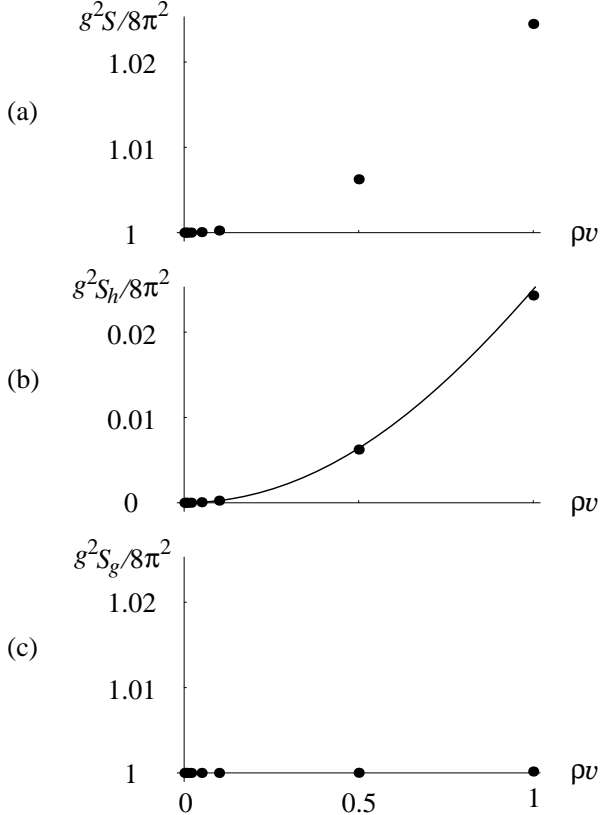


Fig. 17. (a) The action S (in unit of $g^2/8\pi^2$) of the numerical solution of the valley equation, at $\lambda/g^2 = 1$, as a function of the parameter ρv . (b) The contribution from the Higgs sector, S_h . The solid line shows the behavior of the analytical result that $g^2 S_h/8\pi^2 = (\rho v)^2/4 - (\rho v)^4 \ln(\rho v)/32$. (c) The contribution from the gauge sector, S_g .

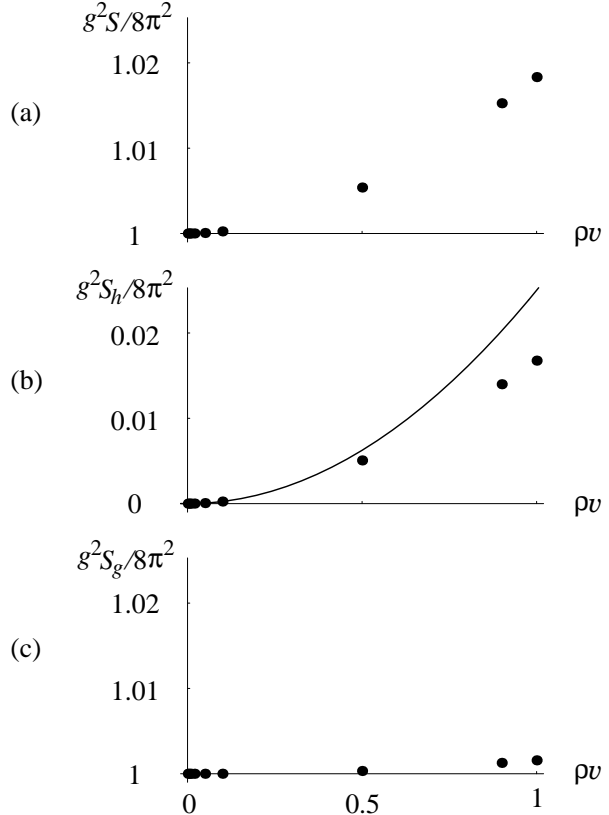


Fig. 18. (a) The action S (in units $g^2/8\pi^2$) of the numerical solution of the constrained instanton, at $\lambda/g^2 = 1$, as a function of the parameter ρv . (b) The contribution from the Higgs sector, S_h . The solid line shows the behavior of the analytical result that $g^2 S_h/8\pi^2 = (\rho v)^2/4$. (c) The contribution from the gauge sector, S_g .

the gauge part S_g and from the Higgs part S_h are in (b) and (c) respectively. The solid line shows the behavior of S_h of the analytical result (4.123). From Fig. 17 (c), it turns that S_g is almost independent of ρv . This figure shows that our numerical solutions are quite consistent with (4.123), even when $\rho v = 1.0$.

The values of the action of the constrained instanton for $\rho v = 0.001 \sim 1.0$ are plotted in Fig. 18. When $\rho v \gtrsim 0.5$, we can no longer use the analytical result (4.128). This is attributed to the large deformation from the original instanton. We notice that the action of the constrained instanton is smaller than that of the valley instanton for the same value of ρv . This result is natural at the point that the parameter ρv corresponds to the scale parameter. This point was elaborated upon in section 3, using the toy model (3.23). To repeat, the fact

that the constrained instanton has the smaller action than the valley instanton for the same value of ρv does not mean that the constrained instanton gives more important contribution to the functional integral than the valley instanton.

We summarize all the numerical data in Table II and III, for the valley instanton and for the constrained instanton, respectively.

ρv	ν	$h_{(1)}$	$f_{(2)}^a$	$f_{(1)}^h$	$g^2 S/8\pi^2$
0.001	0.2500	-1.000	0.5001	0.2500	1.000000
0.005	0.2500	-1.000	0.5001	0.2500	1.000006
0.01	0.2501	-1.000	0.5001	0.2500	1.000025
0.02	0.2501	-1.000	0.5003	0.2501	1.000100
0.05	0.2503	-1.000	0.5014	0.2505	1.000625
0.1	0.2509	-1.000	0.5044	0.2515	1.002503
0.5	0.2537	-1.007	0.5478	0.2669	1.062550
1.0	0.2521	-1.021	0.6226	0.2926	1.244646

Table II. The numerical data of the valley instanton in the gauge-Higgs system.

ρv	$\tilde{\sigma}$	$h_{(1)}$	$\rho_0 v$	$g^2 S/8\pi^2$
0.001	0.1042	-1.000	0.000100	1.000000
0.005	0.1042	-1.000	0.005000	1.000006
0.01	0.1041	-1.000	0.010000	1.000025
0.02	0.1040	-1.000	0.019998	1.000100
0.05	0.1035	-1.002	0.049972	1.000623
0.1	0.1019	-1.005	0.099779	1.002471
0.5	0.0798	-1.070	0.481738	1.053903
0.9	0.0637	-1.144	0.833000	1.152691
1.0	0.0609	-1.162	0.917406	1.183336

Table III. The numerical data of the constrained instanton in the gauge-Higgs system.

In Table III, we show the parameter ρ_0 used as “ ρ ” in Ref. 10). The parameter ρ_0 is defined by,

$$O = c_0 \rho_0^{4-d}, \quad (4.133)$$

where d is a dimension of the operator and c_0 is a conveniently chosen constant. For $O_A = ig^2 \int d^4x \text{tr} F_{\mu\nu} F_{\nu\rho} F_{\rho\mu}$ and $O_H = 0$, we choose that $c_0 = 96\pi^2/5g^2$ so that $\rho_0 = \rho$ as $\rho v \rightarrow 0$. We find that ρ_0 nearly agrees with ρ .

4.5. Valley calculation of the B and L violation

In this subsection, we calculate the cross section for the process of the type $\bar{q} + \bar{q} \rightarrow (3n_f - 2)q + n_f l + n_w W + n_h H$, using the valley instanton.³¹⁾ As explained in section 2, Ringwald and Espinosa studied this process by using the constrained instanton.^{5),6)} They suggested that the amplitudes of the multi-boson process increase with the energy and reach 1pb for a center of mass energy of O(10) TeV. Unfortunately, the high-energy behavior of the process with many bosons, which is most interesting, is out of the validity of their calculations. One of the problem that they used the analytically constructed configuration given in subsection 4.4.2. In the process with many bosons, the large radius instanton dominates the path-integral. As is shown in subsection 4.4.3, the large radius constrained instanton is not approximated well by the analytically constructed configuration. On the other hand, the valley instanton

can be approximated by the analytically constructed configuration even for the large radius one. (See subsection 4.4.3.) Thus the analytically constructed configuration can be used in the calculation. Although induced vertex by the valley instanton is similar to that given by Ref. 5) and 6), the latter can not be justified in the calculation of the process with many bosons.

Another problem of Ref. 6) is that the orientation effects of the instanton are not taken into account. The integration of the orientation in the Lorentz $SU(2)_R$ rotations is not trivial but very important especially for the process with many bosons. Moreover, in considering the multi-boson processes at high energies, masses of the gauge boson, Higgs particle and top quark can not be neglected. All the effects are incorporated in the following calculations.

4.5.1. Valley instanton in the electroweak theory

We consider the standard model with n_f generations of quarks and leptons. For simplicity, we set $SU(3)_c$ and $U(1)_Y$ coupling constant to be zero. Thus we treat the simplified standard model that reduces to an $SU(2)$ gauge-Higgs system with fermions. As for quarks, we have the left-handed doublets $q_L^{i\alpha}$ and the right-handed singlets $q_R^{i\alpha}$, where $\alpha = 1, 2, 3$ is the color index and $i = 1, \dots, n_f$ is the index of the generations. Similarly, we have the left-handed doublets l_L^i and the right-handed singlets l_R^i for leptons. The bosonic part of the action is given by

$$S_g = \frac{1}{2g^2} \int d^4x \operatorname{tr} F_{\mu\nu} F_{\mu\nu}, \quad (4.134)$$

$$S_h = \frac{1}{\lambda} \int d^4x \left\{ (D_\mu H)^\dagger (D_\mu H) + \frac{1}{8} (H^\dagger H - v^2)^2 \right\}, \quad (4.135)$$

where $F_{\mu\nu} = \partial_\mu A_\nu - \partial_\nu A_\mu - i[A_\mu, A_\nu]$ and $D_\mu = \partial_\mu - iA_\mu$. The masses of the gauge boson and the Higgs boson are

$$m_W = \sqrt{\frac{g^2}{2\lambda}} v, \quad m_H = \frac{1}{\sqrt{2}} v. \quad (4.136)$$

The fermionic part of the action is

$$S_q = \int d^4x (i q_L^\dagger \sigma_\mu D_\mu q_L - i u_R^\dagger \bar{\sigma}_\mu \partial_\mu u_R - i d_R^\dagger \bar{\sigma}_\mu \partial_\mu d_R + y_u q_L^\dagger \epsilon H^* u_R - y_d q_L^\dagger H d_R + h.c.), \quad (4.137)$$

$$S_l = \int d^4x (i l_L^\dagger \sigma_\mu D_\mu l_L - i e_R^\dagger \bar{\sigma}_\mu \partial_\mu e_R - y_l l_L^\dagger H e_R + h.c.), \quad (4.138)$$

where $\epsilon^{\alpha\beta} = -\epsilon_{\alpha\beta} = i\sigma^2$, $\sigma_\mu = (\sigma, i)$ and $\bar{\sigma}_\mu = (\sigma, -i)$. The masses of fermions are given by $m_{u,d,l} = y_{u,d,l} v$. The total action is given by

$$S = S_g + S_h + \sum_{i=1}^{n_f} \left(S_l + \sum_{\alpha=1}^3 S_q \right). \quad (4.139)$$

As was shown in the previous subsection, the dominating configuration in the path-integral of the bosonic variables is the valley instanton. The valley instanton is given by the following;

$$A_\mu(x) = \frac{x_\nu}{x^2} U \bar{\sigma}_{\mu\nu} U^\dagger \cdot 2a(r), \quad (4.140)$$

$$H(x) = v(1 - h(r))\eta, \quad (4.141)$$

where U is a Lorentz $SU(2)_R$ matrix, η is a constant isospinor, and a and h are real dimensionless functions of dimensionless variable r , which is defined by $r = \sqrt{x^2}/\rho$. We choose η_r as $(0,1)$.

Near the origin of the valley instanton, $r \ll (\rho m_{w,H})^{-1/2}$, the valley instanton is given by,

$$a(r) = \frac{1}{1+r^2}, \quad h(r) = 1 - \left(\frac{r^2}{1+r^2} \right)^{1/2}, \quad (4.142)$$

where we ignore the correction terms that go to zero as $\rho v \rightarrow 0$, since they are too small comparing with the leading terms. As r becomes larger, the leading terms are getting smaller and so the correction terms become more important;

$$a(r) = \frac{1}{r^2} + o((\rho v)^2), \quad h(r) = \frac{1}{2r^2} - \frac{(\rho v)^2}{16} \ln 2 + \dots, \quad (4.143)$$

for $(\rho m_{w,H})^{-1/2} \ll r \ll (\rho m_{w,H})^{-1}$. Finally, far from the origin, $r \gg (\rho m_{w,H})^{-1/2}$, the solution is given by the following:

$$\begin{aligned} a(r) &= \frac{\pi^2}{2\nu} r \frac{d}{dr} G_{\rho m_w}(r) + \frac{1}{\nu} f^a(r), \\ h(r) &= -\frac{\pi^2}{2\nu} G_{\rho m_H}(r) + \frac{1}{\nu} f^h(r), \end{aligned} \quad (4.144)$$

where $\nu = 1/4$ for $\rho v = 0$, and by the numerical calculation, we obtain $\nu \sim 1/4$ for $\rho v \lesssim 1$. In (4.144), we ignore correction terms, since they are too small. The function $G_m(r)$ is

$$G_m(r) = \frac{m K_1(mr)}{(2\pi)^2 r}, \quad (4.145)$$

where K_1 is a modified Bessel function. The functions f and h decay exponentially at large r .

The fermionic zero mode around the valley instanton is given by;

$$q_{Lr}^{\dot{\alpha}}(x) = -\frac{1}{\pi\rho^3} x_\nu \bar{\sigma}_\nu^{\dot{\alpha}\alpha} U_\alpha^{\dagger\beta} \left(-\epsilon_{rs} \eta^{\dagger s} \eta_\beta u_L(r) + \eta_r \epsilon_{\beta\gamma} \eta^{\dagger\gamma} d_L(r) \right), \quad (4.146)$$

$$u_{R\alpha}(x) = \frac{i}{2\pi} \frac{m_u}{\rho} u_R(r) U_\alpha^{\dagger\beta} \eta_\beta, \quad (4.147)$$

$$d_{R\alpha}(x) = \frac{i}{2\pi} \frac{m_d}{\rho} d_R(r) U_\alpha^{\dagger\beta} \epsilon_{\beta\gamma} \eta^{\dagger\gamma}, \quad (4.148)$$

where the Greek and the Roman letters denote indices of spinor and isospinor, respectively. For small ρv , the solution is given approximately, by the following;

$$u_L(r) = \begin{cases} \frac{1}{r(r^2 + 1)^{3/2}}, & \text{if } r \ll (\rho m_u)^{-1/2}; \\ -2\pi^2 \frac{1}{r} \frac{d}{dr} G_{\rho m_u}(r), & \text{if } r \gg (\rho m_u)^{-1/2}; \end{cases} \quad (4.149)$$

$$u_R(r) = \begin{cases} \frac{1}{r^2 + 1}, & \text{if } r \ll (\rho m_u)^{-1/2}; \\ 2\pi^2 G_{\rho m_u}(r), & \text{if } r \gg (\rho m_u)^{-1/2}, \end{cases} \quad (4.150)$$

and d_L and d_R are obtained by replacing m_u with m_d . The above approximative behavior is correct even though ρv is $O(1)$, since the valley instanton keep its shape unchanged as was seen in section 4.4.3.

4.5.2. Calculation of the cross section

To evaluate the multi-point Green function, we must introduce collective coordinates x_0 and U to restore the translational and Lorentz invariance as the valley instanton breaks these symmetries. In addition to them, the ρ integral must be brought into, because along the valley direction the action varies gently and the corresponding integration can not be approximated by the Gaussian integration.

Since the valley instanton is not a classical solution, a slight complication arises to introduce the collective coordinates. For the classical solution, corresponding to the broken symmetries, there exist zero modes and the collective coordinates are introduced naturally to extract these zero modes from the functional integral. However, the existence of the zero modes is not guaranteed for the valley instanton. In Ref. 31), another collective coordinate method have been used. The point is that the collective coordinates for the translations and the Lorentz $SU(2)_R$ rotations can be treated as transformation parameters of a kind of “gauge symmetries”.³²⁾ The orbits of the “gauge symmetries” can be extracted by the usual Faddeev-Popov method and they becomes the collective coordinates for the translations and the Lorentz $SU(2)_R$ rotations. As well as the usual gauge symmetry, the translation and the Lorentz invariance of the Green function is automatically guaranteed. For the collective coordinate of the valley direction, we bring into it so as the quantum fluctuations around the valley instanton are restricted to be orthogonal to the valley direction.¹¹⁾ From this prescription, liner terms of the quantum fluctuation drop naturally from the action while we do not treat the classical solution.

Since the valley instanton is very similar to the original instanton, we approximate the determinant and Jacobian of the valley instanton by one of the original instanton²⁾. Then

the Fourier transformed Green function is given by,

$$\begin{aligned} \tilde{G}(p, q, k) &= e^{-8\pi^2/g^2} g^{-8} \int dU \int d\rho e^{-2\pi^2(\rho v)^2/\lambda} \rho^{2n_f-5} c(\rho\mu)^{(43-8n_f)/6} \\ &\quad \times \tilde{\psi}(p_1) \cdots \tilde{A}_\mu(q_1) \cdots \tilde{\phi}(k_1) \cdots \end{aligned} \quad (4.151)$$

Here the Fourier transformations of the fermionic zero mode $\tilde{\psi}$ is given by

$$\tilde{\psi} = \begin{pmatrix} \tilde{\psi}_{R\alpha} \\ \tilde{\psi}_L^{\dot{\alpha}} \end{pmatrix} = 2\pi i \rho \begin{pmatrix} -m_f U^\dagger \chi \\ \bar{\not{p}} U^\dagger \chi \end{pmatrix} \frac{1}{p^2 + m_f^2} + \cdots, \quad (4.152)$$

where \cdots includes the regular term in the limit: $p^2 + m_f^2 \rightarrow 0$, and χ_α is the constant spinor, $(0, -1)$ for $\psi = u, \nu$ and $(1, 0)$ for $\psi = d, e$. The Fourier transforms of the valley instanton, \tilde{A}_μ is given by

$$\tilde{A}_\mu = -\frac{1}{\nu} \pi^2 i \rho^2 \frac{q_\nu U \bar{\sigma}_{\mu\nu} U^\dagger}{q^2 + m_w^2} + \cdots. \quad (4.153)$$

We define the shifted Higgs field ϕ by $H = (v + \phi)\eta$ and the Fourier transform is given by,

$$\tilde{\phi} = \frac{1}{2\nu} \pi^2 \rho^2 \frac{v}{k^2 + m_h^2} + \cdots. \quad (4.154)$$

The integration of the valley parameter ρv is given by

$$\int_0^\infty d(\rho v) e^{-2\pi^2(\rho v)^2/\lambda} (\rho v)^{2t-1} = \frac{1}{2} \left(\frac{\lambda}{2\pi^2} \right)^t \Gamma(t), \quad (4.155)$$

where $t = \frac{7}{3}n_f + n_w + n_h + \frac{19}{12}$. The integration is dominated by the contribution around the saddle point;

$$\rho v_s = \left\{ \frac{\lambda}{2\pi^2} \left(t - \frac{1}{2} \right) \right\}^{1/2} \quad (4.156)$$

Therefore, we can check the consistency of the approximation by this value of the saddle point. The saddle point ρv_s depends on the number of bosons monotonously. The valley instanton is quite similar to the original instanton even at $\rho v = 1$, and therefore the approximation is valid for $n_w + n_h \sim 40$, if we assume $m_H = m_W$ and use $g^2 \sim 0.42$. On the other hand, the constrained instanton is deviated from the original instanton at $\rho v = 0.5$ and so the approximation breaks for $n_w + n_h \sim 4$. Therefore we can calculate the amplitude of the multi-boson process, using the valley instanton. Finally, we obtain the Green function;

$$\begin{aligned} \tilde{G}(p, q, k) &= (-i)^{n_w} c' \cdot 2^{-n_h/2} \left(\frac{\mu}{m_W} \right)^{(43-8n_f)/6} m_W^{-6n_f-2n_w-n_h+4} e^{-8\pi^2/g^2} \\ &\quad \times g^{14n_f/3+n_w+n_h-29/6} \int dUL(U; p, q, k), \end{aligned} \quad (4.157)$$

where

$$\begin{aligned} c' &= c \cdot 2^{-2n_f/3-25/6} \pi^{-2n_f/3-19/6} \Gamma(t), \\ &= 1.26 \times 10^6 \cdot e^{6.516n_f} \cdot \Gamma(t), \end{aligned} \quad (4.158)$$

and $L(U; p, q, k)$ is defined by,

$$L(U; p, q, k) = \prod_{i=1}^{4n_f} \begin{pmatrix} -m_f U^\dagger \chi \\ \bar{p}_i U^\dagger \chi \end{pmatrix} \frac{1}{p_i^2 + m_f^2} \prod_{j=1}^{n_w} \frac{q_{j\nu} U \bar{\sigma}_{\mu\nu} U^\dagger}{q_j^2 + m_w^2} \prod_{l=1}^{n_h} \frac{1}{k_l^2 + m_H^2}. \quad (4.159)$$

We ignore the momentum dependence that goes to zero on mass-shell. Performing the LSZ procedure, we obtain the invariant amplitude T_{n_f, n_w, n_h} . Summing up the polarization and charge of the gauge field, isospinor and spinor of the fermion field, we obtain the amplitude;

$$\begin{aligned} \sum |T_{n_f, n_w, n_h}|^2 &= c'^2 2^{-n_w - n_h} \left(\frac{\mu}{m_H} \right)^{(43-8n_f)/3} (m_W^2)^{-6n_f - 2n_w - n_h + 4} e^{-16\pi^2/g^2} \\ &\quad \times (g^2)^{14n_f/3 + n_w + n_h - 29/6} \int dU \prod_{i=1}^{4n_f} \text{tr}(\bar{p}_i U) \prod_{j=1}^{n_w} (-) g^{\mu\rho} q_j^\nu q_j^\sigma \text{tr}(\sigma_{\mu\nu} U \bar{\sigma}_{\rho\sigma} U^\dagger). \end{aligned} \quad (4.160)$$

The cross section is given by the following;

$$\begin{aligned} \sigma &= \frac{1}{n_w! n_h!} \frac{1}{2^4} \int \prod_{i=3}^{4n_f} \frac{d^3 p_i}{(2\pi)^3 2E_{p_i}} \prod_{j=1}^{n_w} \frac{d^3 q_j}{(2\pi)^3 2E_{q_j}} \prod_{l=1}^{n_h} \frac{d^3 k_l}{(2\pi)^3 2E_{k_l}} (2\pi)^4 \delta^{(4)}(p_{\text{in}} - p_{\text{out}}) \\ &\quad \times \sum |T_{n_f, n_w, n_h}|^2 \cdot \frac{1}{4\sqrt{(p_1 \cdot p_2)^2 - m_1^2 m_2^2}} \\ &= \frac{c'^2}{n_w! n_h!} 2^{-n_h - 5} (2\pi)^{-12n_f - 3n_w - 3n_h + 10} \left(\frac{\mu}{m_W} \right)^{(43-8n_f)/3} (m_W)^{-6n_f - 2n_w - n_h + 4} \\ &\quad \times e^{-16\pi^2/g^2} (g^2)^{14n_f/3 + n_w + n_h - 29/6} \cdot I_{2n_f, n_w, n_h}(s) \cdot s^{-1}, \end{aligned} \quad (4.161)$$

where $s = p_{\text{in}}^2 = (p_1 + p_2)^2$ and the masses of fermions of the initial state are ignored. We denote the sum of the momentums of the final state by p_{out} . All the information about phase space and group integration is encoded in the function $I_{2n_f, n_w, n_h}(s)$. We define $I_{l, m, n}(s)$

$$\begin{aligned} I_{l, m, n}(s) &= \int \prod_{i=3}^{2l} \frac{d^3 p_i}{2E_{p_i}} \prod_{j=1}^m \frac{d^3 q_j}{2E_{q_j}} \prod_{l=1}^n \frac{d^3 k_l}{2E_{k_l}} \delta^{(4)}(p_{\text{in}} - p_{\text{out}}) \\ &\quad \times 2^m \int dU \prod_{i=1}^{2l} \text{tr}(\bar{p}_i U) \prod_{j=1}^m (-) g^{\mu\rho} q_j^\nu q_j^\sigma \text{tr}(\sigma_{\mu\nu} U \bar{\sigma}_{\rho\sigma} U^\dagger) \\ &= \int \prod_{i=3}^{2l} \frac{d^3 p_i}{2E_{p_i}} \prod_{j=1}^m \frac{d^3 q_j}{2E_{q_j}} \prod_{l=1}^n \frac{d^3 k_l}{2E_{k_l}} \delta^{(4)}(p_{\text{in}} - p_{\text{out}}) \\ &\quad \times \int dU \prod_{i=1}^{2l} \text{tr}(\bar{p}_i U) \prod_{j=1}^m \left[\left\{ \text{tr}(\bar{q}_j U) \right\}^2 - m_W^2 \right]. \end{aligned} \quad (4.162)$$

To evaluate the function $I_{l,m,n}(s)$, we consider the Laplace transformation of this function. At first, we assume that p_{in} , p_1 and p_2 are independent variables, and at last we input $p_{\text{in}} = p_1 + p_2$. The Laplace transform $\Phi_{l,m,n}(\alpha; p_1, p_2)$ is given by,

$$\begin{aligned}\Phi_{l,m,n}(\alpha; p_1, p_2) &= \int d^4 p_{\text{in}} e^{-\alpha p_{\text{in}}} I_{l,m,n}(p_{\text{in}}; p_1, p_2) \\ &= \int dU \text{tr}(\bar{\boldsymbol{p}}_1 U) \text{tr}(\bar{\boldsymbol{p}}_2 U) \phi_f(\alpha, U)^{2l-2} \phi_g(\alpha, U)^m \phi_h(\alpha)^n,\end{aligned}\quad (4.163)$$

where

$$\phi_f(\alpha, U) = \int \frac{d^3 p}{2E_p} \text{tr}(\bar{\boldsymbol{p}} U) e^{-\alpha p} = 2\pi \frac{m_f^2}{\alpha^2} K_2(\alpha m_f) \text{tr}(\bar{\boldsymbol{\phi}} U), \quad (4.164)$$

$$\phi_g(\alpha, U) = \int \frac{d^3 q}{2E_q} \left[\left\{ \text{tr}(\bar{\boldsymbol{q}} U) \right\}^2 - m_w^2 \right] e^{-\alpha q} = \frac{2\pi m_w^3}{\alpha^3} K_3(\alpha m_w) \left[\left\{ \text{tr}(\bar{\boldsymbol{\phi}} U) \right\}^2 - \alpha^2 \right], \quad (4.165)$$

$$\phi_h(\alpha) = \int \frac{d^3 k}{2E_k} e^{-\alpha k} = \frac{2\pi m_H}{\alpha} K_1(\alpha m_H). \quad (4.166)$$

The above functions K_ν are the modified Bessel functions and $\alpha = \sqrt{\alpha^2}$. Then we can perform the group integration easily,

$$\begin{aligned}& \int dU \text{tr}(\bar{\boldsymbol{p}}_1 U) \text{tr}(\bar{\boldsymbol{p}}_2 U) \left\{ \text{tr}(\bar{\boldsymbol{\phi}} U) \right\}^{2l-2} \left[\left\{ \text{tr}(\bar{\boldsymbol{\phi}} U) \right\}^2 - \alpha^2 \right]^m \\ &= \sum_{i=0}^m {}_m C_i \int dU \text{tr}(\bar{\boldsymbol{p}}_1 U) \text{tr}(\bar{\boldsymbol{p}}_2 U) \left\{ \text{tr}(\bar{\boldsymbol{\phi}} U) \right\}^{2l-2+2i} (-\alpha^2)^{n-i} \\ &= \left\{ C_0 (p_1 \cdot \alpha) (p_2 \cdot \alpha) + C_1 (p_1 \cdot p_2) \alpha^2 \right\} \alpha^{2(l+m-2)},\end{aligned}\quad (4.167)$$

where

$$C_0 = 4 \sum_{i=0}^m (-)^{m-i} {}_m C_i \frac{\{2(l+i-1)\}!}{(l+i+1)!(l+i-2)!}, \quad (4.168)$$

$$C_1 = 2 \sum_{i=0}^m (-)^{m-i} {}_m C_i \frac{\{2(l+i-1)\}!}{(l+i+1)!(l+i-1)!}. \quad (4.169)$$

Finally, using the inverse Laplace transformation, we obtain the function $I_{l,m,n}$. We can evaluate $I_{l,m,n}$ analytically in the case of the relativistic limit and the non-relativistic limit. In the relativistic limit, $I_{l,m,n}$ is given by,

$$I_{l,m,n} = C_{l,m,n}^{\text{ER}} S^{3l+2m+n-4} \quad (4.170)$$

where

$$\begin{aligned}C_{l,m,n}^{\text{ER}} &= 2^m \left(\frac{\pi}{2} \right)^{2l+m+n-3} \left\{ (3l+2m+n-3)!(3l+2m+n-5)! \right\}^{-1} \\ &\times \sum_{i=0}^m (-)^{m-i} {}_m C_i \frac{\{2(l+i-1)\}!}{(l+i+1)!(l+i-1)!} \{1 + (l+i)(3l+2m+n-4)\}.\end{aligned}\quad (4.171)$$

In the non-relativistic limit, we obtain

$$I_{l,m,n} = C_{l,m,n}^{\text{NR}} m_f^{3/2} m_W^{5m/2} m_H^{n/2} (\sqrt{s} - M)^{6l+3(m+n)/2-10} \cdot s^{1/4}, \quad (4.172)$$

where

$$C_{l,m,n}^{\text{NR}} = \left\{ \left(6l + \frac{3}{2}m + \frac{3}{2}n - 10 \right)! \right\}^{-1} \cdot 2^{4l+(m+n)/2-7} \pi^{2l+3(m+n)/2-3} \\ \times \sum_{i=0}^m (-)^{m-i} {}_m C_i \frac{\{2(l+i-1)\}!}{(l+i+1)!(l+i-1)!} (l+i). \quad (4.173)$$

In the general cases, we can perform the inverse Laplace transformation numerically, using the steepest descent approximation. We show the result in Fig. 19 for the case where $n_w = 75$ and $n_h = 0$. In Fig. 19, the solid line denotes the numerical result by the steepest descent method. The dashed line and the dotted line denote the approximate result in the non-relativistic limit and extremely relativistic limit, respectively. We show cross sections for the various values of n_w and n_h in Fig. 20 at $\sqrt{s}=15.55$ TeV. From this, we understand that the gauge boson plays an important role rather than the Higgs particle. In Fig. 21, we show the energy dependence of the cross section for $n_w=0, 20, 40, 75$ and 100 , and $n_h=0$. We show the unitarity bound as a dashed line in Fig. 21. The approximation breaks in the region of the energy where the cross section overcomes the unitarity bound. In the region, the multi-instanton effect⁷⁾(see section 2) or interaction between the gauge bosons in the final state²⁶⁾ are important, which are not evaluated in our analysis. Since the asymptotic behavior of the valley instanton is different from the constrained instanton, a naive calculation yields that the interaction between the valley instanton and the anti valley instanton is different from that between the constrained instanton and the anti constrained instanton. Therefore, the analysis given in section 2 must be reconsidered. This is interesting problem, but remains as an open question for now.

§5. Complex-time methods

As we have seen so far in this paper, the imaginary-time path-integral formalism combined with the proper valley method has been successful for the treatment of the quantum tunneling phenomena. In spite of this, some basic as well as practical questions related to analytic continuation remain. How does the boundary condition matches that of the valley configurations? In estimating many-point Green functions, how does the external fields enter (affect) the imaginary time configuration? [This is crucial for the validity of the path-deformations in the valley calculation, as well as bounce calculations.] Some other points are elaborated by Boyanovsky, Willey and Holman.¹⁷⁾

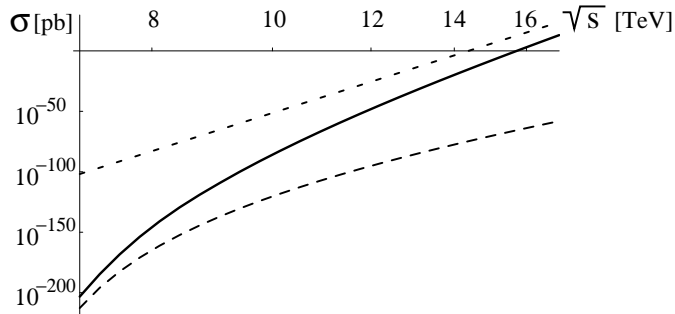


Fig. 19. The energy dependence of the cross section for $n_w = 75$ and $n_h = 0$. The solid line denotes the result by the saddle point approximation. The dashed line and the dotted line denote the approximate result in the non-relativistic limit and extremely relativistic limit, respectively.

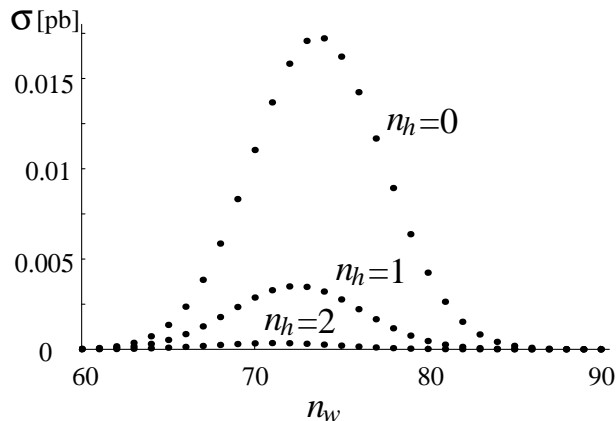


Fig. 20. The cross section for the various n_w and n_h at $s^{1/2} = 15.55$ TeV.

In quantum mechanics, the complex-time method has been studied by various authors. (33), (34), (35), (36), (37), (38), (39) It was argued that it allows semi-classical approximation for tunneling phenomena and overcomes various problems associated with the pure-imaginary-time method. In it, one considers the analytic continuation of the time-integral in Fourier transform of the Feynman kernel. The existence of the tunneling leads to the existence of the complex saddle-points in the time-plane. It was claimed that semi-classical approximation is done by deforming the time-integral so that it goes through all such saddle-points. (39)

This gives one hope that calculations in field theory may be improved by using the complex-time method. Indeed, Son and Rubakov (40), (41), (42) adopted a complex-time method

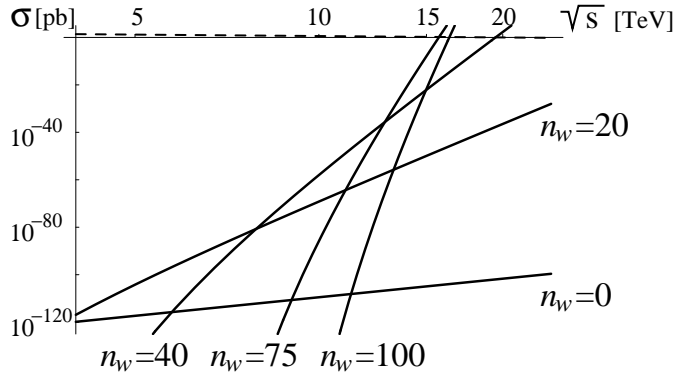


Fig. 21. The energy dependence of the cross section for $n_w=0, 20, 40, 75$ and 100 , and $n_h=0$. A dashed line denotes the unitarity bound.

for the estimate of the cross section. They used periodic instanton-anti-instanton solution in imaginary time, and the initial Minkowski state overlaps with the instanton as a coherent state.

Closer look, however, reveals many questions unanswered so far.⁴³⁾ It is known that the complex-time plane is plagued with singularities and infinite number of saddle-points, which form lattice structure. Among saddle-points, there are two kinds, those that are solutions of the equation of motions (we shall call these “physical saddle-points” in this paper), and those that are not (“unphysical saddle-points”). How the path is deformed to avoid the singularities and to go through only the physical saddle-points is unknown. One simply assumes that all and only the physical saddle-points contribute. Even so, the weight of each saddle-point is a riddle. They are determined so that the result agrees with that of the WKB approximation. It is not known how it comes about from the path.

In this section, we give the solution of these problems, based on a reduction formula in the number of the turning points of the path. In the first subsection, we give a brief overview of the saddle-point calculations in complex-time. There we elaborate some of the points briefly mentioned above. In order to solve the riddles pointed in this subsection, we analyze the orthonormality of the WKB wavefunctions and construct the Green function from them in the subsection 5.2. This way, the arbitrariness in the path-integral formulation is avoided and the relevant Green functions are constructed from the first principle. Based on this construction of the Green functions, we derive the connection formula for the WKB wavefunction in the subsection 5.3, where it leads to the reduction formula for Green function. Expanding this formula, we obtain a series, which can be interpreted as a sum over the

physical saddle-points. The weights and the phases of saddle-points are determined from this formula.

5.1. Saddle-point method

We consider one-dimensional quantum mechanics with action;

$$S = \int dt \left[\frac{1}{2} \dot{x}^2 - V(x) \right]. \quad (5.1)$$

The potential $V(x)$ is assumed to be smooth enough to allow WKB approximation in asymptotic regions I ($x \rightarrow -\infty$) and II ($x \rightarrow \infty$). The finite-time Green function (Feynman kernel) is defined by the following in the Heisenberg representation;

$$G(x_i, x_f; T) = \langle x_f | e^{-iHT} | x_i \rangle, \quad (5.2)$$

in terms of the Hamiltonian of the system, H . The advanced and retarded resolvents are, respectively;

$$G^A(x_i, x_f; E) = i \int_{-\infty}^0 dT e^{i(E-i\delta)T} G(x_i, x_f; T) = \langle x_f | \frac{1}{E - i\delta - H} | x_i \rangle, \quad (5.3)$$

$$G^R(x_i, x_f; E) = -i \int_0^{\infty} dT e^{i(E+i\delta)T} G(x_i, x_f; T) = \langle x_f | \frac{1}{E + i\delta - H} | x_i \rangle, \quad (5.4)$$

where real-positive δ is introduced to guarantee the convergence of the integrals. The poles of these Green functions come from the bound states, and the cut from the continuous spectra.

Let us first look at the saddle-point approximation for the path integral,

$$G(x_i, x_f; T) = \int_{x(0)=x_i}^{x(T)=x_f} \mathcal{D}x e^{iS}. \quad (5.5)$$

One obtains the following from the saddle-point method;

$$G(x_i, x_f; T) = \sum_{x_{\text{cl}}} \left[\frac{2\pi \dot{x}_{\text{cl}}(0) \dot{x}_{\text{cl}}(T)}{i \partial^2 S_{\text{cl}} / \partial T^2} \right]^{-1/2} e^{iS_{\text{cl}}}, \quad (5.6)$$

where x_{cl} is the solution of the classical equation of motion and S_{cl} is the action evaluated at the classical solution. This approximation is valid as long as both x_i and x_f are far from the turning points where classical velocities vanish. Substituting (5.6) into the retarded resolvent in (5.3), (5.4), one arrives at the following expression;

$$G^R(x_i, x_f; E) = -i \int_0^{\infty} dT \sum_{x_{\text{cl}}} \left[\frac{2\pi \dot{x}_{\text{cl}}(0) \dot{x}_{\text{cl}}(T)}{i \partial^2 S_{\text{cl}} / \partial T^2} \right]^{-1/2} e^{i(ET+S_{\text{cl}})}. \quad (5.7)$$

In the above, we absorbed the infinitesimal imaginary convergence factor ($i\delta$) in E .

In calculating (5.7), one hopes to apply the saddle-point approximation to the T -integral. The saddle-point condition (the stable-phase condition, to be more exact) is then,

$$E = -\frac{\partial S_{\text{cl}}}{\partial T} = \frac{1}{2}\dot{x}_{\text{cl}}^2 + V(x_{\text{cl}}) . \quad (5.8)$$

In other words, the solution of the equation of motion $x_{\text{cl}}(t)$ has to have the energy E .

Let us consider a situation depicted in Fig. 22. Both the initial point x_i and the final point x_f lie in the forbidden region. There is no real-time solution of the equation of motion. Thus no semi-classical approximation is possible for the real-time formalism.

If one assumes that the expression (5.6) gives correct analytic continuation of the Green function in the complex T -plane when complex- T solutions of the equation of motion exist, one could go to the complex T -plane and apply the saddle-point method. One then arrives at the following expression;

$$G(x_i, x_f; E) = -i \sum_{T_s} \sum_{x_{\text{cl}}} |\dot{x}_{\text{cl}}(0)\dot{x}_{\text{cl}}(T_s)|^{-1/2} w(T_s) p(T_s) e^{iW_{\text{cl}}(T_s)}, \quad (5.9)$$

where T_s is given by (5.8). Here $W_{\text{cl}}(T_s)$ is the WKB phase, $w(T_s)$ is weight and $p(T_s)$ is phase for the corresponding saddle-point. The original contour is deformed to pass the saddle-points by a series of steepest descent paths from the origin $T = 0$ to the positive infinity on the real axes ($\text{Re } T = \infty, \text{Im } T = 0$). The weight of a saddle-point, $w(x_{\text{cl}})$, is determined by how the contour crosses the saddle-point: If the contour does not cross the saddle-point, the corresponding weight is zero. If the contour crosses it along the steepest descent direction, the weight is 1. In case the contour reaches a sub-dominant saddle-point from the direction orthogonal to the steepest descent and leaves it along the steepest descent direction, the weight is 1/2 (as in the calculation of the false vacuum decay). The phase of a saddle-point, $p(T_s)$ comes from the square root in (5.7).

Carlitz and Nicole applied this method to linear potential, quadratic well and quadratic barrier, all of which are exactly solvable. Using the exact expression for the Green function

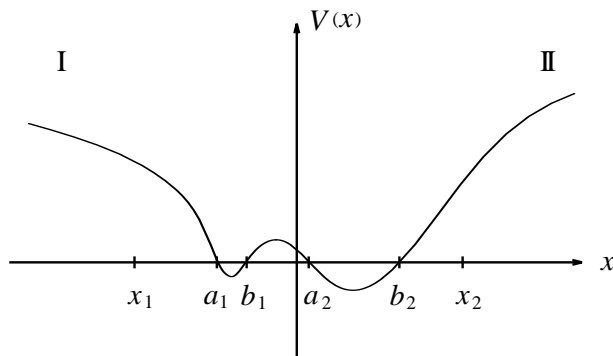


Fig. 22. A potential $V(X)$ with asymptotic regions I and II.

(5.7), they found that the saddle-points explained above, namely the ones associated with the complex-time solution, indeed lead to saddle-points in the T -plane [we shall call these “physical saddle-points”]. They, however found more: there are saddle-points that are *not* associated with any solutions of equations of motion (unphysical ones), and also singularities due to the periodicities. Deforming the T -integration path to avoid singularities, they found that the path indeed goes through only the physical saddle-points. As a result, the weights and phases in (5.9) are determined, which leads to the correct WKB result.

In the case of a double-well potential, the deformation of the integration contour is not specified, which is understandable in view of the fact that the analytic structure of (5.2) in complex T -plane is fairly complicated. The claim made in the literatures is simply that the contour passes all saddle-points that correspond to classical trajectories with weights that are extracted from the above calculation.

The problem lies in the fact that we do not know the contour which passes all physical saddle-points that are distributed in complex-time plane. Because of this, we cannot determine the weights of the saddle-points. In the case when x_i and x_f are in the forbidden region on the right side of the double-well potential as depicted in Fig. 22, saddle-points in complex T -plane are given by

$$T_s = \pm T(b_2, x_i) \pm T(b_2, x_f) + lT(a_1, b_1) + mT(b_1, a_2) + nT(a_2, b_2) \quad (5.10)$$

$$l, m, n = 0, \pm 1, \pm 2, \dots, \quad (5.11)$$

where

$$T(x, y) = 2 \int_x^y \frac{dx'}{\sqrt{2(E - V(x'))}}. \quad (5.12)$$

Notice that $T(x, y)$ is pure imaginary if (x, y) is in a forbidden region. These saddle-points T_s are shown as solid circles in Fig. 23. The unphysical saddle-points are also shown as open circles in the same figure. We know of no contour which passes only the physical ones and avoids the unphysical ones. Thus so far the complex-time method has not been worked out for the double-well and more complicated potentials.

5.2. Green function and the WKB wavefunctions

We shall examine the Green functions by using the complete orthonormal set of the eigenfunctions $\{|\psi_n\rangle\}$ of H . For example, the retarded Green function in (5.3), (5.4) is written as

$$G^R(x_i, x_f; E) = \sum_n \frac{\langle x_f | \psi_n \rangle \langle \psi_n | x_i \rangle}{E + i\delta - \lambda_n}, \quad (5.13)$$

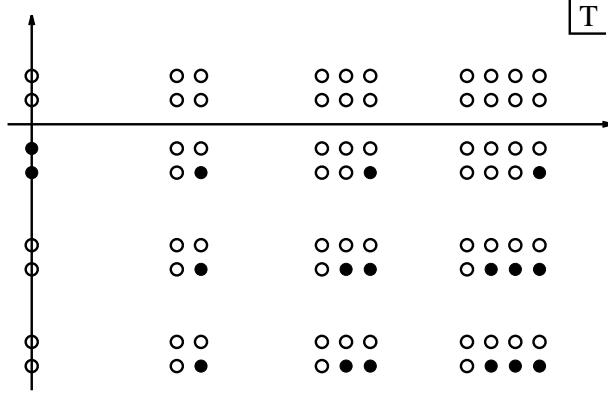


Fig. 23. Positions of saddle-points in complex T -plane.

where the sum over the complete set is actually made of the integration over the continuum spectrum and sum over the discrete bound states.

In order to study the Green functions in the asymptotic region, we use the WKB approximation for the wavefunctions $\psi(x) = \langle x|\psi\rangle$. For a state with the eigenvalue λ in the continuum spectrum, the second-order WKB approximation yields the following;

$$\psi_\lambda(x) = \frac{1}{\sqrt{2\pi p(x)}} \times \begin{cases} \left(A_\lambda e^{i \int_x^{x_1} p(x') dx'} + B_\lambda e^{-i \int_x^{x_1} p(x') dx'} \right), & \text{for } x \in \text{I}, \\ \left(C_\lambda e^{-i \int_x^{x_2} p(x') dx'} + D_\lambda e^{i \int_x^{x_2} p(x') dx'} \right), & \text{for } x \in \text{II}, \end{cases} \quad (5.14)$$

where $p(x) = \sqrt{2(\lambda - V(x))}$. We choose the limits x_1 and x_2 of the integrations to be the nearest turning points for definiteness. Among the coefficients A , B , C , and D , only two are independent. Their inter-relation is linear due to the superposition principle and can be written as follows⁴⁴);

$$\begin{pmatrix} A_\lambda \\ B_\lambda \end{pmatrix} = S(\lambda) \begin{pmatrix} C_\lambda \\ D_\lambda \end{pmatrix}. \quad (5.15)$$

The 2×2 matrix $S(\lambda)$ is determined by the shape of the potential $V(x)$ in the intermediate region between x_1 and x_2 . The flux conservation law is satisfied for the Schrödinger equation;

$$\frac{d}{dx} j = 0, \quad j = \frac{i}{2} \left(\frac{d\psi^*}{dx} \psi - \psi^* \frac{d\psi}{dx} \right). \quad (5.16)$$

Substituting the WKB expression (5.14) into the above, we find that

$$j = \frac{1}{2\pi} (|A|^2 - |B|^2) = \frac{1}{2\pi} (|C|^2 - |D|^2). \quad (5.17)$$

This results in the following relation between the matrix elements of $S(\lambda)$;

$$|S_{11}|^2 - |S_{21}|^2 = 1, \quad |S_{12}|^2 - |S_{22}|^2 = 1, \quad (5.18)$$

$$S_{11}^* S_{12} - S_{21}^* S_{22} = 0. \quad (5.19)$$

As a result, the matrix $S(\lambda)$ is parameterized by three real functions $\alpha(\lambda)$, $\beta(\lambda)$, and $\rho(\lambda)$ as follows;

$$S(\lambda) = \begin{pmatrix} e^{i\alpha} \cosh \rho & e^{i\beta} \sinh \rho \\ e^{-i\beta} \sinh \rho & e^{-i\alpha} \cosh \rho \end{pmatrix}. \quad (5.20)$$

For a given eigenvalue λ , there are two independent eigenfunctions. In order to construct them, we look at the inner-product of the eigenfunction $\psi_\lambda(x)$ with coefficients $(A_\lambda, B_\lambda, C_\lambda, D_\lambda)$ and another eigenfunction $\tilde{\psi}_{\lambda'}(x)$ with $(\tilde{A}_{\lambda'}, \tilde{B}_{\lambda'}, \tilde{C}_{\lambda'}, \tilde{D}_{\lambda'})$. Integration in the asymptotic regions determines the coefficient of the delta function $\delta(\lambda - \lambda')$ completely, as the delta function can come only from the infinite integrations. [In order to calculate the finite terms we need to solve the Schrödinger equation completely. But this is not necessary for the current purpose.] In fact, integration in the region II yields,

$$\begin{aligned} \int_{x_2}^{\infty} dx \psi_\lambda^*(x) \tilde{\psi}_{\lambda'}(x) &= \frac{1}{2\pi} \int_{x_2}^{\infty} \frac{dx}{\sqrt{p(x)p'(x)}} \\ &\times \left(C_\lambda^* \tilde{C}_{\lambda'} e^{i \int_{x_2}^x (p(x') - p'(x')) dx'} + D_\lambda^* \tilde{D}_{\lambda'} e^{-i \int_{x_2}^x (p(x') - p'(x')) dx'} \right. \\ &\left. + C_\lambda^* \tilde{D}_{\lambda'} e^{i \int_{x_2}^x (p(x') + p'(x')) dx'} + D_\lambda^* \tilde{C}_{\lambda'} e^{-i \int_{x_2}^x (p(x') + p'(x')) dx'} \right), \end{aligned} \quad (5.21)$$

As we are interested in the singularity of the above for $\lambda = \lambda'$, we expand the exponent using the following for $\lambda \sim \lambda'$,

$$p(x') - p'(x') \simeq \frac{(\lambda - \lambda')}{p(x')}. \quad (5.22)$$

By using a new coordinate y defined by $dy = dx/p(x)$, we find the contribution from the first two terms to the delta function;

$$\begin{aligned} \int_{x_2}^{\infty} dx \psi_\lambda^*(x) \tilde{\psi}_{\lambda'}(x) &= \frac{1}{2\pi} \int_{y_2}^{\infty} dy \left(C_\lambda^* \tilde{C}_\lambda e^{i(\lambda - \lambda')(y - y_2)} + D_\lambda^* \tilde{D}_\lambda e^{-i(\lambda - \lambda')(y - y_2)} \right) + \dots \\ &= \frac{1}{2} \left(C_\lambda^* \tilde{C}_\lambda + D_\lambda^* \tilde{D}_\lambda \right) \delta(\lambda - \lambda') + \dots, \end{aligned} \quad (5.23)$$

where we have neglected all the finite terms. Doing the similar calculation for the region I, we find

$$\int_{-\infty}^{\infty} dx \psi_\lambda^*(x) \tilde{\psi}_{\lambda'}(x) = \frac{1}{2} \left(A_\lambda^* \tilde{A}_\lambda + B_\lambda^* \tilde{B}_\lambda + C_\lambda^* \tilde{C}_\lambda + D_\lambda^* \tilde{D}_\lambda \right) \delta(\lambda - \lambda'). \quad (5.24)$$

Using the above result, we choose our orthonormal eigenfunctions for a given λ as the following;

$$(A_\lambda, B_\lambda, C_\lambda, D_\lambda)^{(1)} = \left(\frac{e^{i\alpha}}{\cosh \rho}, 0, 1, -e^{i(\alpha-\beta)} \tanh \rho \right), \quad (5.25)$$

$$(A_\lambda, B_\lambda, C_\lambda, D_\lambda)^{(2)} = \left(e^{i(\alpha+\beta)} \tanh \rho, 1, 0, \frac{e^{i\alpha}}{\cosh \rho} \right). \quad (5.26)$$

[The above corresponds to two incoming states. There are of course other choices, such as stationary states, but all of those reads to the same result for the Feynman kernel.]

Let us first look at the case when both x_i and x_f are in an allowed region in II. From (5.25) and (5.26), we find that

$$\sum_{i=1,2} \psi_\lambda^{(i)}(x_f) \psi_\lambda^{(i)*}(x_i) = \frac{1}{2\pi \sqrt{p(x_i)p(x_f)}} \quad (5.27)$$

$$\times \left[e^{i \int_{x_i}^{x_f} p(x') dx'} - e^{i \left(\int_{x_2}^{x_i} p(x') dx' + \int_{x_2}^{x_f} p(x') dx' \right)} e^{i(\alpha-\beta)} \tanh \rho + (\text{c.c.}) \right] \quad (5.28)$$

$$(5.29)$$

The complex conjugate part can be understood as the same function below the cut on the real-axis of the complex λ -plane (see Fig. 24). This is guaranteed by the fact that as λ moves below the cut, the role of the coefficients A and B is exchanged and likewise for C and D , and as a result, the phases α and β change their signs, while ρ does not. Therefore the sum over the continuous spectra in the Feynman kernel (5.13) is written as the following λ -integration;

$$G^R(x_i, x_f; E) = \frac{1}{2\pi} \int_C d\lambda \frac{1}{E + i\delta - \lambda} \frac{1}{\sqrt{p(x_i)p(x_f)}}$$

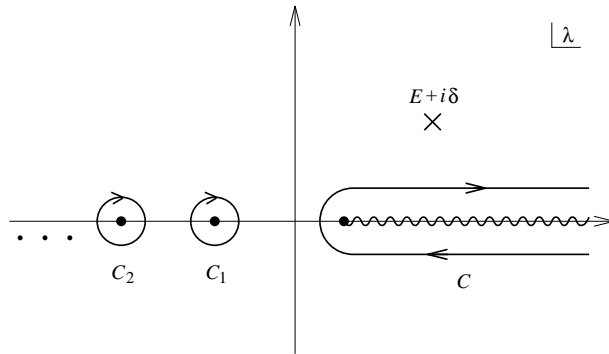


Fig. 24. The complex-plane of the eigenvalue λ . The cut on the real-axis is the continuous spectra and the poles are the bound states.

$$\times \begin{cases} e^{i \int_{x_2}^{x_i} p(x') dx'} \left[e^{-i \int_{x_2}^{x_f} p(x') dx'} - e^{i \int_{x_2}^{x_f} p(x') dx'} e^{i(\alpha-\beta) \tanh \rho} \right] & \text{for } x_i > x_f, \\ e^{i \int_{x_2}^{x_f} p(x') dx'} \left[e^{-i \int_{x_2}^{x_i} p(x') dx'} - e^{i \int_{x_2}^{x_i} p(x') dx'} e^{i(\alpha-\beta) \tanh \rho} \right] & \text{for } x_f > x_i. \end{cases} \quad (5.30)$$

The integration contour C in the complex λ -plane is as in Fig. 24. In (5.30), we have chosen the integrand so that it converges for $|\lambda| \rightarrow \infty$, which we need later. As for the discrete spectrum, it is determined by the absence of the diverging behavior of the wavefunction, which translates into the condition that for $C = 0$, $A = 0$. From (5.20), we thus find that $\sinh \rho = 0$ when λ is equal to a discrete eigenvalue of H . This allows us to write the sum over the discrete spectra as pole integrations of the second term in (5.30) depicted in Fig. 24. Connecting all the contours and closing it at the infinity, we find that the whole contour enclose the pole at $\lambda = E + i\delta$. Thus we end up with the expression

$$G^R(x_i, x_f; E) = -\frac{i}{\sqrt{p(x_i)p(x_f)}} \quad (5.31)$$

$$\times \begin{cases} e^{i \int_{x_2}^{x_i} p(x') dx'} \left(e^{-i \int_{x_2}^{x_f} p(x') dx'} + iR e^{i \int_{x_2}^{x_f} p(x') dx'} \right) & \text{for } x_i > x_f, \\ e^{i \int_{x_2}^{x_i} p(x') dx'} \left(e^{-i \int_{x_2}^{x_f} p(x') dx'} + iR e^{i \int_{x_2}^{x_f} p(x') dx'} \right) & \text{for } x_f > x_i, \end{cases} \quad (5.32)$$

where we defined the ‘‘reflection coefficient’’ R by the following,

$$R = i \frac{S_{21}}{S_{22}} = i e^{i(\alpha-\beta) \tanh \rho}. \quad (5.33)$$

We note that this expression (5.32) is valid for a general value of E with proper analytic continuation of the coefficients. Therefore, if any end-points are in a forbidden region, simple analytic continuation of (5.32) is appropriate. We shall use this result in the next subsection.

5.3. Reduction formula and its expansion

In this subsection, we derive a formula for evaluating the Green function in a system with an arbitrary potential to which we can apply the WKB approximation. We consider a general potential which has arbitrary number of wells, and show that the Green function is given by summing up all contributions of classical paths.

Let us consider the case when x_i and x_f lie in the forbidden region on the same sides of the wells. The potential which has n wells is depicted in Fig. 25. By the analytical continuation of (5.32) in E , we find the retarded resolvent in the following form;

$$G^R(x_i, x_f; E) = -|p(x_i)p(x_f)|^{-1/2} e^{-\Delta_i} \left(e^{\Delta_f} + iR_n e^{-\Delta_f} \right), \quad (5.34)$$

where

$$\Delta_{i,f} \equiv \int_{b_n}^{x_{i,f}} dx |p(x)|. \quad (5.35)$$

In order to specify the fact that this expression is for n wells, we attach the subscript (n) to the coefficients hereafter.

Due to the existence of the intermediate region (b_{n-1}, a_n) , the matrix $S^{(n)}$, which connects the regions I and II, can be written in terms of the matrices $S^{(n-1)}$ that connects regions I and (b_{n-1}, a_n) and \tilde{S} for (b_{n-1}, a_n) and II. If we apply the linear WKB connection formula for the latter region, which we can obtain from the saddle-point method for a linear potential, we obtain the following;

$$S^{(n)}(E) = S^{(n-1)}(E) \begin{pmatrix} e^{-\Delta_{n-1}} & 0 \\ 0 & e^{\Delta_{n-1}} \end{pmatrix} \begin{pmatrix} \frac{i}{2} & -\frac{i}{2} \\ 1 & 1 \end{pmatrix} \quad (5.36)$$

$$\times \begin{pmatrix} e^{-i(W_n + \frac{\pi}{2})} & 0 \\ 0 & e^{i(W_n + \frac{\pi}{2})} \end{pmatrix} \begin{pmatrix} \frac{1}{2} & i \\ \frac{1}{2} & -i \end{pmatrix} \quad (5.37)$$

$$= S^{(n-1)}(E) \begin{pmatrix} \frac{1}{2}e^{-\Delta_{n-1}} \cos W_n & e^{-\Delta_{n-1}} \sin W_n \\ -e^{\Delta_{n-1}} \sin W_n & 2e^{\Delta_{n-1}} \cos W_n \end{pmatrix}, \quad (5.38)$$

where W_n and Δ_{n-1} are defined by,

$$W_n = \int_{a_n}^{b_n} dx |p(x)|, \quad (5.39)$$

$$\Delta_{n-1} = \int_{b_{n-1}}^{a_n} dx |p(x)|. \quad (5.40)$$

Therefore, we find the relations;

$$S_{21}^{(n)} = \frac{1}{2} S_{21}^{(n-1)} e^{-\Delta_{n-1}} \cos W_n - S_{22}^{(n-1)} e^{\Delta_{n-1}} \sin W_n, \quad (5.41)$$

$$S_{22}^{(n)} = S_{21}^{(n-1)} e^{-\Delta_{n-1}} \sin W_n + 2S_{22}^{(n-1)} e^{\Delta_{n-1}} \cos W_n. \quad (5.42)$$

From (5.33), (5.41) and (5.42), we find that R_n can be written as the following;

$$R_n = \frac{i}{2} \frac{-\sin W_n - \frac{i}{2} e^{-2\Delta_{n-1}} R_{n-1} \cos W_n}{\cos W_n - \frac{i}{2} e^{-2\Delta_{n-1}} R_{n-1} \sin W_n}. \quad (5.43)$$

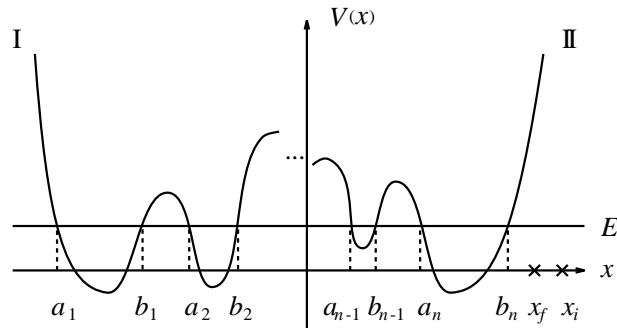


Fig. 25. A potential with n wells we consider. The turning points are denoted by a_i and b_i , for left and right of the i -th well, respectively ($i = 1 \sim n$).

We find it most convenient to rewrite this to the following two expressions;

$$R_n = \frac{1}{2} \frac{1 - \tilde{R}_n e^{2iW_n}}{1 + \tilde{R}_n e^{2iW_n}}, \quad (5.44)$$

$$\tilde{R}_n = \frac{1 - \frac{1}{2} R_{n-1} e^{-2\Delta_{n-1}}}{1 + \frac{1}{2} R_{n-1} e^{-2\Delta_{n-1}}}. \quad (5.45)$$

Defined in this manner, the function R_{n-1} corresponds to the reflection amplitude at the turning point b_{n-1} .

In order to see the correspondence between these expressions and the saddle-point method, let us expand (5.44) in an infinite series as follows;

$$iR_n = \frac{i}{2} + (-i\tilde{R}_n) e^{2iW_n} + (-i\tilde{R}_n)^2 (-i) e^{4iW_n} + \dots \quad (5.46)$$

The convergence of this series is guaranteed by the implicit factor $i\delta$. The retarded resolvent is then,

$$\begin{aligned} G^R(x_i, x_f; E) &= -|p(x_i)p(x_f)|^{-1/2} \\ &\times \left[e^{-(\Delta_i - \Delta_f)} + \left\{ \frac{i}{2} + (-i\tilde{R}_n) e^{2iW_n} + (-i\tilde{R}_n)^2 (-i) e^{4iW_n} + \dots \right\} e^{-(\Delta_i + \Delta_f)} \right]. \end{aligned} \quad (5.47)$$

This is the expression to be compared to the saddle-point expression (5.7). If we choose T to be negative imaginary, $-i\tau$, the factor in the exponent is,

$$i(ET + S_{cl}) = E\tau - S_E = - \int d\tau \left(\frac{dx}{d\tau} \right)^2 = - \int dx |p(x)|. \quad (5.48)$$

Therefore, the two factors $\Delta_{i,f}$ is equal to the above quantity for the path from $x_{i,f}$ to the turning point b_n . The first term in (5.47) corresponds the contribution of the pure-imaginary-time path that starts from x_i and reaches x_f directly. The factor $e^{-(\Delta_i + \Delta_f)}$ in the rest of the terms is for the path from x_i to the turning point b_n and then from b_n to x_f . The expansion of iR_n is understood as contributions of the paths that oscillate in the allowed region (a_n, b_n) . Various factors have unique interpretations as factors coming from the turning points. This is most conveniently depicted in Fig. 26. Similarly to (5.46), the expression (5.45) is expanded as the following,

$$-i\tilde{R}_n = -i + (iR_{n-1}) e^{-2\Delta_{n-1}} + (iR_{n-1})^2 \left(\frac{i}{2}\right) e^{-4\Delta_{n-1}} + \dots \quad (5.49)$$

The corresponding diagrams are illustrated in Fig. 27.

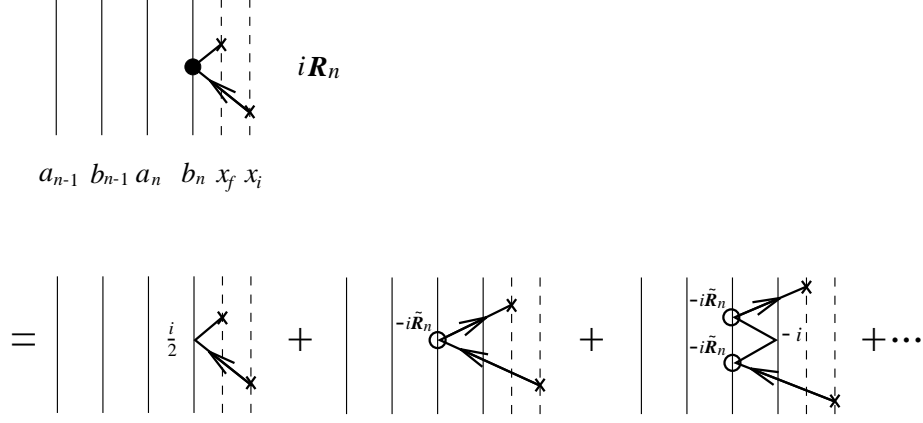


Fig. 26. Diagrammatic representation of the expansion of iR_n . The information of the region left of a_n is contained in $-i\tilde{R}_n$.

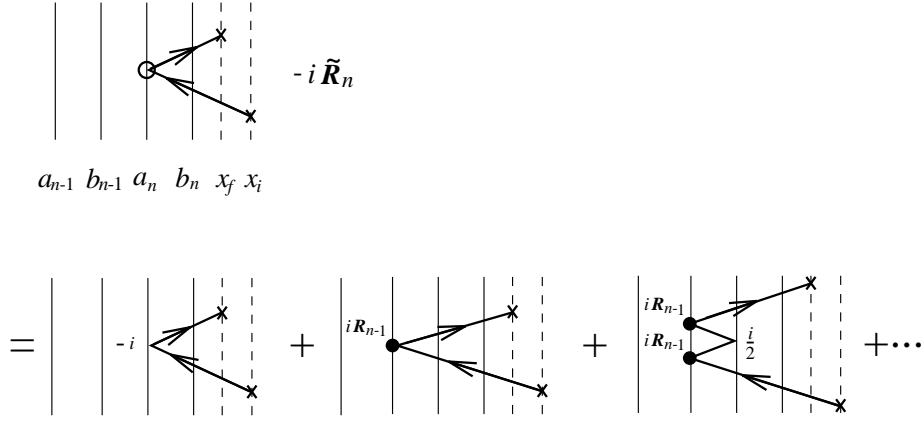


Fig. 27. Diagrammatic representation of the expansion of $-i\tilde{R}_n$. The each path corresponds to a group of paths with different number of oscillation in the forbidden region (b_{n-1}, a_n) .

We have so far derived the expressions that results from the WKB approximation for the n -th well. This procedure can be applied recursively for the rest of the wells. At the end, we are left with R_1 , which is given by

$$iR_1 = \frac{1}{2} \tan W_1 = \frac{i}{2} + (-i) e^{-2iW_1} + (-i)^3 e^{-4iW_1} + \dots, \quad (5.50)$$

where W_1 is defined by (5.39) by replacing n with 1. Therefore we find that R_1 is expressed as a sum of the contribution of the classical paths which evolve in the first well.

Combining (5.47), (5.49), and (5.50), we find all complex-time paths are included in the expression of the resolvent G^R . Therefore, the resulting Green function in a n -well potential is given by

$$G^R(x_i, x_f; E) = -|p(x_i)p(x_f)|^{-1/2} \sum_{x_{cl}} f(x_{cl}) e^{iW(x_i, x_f; E)}. \quad (5.51)$$

where $f(x_{cl})$ is determined by the number of reflections and transmissions which the classical path contains, and $W(x_i, x_f; E)$ is determined by what wells the path crosses and what barriers it tunnels through. The rules for calculating $f(x_{cl})$ is the following: When a path has a reflection in the allowed region, it obtains $-i$. In the case of a reflection in the forbidden region, it gets $i/2$.

Let us next examine the case when x_i, x_f are on opposite sides of the wells. Applying the analysis similar to the one in the previous section, we find that the Green function is expressed as follows;

$$G^R(x_i, x_f; E) = -|p(x_i)p(x_f)|^{-1/2} T_n e^{-\Delta_i - \Delta_f} . \quad (5.52)$$

where T_n is the (analytically-continued) transmission amplitude

$$T_n = \frac{1}{S_{22}^{(n)}} . \quad (5.53)$$

Just as the previous case, we can express T_n in terms of T_{n-1} as in the following;

$$T_n = \frac{1}{S_{21}^{(n-1)} e^{-\Delta_{n-1}} \sin W_n + 2S_{22}^{(n-1)} e^{\Delta_{n-1}} \cos W_n} \quad (5.54)$$

$$= \frac{T_{n-1} e^{-\Delta_{n-1} + iW_n}}{1 + \frac{1}{2} R_{n-1} e^{-2\Delta_{n-1}} + e^{2iW_n} \left(1 - \frac{1}{2} R_{n-1} e^{-2\Delta_{n-1}}\right)} \quad (5.55)$$

$$= \frac{e^{-\Delta_{n-1}}}{1 + \frac{1}{2} R_{n-1} e^{-2\Delta_{n-1}}} \frac{e^{iW_n}}{1 + \tilde{R}_n e^{2iW_n}} T_{n-1} . \quad (5.56)$$

In the above, we have used (5.33), (5.42) and (5.45). Let us show that T_n consists of all contributions of classical paths. The second factor in (5.56) is expanded in the following way,

$$\frac{e^{iW_n}}{1 + \tilde{R}_n e^{2iW_n}} = e^{iW_n} + (-i)(-i\tilde{R}_n) e^{3iW_n} + (-i)^2(-i\tilde{R}_n)^2 e^{5iW_n} + \dots , \quad (5.57)$$

which corresponds to the diagrams in Fig. 28 (a). The first factor in (5.56) is expanded as,

$$\frac{e^{-\Delta_{n-1}}}{1 + \frac{1}{2} R_{n-1} e^{-2\Delta_{n-1}}} = e^{-\Delta_{n-1}} + \left(\frac{i}{2}\right)(iR_{n-1}) e^{-3\Delta_{n-1}} + \left(\frac{i}{2}\right)^2(iR_{n-1})^2 e^{-5\Delta_{n-1}} + \dots \quad (5.58)$$

which is illustrated in Fig. 28 (b). As the previous case, repeating this procedure, we reach T_1 , which is given by

$$T_1 = \frac{1}{2 \cos W_1} \quad (5.59)$$

$$= e^{iW_1} + (-i)^2 e^{3iW_1} + (-i)^4 e^{5iW_1} + \dots . \quad (5.60)$$

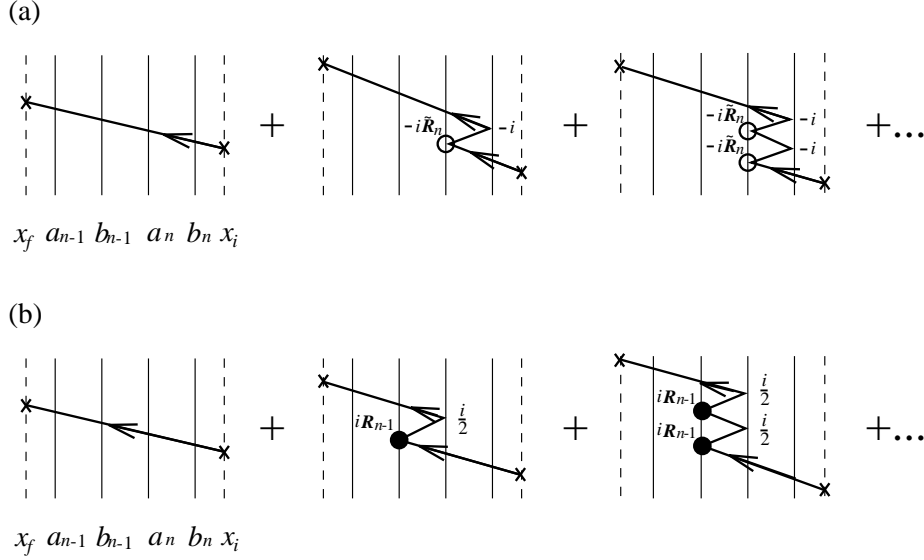


Fig. 28. Classical paths traversing in the n -th well and tunneling through the $(n - 1)$ -th barrier.

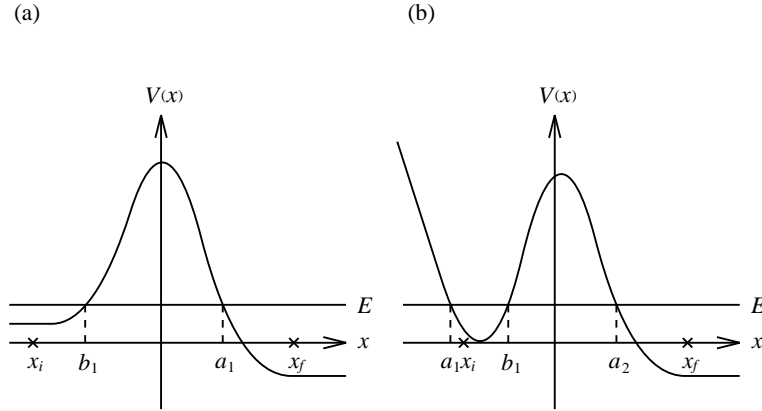


Fig. 29. A scattering process against a potential barrier and a metastable system.

Therefore we conclude that T_n consists of all contributions of classical paths.

The above analysis can be applied to other cases with various locations of x_i and x_f . Thus we verify that thus constructed resolvent can be always interpreted as sum over the complex-time classical paths.

This formalism is valid for a scattering process and metastable system (Fig. 29) as well as for a stationary system. It is apparent from this derivation that this complex-time method reproduces the result of the WKB approximation with the linear connection formula. The potential we consider is given in Fig. 29 (b). The turning points are labeled in the figure by a_1 , b_1 , and a_2 . First we consider the case when x_i is in the well and x_f is outside of the

barrier. The analysis similar to the above yields the Green function as in the following;

$$G^R(x_i, x_f; E) = -i|p(x_i)p(x_f)|^{-1/2} \frac{(e^{-iW_i} - ie^{iW_i}) e^{iW_1 - \Delta_1 + iW_f}}{(1 + \tilde{R}e^{2iW_1})(1 + \frac{1}{4}e^{-2\Delta_1})}, \quad (5.61)$$

where \tilde{R} is given by

$$-i\tilde{R} = -i \frac{1 - \frac{1}{4}e^{-2\Delta_1}}{1 + \frac{1}{4}e^{-2\Delta_1}} \quad (5.62)$$

$$= -i + \frac{i}{2}e^{-2\Delta_1} + \left(\frac{i}{2}\right)^3 e^{-4\Delta_1} + \dots \quad (5.63)$$

From (5.61) and (5.63), we find again that the resolvent is equal to the sum over the physical saddle-points. We find that the poles of the Green function are determined by the following;

$$1 + e^{2iW_1} + \frac{1}{4}e^{-2\Delta_1} (1 - e^{2iW_1}) = 0. \quad (5.64)$$

Let us solve this equation iteratively. Then we obtain

$$W_1(E) = \left(n + \frac{1}{2}\right) \pi - \frac{i}{4}e^{-2\Delta_1}. \quad (5.65)$$

From (5.65), we find an imaginary part of the energy eigenvalue

$$\text{Im } E_n = -\frac{i}{2T(E_n)}e^{-2\Delta_1}, \quad (5.66)$$

where $T(E_n)$ is the period of the classical path between the turning points a_1, b_1

$$T(E) = 2 \int_{a_1}^{b_1} \frac{dx}{\sqrt{2(E - V(x))}}. \quad (5.67)$$

We find the decay rate of this metastable system. We note that the factor $1/2$ in (5.66) comes from the weight $1/2^n$ of the saddle-points with n reflections in the forbidden region.

Let us apply this method to a scattering process against a potential barrier in Fig. 29 (a). When x_i and x_f are separated by the barrier, the Green function is given by

$$\begin{aligned} G^R(x_i, x_f; E) &= -i|p(x_i)p(x_f)|^{-1/2} \tilde{T} e^{i(W_i + W_f)} \\ &= -i|p(x_i)p(x_f)|^{-1/2} \sum_{k=1}^{\infty} e^{i(W_i + W_f) - (2k-1)\Delta_1} \left(\frac{i}{2}\right)^{2(k-1)}, \end{aligned} \quad (5.68)$$

where we have used the WKB expression for the transmission coefficient \tilde{T} ;

$$\tilde{T} = \frac{e^{-\Delta_1}}{1 + \frac{1}{4}e^{-2\Delta_1}}. \quad (5.69)$$

When x_i and x_f are on the same side, the Green function is given by

$$\begin{aligned} G^R(x_i, x_f; E) &= -i|p(x_i)p(x_f)|^{-1/2}e^{iW_i} \left[e^{-iW_f} - i\tilde{R}e^{iW_f} \right] \\ &= -i|p(x_i)p(x_f)|^{-1/2}e^{iW_i} \left[e^{-iW_f} + \frac{i}{2}e^{iW_f} + \sum_{k=1}^{\infty} e^{iW_f-2k\Delta_1}(-i)^{2k-1} \right], \end{aligned} \quad (5.70)$$

where we have used the expression for the reflection amplitude,

$$-i\tilde{R} = -i \frac{1 - \frac{1}{4}e^{-2\Delta_1}}{1 + \frac{1}{4}e^{-2\Delta_1}}. \quad (5.71)$$

The coefficients \tilde{T} and \tilde{R} satisfy the unitarity condition

$$|\tilde{T}|^2 + |\tilde{R}|^2 = 1. \quad (5.72)$$

We again confirm the validity of the sum over the physical saddle-points. The weight $1/2^n$ is crucial for (5.72).

We have given the re-formulation of the complex-time method. In quantum mechanics, using the connection formula for the wavefunctions, we constructed the reduction formula in the number of the turning points for the Green function. This yields series expansions, which can be understood as sum over in the classical complex-time trajectories. This is understood as a sum over the physical saddle-points with specific weights and phases in the path-integral method. This shows the validity of the method proposed before, in the context of the path-integral method. We confirmed that this method yields results identical with that of the WKB approximation. Thus our construction gives solid basis for the starting point of the complex-time method.

We must elaborate this complex-time formalism so that it could be applied to field theory and two-particle scattering process. Thus somewhat different analysis may be required. One of them could be the combination of the valley method and the current complex-time method. The valley method can be used to identify the imaginary-time tunneling paths, which are converted to collective coordinates. Thus, while the incoming particle are expressed in real-time expressions, the tunneling part may be obtained as the imaginary part of the complex-time development along the valley trajectory. There are rather interesting possibilities along this line, which should be further investigated.

§6. Asymptotic analysis of the perturbation theory

The tunneling phenomenon has some subtle relation to the large order behavior of the perturbative series of the theory. Dyson argued⁴⁵⁾ that the perturbative series in QED is

an asymptotic series. Later, more accurate estimates of the large order behavior of the perturbative series were carried out in many models.⁴⁶⁾ Although asymptotic series are divergent, it allows summation techniques, such as Borel summation and Padé approximation. In theories with tunneling phenomena, the perturbative series, however, are generally not Borel-summable. In such a case, the Borel integral encounters singularities, which are related to the existence of the nonperturbative tunneling phenomena. Therefore, only after the perturbative and nonperturbative effects are combined the physical quantities are well-defined.

The consideration of the valley, described in detail in this paper, provides an insight into this interplay between the perturbative and non-perturbative contributions to path-integral: In the context of the the high energy behavior of the B and L violating amplitude considered in section 2, we have noted that the contribution of the configuration which has an instanton and an anti-instanton in small separation compared with their size become important. Since this configuration merges into the vacuum continuously, it implies that the perturbative and non-perturbative contributions transmute into each other in this configuration. This situation casts a doubt against our intuitive understanding that there must be a clear separation between the two. For the full understanding of the tunneling phenomena, we consider it necessary to understand this situation. Approaches in this section provide some possible direction for progress. In the first subsection, we show that the valley calculation provides an easy way to evaluate the large order behavior of the perturbative expansion in a model in quantum mechanics.⁴⁷⁾ In the second subsection, the asympton theory, which is an analysis of the perturbative functional, not just the coefficients, is presented.

6.1. *Borel function in the valley method*

We consider the symmetric double-well potential

$$V(\phi; g) = \frac{1}{2}\phi^2(1 - g\phi)^2 \quad (6.1)$$

and evaluate the transition amplitude $\langle 0|e^{-HT}|0\rangle$ by the path-integral Eq. (4.2). We are interested in the perturbative expansion of

$$Z(g^2) \equiv \frac{\langle 0|e^{-HT}|0\rangle}{\langle 0|e^{-H_0T}|0\rangle}, \quad (6.2)$$

($H_0 \equiv (1/2)[p^2 + \phi^2]$ the free part of the Hamiltonian) or the energy shift $E(g^2)$ of the ground state due to the interaction, which is evaluated by

$$E(g^2) = -\lim_{T \rightarrow \infty} \frac{1}{T} \ln Z(g^2). \quad (6.3)$$

The time T is taken sufficiently large, compared with the inverse of the excitation energies.

The perturbative series of $Z(g^2)$ in the present model is a power series in g^2

$$Z_{\text{pert}}(g^2) = 1 + \sum_{n=1}^{\infty} Z_n g^{2n}. \quad (6.4)$$

The coefficient Z_n are evaluated by expanding the action in powers of g ,

$$e^{-S[\phi;g]} = \sum_n g^n F_n[\phi], \quad S[\phi;g] \equiv \int_0^T d\tau \left[\frac{1}{2} (\dot{\phi})^2 + V(\phi;g) \right] \quad (6.5)$$

and path-integrating each term,

$$Z_n = \frac{\int \mathcal{D}\phi F_{2n}[\phi]}{\int \mathcal{D}\phi e^{-S_0[\phi]}}, \quad (6.6)$$

in the background $\phi_B \equiv 0$, where S_0 is the action for the harmonic oscillator

$$S_0 = \int_0^T d\tau \frac{1}{2} \left[(\dot{\phi})^2 + \phi^2 \right]. \quad (6.7)$$

Note that the functional $F_n[\phi]$ with odd n has odd powers of ϕ and gives no contribution. Although Z_n are well-defined objects, the infinite series (6.4) does not converge; (27), (28), (45), (48), (49), (50) it is known to be asymptotic to $Z(g^2)$.

The Borel summation method is a powerful one to analyze the asymptotic series Eq. (6.4). To apply the method, we first calculate the Borel function $B(t)$ defined by a series

$$B(t) = \sum_n \frac{Z_n}{n!} t^n. \quad (6.8)$$

$Z(g^2)$ is recovered, at least formally, by the integral

$$Z(g^2) = \int_0^\infty dt e^{-t} B(tg^2) = \frac{1}{g^2} \int_0^\infty dt e^{-t/g^2} B(t) \quad (6.9)$$

since

$$\int_0^\infty dt e^{-t} t^n = n!. \quad (6.10)$$

Note the series (6.8) has wider region of convergence in the complex t -plane than the series (6.4) has in g^2 -plane. This may give a chance to get a meaningful answer even from the non-convergent series.

We intend to calculate the Borel function of the present model not by the series expansion (6.8), but in a rather direct way using the valley method. It is well-known that the present model possesses the instanton (I) and anti-instanton (\bar{I}), the solutions of the Euclidean equation of motion that travel between $\phi = 0$ and $\phi = 1/g$. Applying the proper valley equation, we have further found there exist the valley trajectory that starts as a small fluctuation at the vacuum and reaches to the I- \bar{I} pair at the end.¹¹⁾ We first approximate

$Z(g^2)$ to an integral over the valley trajectory $\phi_V(\alpha)$, where α can be any variable that parameterize the valley. In another word, we adopt a line $\phi_V(\alpha)$ in the functional space as the background for calculating $Z(g^2)$, instead of using a single point ϕ_B as in the perturbative calculation. The explicit expression as the collective coordinate integral is obtained by the Faddeev-Popov (FP) method as explained in section 3. To avoid the cumbersome g dependence in the background valley $\phi_V(\alpha)$, we rescale S and ϕ as

$$\phi \rightarrow g\phi \quad (6.11)$$

$$S[\phi; g] \rightarrow g^2 S[\phi]. \quad (6.12)$$

With this transformation, g drops out from the action and $\phi_V(\alpha)$ becomes g invariant. We now obtain

$$Z(g^2) = \int d\alpha e^{-S[\phi_V(\alpha)]/g^2} \left| \frac{dS[\phi_V(\alpha)]}{d\alpha} \right| \left| \frac{\delta S}{\delta\phi_V(\alpha)} \right|^{-1} \mathcal{Z}, \quad (6.13)$$

where

$$\begin{aligned} \mathcal{Z} = & \frac{\mathcal{N}}{(\sqrt{2\pi}g)\langle 0|e^{-H_0T}|0\rangle} \int [d\varphi]' \exp\left(-\frac{1}{2}(\varphi \cdot D(\alpha) \cdot \varphi) - S'_{\text{int}}[\varphi; g]\right) \\ & \times \left[1 - \frac{g(\varphi \cdot D(\alpha) \cdot d\phi_V(\alpha)/d\alpha)}{dS[\phi_V(\alpha)]/d\alpha} \right]. \end{aligned} \quad (6.14)$$

In Eq. (6.14), $\varphi \equiv g(\phi - \phi_V(\alpha))$ represents the fluctuations around ϕ_V , $[d\varphi]'$ is the functional measure except the mode parallel to $\delta S/\delta\phi$ that was removed by the FP method, $1/\sqrt{2\pi}g$ comes from this elimination, $D(\alpha)$ represents $\delta^2 S/\delta\phi_V^2(\alpha)$ and the abbreviation like $\varphi \cdot D(\alpha) \cdot \varphi$ stands for

$$\int_0^T d\tau d\tau' \frac{\delta^2 S}{\delta\phi_V(\alpha)(\tau)\delta\phi_V(\alpha)(\tau')} \varphi(\tau)\varphi(\tau'),$$

S'_{int} is the remaining action after the value at ϕ_V and the quadratic term $\varphi D\varphi$ are subtracted.

The trick of extracting the Borel function from Eq. (6.13) is to choose the parameter α as the value t of the action of the valley, so that $t = S[\phi_V(t)]$. Then Eq. (6.13) is written as

$$Z(g^2) = \int_0^{S_{\text{cl}}} dt e^{-t/g^2} \left| \frac{\delta S}{\delta\phi_V(t)} \right|^{-1} \mathcal{Z}, \quad (6.15)$$

where $S_{\text{cl}} = 1/3$ is the twice of the instanton action which the valley action cannot exceed. Note the resemblance of this expression to Eq. (6.9). The integrand

$$B_V(t) \equiv \left| \frac{\delta S}{\delta\phi_V(t)} \right|^{-1} \mathcal{Z} \quad (6.16)$$

is the approximation for the Borel function in terms of the valley method.

Although B_V is an approximation, it suffices to predict the large order behavior of the perturbative expansion. The bottom line is that the large order behavior is controlled by singularities of the Borel function in the complex t -plane and that the valley approximation B_V also reproduces them. The valley approaches asymptotically to the well-separated I- \bar{I} pair $\phi_{\bar{I}}(R)$ with R their separation. The action t behaves

$$t \simeq S_{\text{cl}} - \text{const} \times e^{-R} \quad (6.17)$$

at $\phi_{\bar{I}}$. There exists the normalized quasi-zero mode ϕ_R that causes variation of R , i.e. $\phi_R = (1/\eta)(d\phi_{\bar{I}}/dR)$, where η is the Jacobian between R and ϕ_R . The functional gradient is proportional to the quasi-zero mode according to the definition of our valley equation, $\phi_R = (\delta S/\delta\phi_V)/|\delta S/\delta\phi_V|$. Since $(\delta S/\delta\phi_V) \cdot (d\phi_{\bar{I}}/dR) = dt/dR$, we can conclude

$$\left| \frac{\delta S}{\delta\phi_V(t)} \right|^{-1} \simeq \frac{1}{\sqrt{12}(S_{\text{cl}} - t)}, \quad (6.18)$$

where we have used $\eta = \sqrt{1/12}$. The calculation of \mathcal{Z} is also simple at the well-separated I- \bar{I} pair; to the leading order in g^2 it is approximated to the product of the square of the single instanton determinant and the Jacobian for the overall translation,

$$\mathcal{Z} = \frac{1}{2\pi g^2} \frac{12}{\sqrt{3}} T. \quad (6.19)$$

(The calculations of the determinant and the Jacobian are found in Ref. 9.) Combining these, we obtain

$$B_V(t) \simeq \frac{T}{\pi g^2} \frac{1}{S_{\text{cl}} - t}. \quad (6.20)$$

This simple pole controls the large order behavior of the perturbative expansion of $Z(g^2)$. In fact, inserting its expansion $\sim (T/\pi g^2) \sum_n (S_{\text{cl}})^{-n-1} t^n$ into (6.15) and integrating it over to infinity (neglecting the upper bound), we obtain

$$Z_n \simeq \frac{T}{\pi} S_{\text{cl}}^{-n-1} n!, \quad (6.21)$$

or, for coefficients of perturbative expansion of $E(g^2)$ in powers of g^2 ,

$$E_n \simeq -\frac{1}{\pi} S_{\text{cl}}^{-n-1} n! \quad (6.22)$$

which coincides with the known results.⁴⁹⁾

The singularity of $B_V(t)$ at $t = S_{\text{cl}}$ indicates the non Borel-summability of the expansion. There will be an ambiguity depending on how we turn aside the pole when we perform a

contour integral corresponding to Eq. (6.9) if we only know $B(t)$ from the perturbative expansion. The advantage of using the valley method is that we now know the ambiguity is, at least in the present model, an artifact: the integral has the upper limit at $t = S_{\text{cl}}$. This understanding may provide us to construct a specific prescription to get unambiguous predictions from the perturbative expansion by properly taking into account the non-perturbative contributions in a class of models which is known to be non Borel-summable.*)

6.2. Asymptons

In this subsection, we look into the behavior of the perturbative functional, $F_n[\phi]$ in Eq. (6.5), in the functional space of path-integral and discuss it is dominated by a series of configurations, which we name ‘‘asymptons’’. We will show their contribution indeed reproduces the large order behavior of the perturbative series, which shows the fictitious nature of the non Borel-summability and provides us with the insight into the interplay between the perturbative and the non-perturbative effects.

In the first part of this subsection we present a general formalism for the analysis of the asymptons. Then a simple double-well quantum mechanical model are treated in the next part. The SU(2) gauge field theory is studied in the third part. Then the analysis of the asympton on the valley line is carried out. This subsection ends with the discussion on the consequences of the asymptons and on the summing methods.

6.2.1. General formalism for the asympton analysis

Let us use z_n for each coefficient in the perturbative expansion of a given model (not necessarily the symmetric double-well as in the previous section),

$$z_n = \frac{\int \mathcal{D}\phi F_n[\phi]}{\int \mathcal{D}\phi e^{-S_0[\phi]}}. \quad (6.23)$$

We note that the coefficients z_n are known to grow as a factorial of n for large n in a wide range of models while the expansion (6.5) is convergent for a given configuration ϕ as long as the integrals $\int d\tau(\phi)^m$ are convergent. Our aim here is to understand how this can happen. For this purpose we study the behavior of the functional $F_n[\phi]$ itself. The asympton theory answers this question.^{51), 52)}

The expression for $F_n[\phi]$ is complicated in general. In the limit $n \rightarrow \infty$, however, a compact expression can be obtained. The functional $F_n[\phi]$ is expressed as a contour integral in the complex g -plane as follows;

$$F_n[\phi] = \frac{1}{2\pi i} \oint \frac{dg}{g^{n+1}} e^{-S[\phi, g]} = \frac{1}{2\pi i} \oint \frac{dg}{g} e^{-\tilde{S}[\phi, g]}, \quad (6.24)$$

*) See Ref. 47) for the detailed discussion on this point.

where

$$\tilde{S}[\phi, g] = S[\phi, g] + n \log g. \quad (6.25)$$

We apply the saddle-point approximation to the g -integral (6.24) valid for large n .

In this subsection we deal with theories whose action is a second order polynomial of g , which we express as $S[\phi, g] = c_0[\phi] - gc_1[\phi] + g^2c_2[\phi]$. The saddle points of $\tilde{S}[\phi, g]$ are given by the following;

$$g_{\pm} = \frac{c_1}{4c_2}(1 \pm \sqrt{D}), \quad D \equiv 1 - \frac{8nc_2}{c_1^2}. \quad (6.26)$$

In order to examine the behavior of the perturbative functional, we divide the functional space of ϕ into two regions; the one with $D > 0$ and the one of $D < 0$, for the the expressions of $F_n[\phi]$ obtained in the saddle-point approximation are different depending on the sign of D . As was found in Ref. 51), 52), the region of negative D is of importance. We will concentrate on this case hereafter.

When $D < 0$ the saddle points are complex, which we denote by g_{\pm} as follows;

$$g_{\pm} = |g|e^{\pm i\theta}, \quad |g| = \sqrt{\frac{n}{2c_2}}, \quad \cos \theta = \frac{c_1}{\sqrt{8nc_2}}, \quad (6.27)$$

where $\theta \in [0, \pi/2]$. We obtain the following expressions at the saddle points g_{\pm} ;

$$S_{\pm} = c_0 - n - \frac{n}{2}e^{\pm 2i\theta}, \quad (6.28)$$

$$\tilde{S}_{\pm}'' = \frac{2n}{|g|^2} \sin \theta (\sin \theta \pm i \cos \theta). \quad (6.29)$$

Since $\text{Re}(\tilde{S}_{\pm}'') > 0$ at both saddle points, we choose the integration contour to go through both saddle point along the real axes. The contour integration yields the following expression;

$$F_n[\phi] = \frac{2}{\sqrt{2\pi}} \text{Im} \left[\frac{1}{\sqrt{\tilde{S}_{-}''} g_{-}^n} \frac{\exp(-S[\phi, g_{-}])}{g_{-}^n} \right]. \quad (6.30)$$

We stress here that g_{-} is a functional of ϕ and a function of n , defined by (6.27).

Let us look for peaks of $F_n[\phi]$ in order to understand its the large order behavior. Therefore we must solve the following equation:

$$\frac{\delta F_n[\phi]}{\delta \phi} = \frac{\partial F_n[\phi]}{\partial g_{-}} \Big|_{\phi} \frac{\delta g_{-}}{\delta \phi} + \frac{\delta F_n[\phi]}{\delta \phi} \Big|_{g_{-}} = 0. \quad (6.31)$$

At the leading order of \hbar (which we have neglected to write), the g_{-} derivative in the first term acts on \tilde{S} and is zero due to the saddle-point condition. At the same order, we get the

following expression by using (6.30);

$$\text{Im} \left[\frac{\delta S[\phi, g_-]}{\delta \phi} e^{i\sigma} \right] = 0, \quad (6.32)$$

where

$$\begin{aligned} \sigma &= \arg \left[\frac{1}{\sqrt{\tilde{S}''_- g_-^2}} \frac{e^{-S[\phi, g_-]}}{g_-^n} \right] \\ &= n\left(\theta - \frac{1}{2} \sin 2\theta\right) + \frac{\theta}{2} + \frac{\pi}{4}. \end{aligned} \quad (6.33)$$

This expression (6.32) is similar to the ordinary equation of motion except for the fact that the ‘‘coupling constant’’ g_- and the phase σ are functionals of ϕ . The solutions can be identified by first solving the equation of motion (6.32) for arbitrary constant g_- and σ and then solving the self-consistent equation (6.27) for $|g|$ and θ .

6.2.2. Asymptote for the double-well quantum mechanics

We first consider the quantum mechanics of the double-well potential, whose action and perturbative functionals are given by Eqs. (6.5) and (6.1). Then the equation (6.32), which determine the peaks of $F_n[\phi]$, can be written as follows by using the scaled variable $\varphi \equiv |g|\phi$;

$$-\frac{d^2\varphi}{d\tau^2} + \frac{\partial V_{\text{eff}}(\varphi)}{\partial \varphi} = 0. \quad (6.34)$$

The ‘‘effective potential’’ $V_{\text{eff}}(\varphi)$ in the above is defined by the following;

$$V_{\text{eff}}(\varphi) = \frac{1}{2}\varphi^2 - \kappa_3\varphi^3 + \frac{1}{2}\kappa_4\varphi^4, \quad (6.35)$$

where

$$\kappa_3 = \frac{\sin(\sigma - \theta)}{\sin \sigma}, \quad (6.36)$$

$$\kappa_4 = \frac{\sin(\sigma - 2\theta)}{\sin \sigma}. \quad (6.37)$$

play the role of the ‘‘coupling constants’’. The self-consistent equation (6.27) is now rewritten by using the scaled variable as follows;

$$|g| = \sqrt{\frac{R_4}{n}}, \quad (6.38)$$

$$\cos \theta = \frac{R_3}{2R_4}, \quad (6.39)$$

where

$$R_m = \int d\tau \varphi^m. \quad (6.40)$$

We note that the effective equation of motion (6.34) is independent of $|g|$; it has only two free parameters, n and θ (or alternatively κ_3 and κ_4). Consequently, the only self-consistent equation we need to solve is Eq. (6.39), which determines the value of θ for a given n ; Eq. (6.38) simply determines the value of $|g|$, which will be used for the evaluation of $F_n[\phi]$.

The effective equation (6.34) possess a bounce-like solution;

$$\varphi = \frac{1}{\kappa_3 + \sqrt{\kappa_3^2 - \kappa_4} \cosh \tau}. \quad (6.41)$$

where we have chosen the peak position to be at $\tau = 0$. This solution is apparently meaningful only for $\kappa_3^2 > \kappa_4$, which is a valid assumption as we will see later. Next, we must solve the self-consistent equation (6.39) to determine the value of θ . Substituting the solution (6.41) into Eq. (6.40), we obtain the following equations for $R_{3,4}$;

$$R_3 = -\frac{3\kappa_3}{\kappa_4^2} + \frac{3\kappa_3^2 - \kappa_4}{\kappa_4^{5/2}} \operatorname{arctanh} \frac{\kappa_3}{\sqrt{\kappa_4}}, \quad (6.42)$$

$$R_4 = \frac{-15\kappa_3^2 + 4\kappa_4}{3\kappa_4^3} + \frac{\kappa_3(5\kappa_3^2 - 3\kappa_4)}{\kappa_4^{7/2}} \operatorname{arctanh} \frac{\kappa_3}{\sqrt{\kappa_4}}. \quad (6.43)$$

In order to find solutions, we find it convenient to choose θ and κ_4 . Using the relation $2\kappa_3 \cos \theta = \kappa_4 + 1$, which can be derived from Eqs. (6.36) and (6.37), we express the above functions $R_{3,4}$ as functions of the two parameters, θ and κ_4 . And then we solve two equations (6.37) and (6.39) for θ and κ_4 . (Because Eqs. (6.37) and (6.39) are invariant under the reflection $\theta \rightarrow \pi - \theta$ and $\phi \rightarrow -\phi$, we investigate only the region where $\theta \in [0, \pi/2]$.) In Fig. 30, we plot the numerical solutions of these two equations for $n = 15$; the solid line satisfy Eq. (6.39), and the dashed line Eq. (6.37). The solutions of (6.31) are given by the cross points of these lines. The number of the solutions are obtained from the following consideration: The parameter σ varies from $\pi/4$ to $(n + 3/4)\pi$ when θ varies from 0 to π . Since $\kappa_4 = \cos 2\theta - \sin 2\theta \cot \sigma$, there is always one solution for every region width π in σ . Therefore the number of solutions is either n or $n + 1$. All these solutions are the configurations that are stationary points of the perturbative functional $F_n[\phi]$, which we have named the ‘‘asymptons’’.

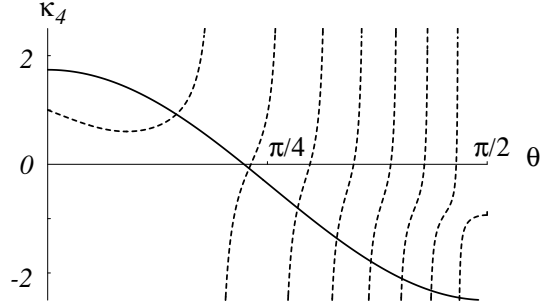


Fig. 30. The solid line satisfy Eq. (6·39),
and the dashed line Eq. (6·37)($n=15$).

In order to see which asympton dominates the path-integral, we have evaluated the value of $F_n[\phi]$ at an asymptons, $\phi_+(\theta_{asym} \in [0, \pi/2])$, and its partner (“anti-asympton”) $\phi_- \equiv -\phi_+(\pi - \theta_{asym} \in [\pi/2, \pi])$. The result is the following;

$$F_n[\phi_+] = \frac{1}{\sqrt{\pi n \sin \theta}} \left(\frac{n}{R_4} \exp(-\kappa_4 - 2 \sin^2 \theta) \right)^{n/2} \sin \sigma, \quad (6·44)$$

$$F_n[\phi_-] = (-)^n F_n[\phi_+]. \quad (6·45)$$

Most notable is the factor $n^{n/2}$ in $F_n[\phi]$. This agrees with the leading term of the known large order behavior of the coefficients, $z_n \sim n^{n/2}$. In this sense the existence of the asympton explains the non-Borel summability in the perturbation series. We note that Eq. (6·45) shows that for odd n the contribution of the asympton and the anti-asympton cancel. This is in agreement with the fact that $z_n = 0$ for odd n .

The expression Eq. (6·44) shows that the leading asympton is the one with the largest $e^{-\kappa_4 - 2 \sin^2 \theta} / R_4$ ($\equiv f(\kappa_4, \theta)$). Fig. 31 shows the behavior of $f(\kappa_4, \theta)$ in the (κ_4, θ) space. The solid line satisfy Eq. (6·39). On this line, the values of $f(\kappa_4, \theta)$ is represented by Fig. 32. The maximum point is numerically $\theta \sim 0.6$ ($\kappa_4 \sim 0.3$). The asympton, of which the value of θ is most close to that of the maximum point, is the leading asympton.

6.2.3. Asympton in the $SU(2)$ gauge field theory

The analysis we have done for the quantum mechanics can be straightforwardly extended to the $SU(2)$ gauge field theory. This may provide the way to predict the large order behavior

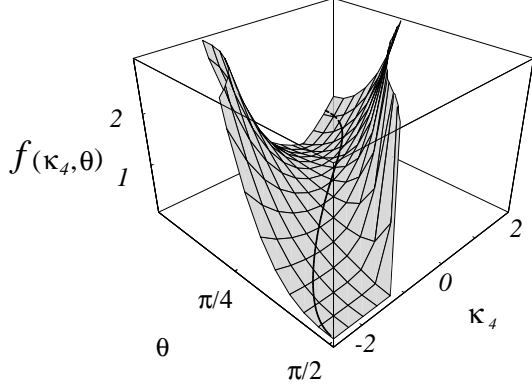


Fig. 31. The function $f(\kappa_4, \theta)$ in the (κ_4, θ) space.

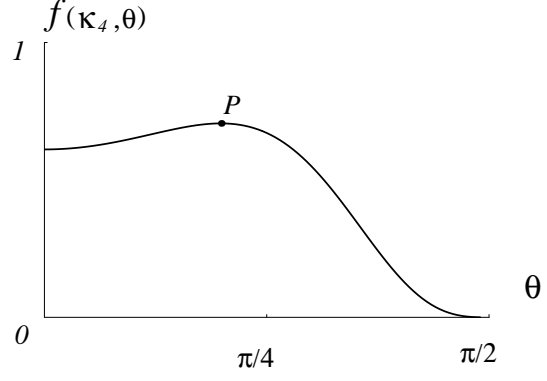


Fig. 32. The values of $f(\kappa_4, \theta)$ on the line that satisfies Eq. (6.39)

of the model.*) The action of this model is

$$S[A_\mu, g] = \frac{1}{2} \int d^4x \text{Tr}(F_{\mu\nu} F_{\mu\nu}), \quad (6.46)$$

where we define the field strength as,

$$F_{\mu\nu} = \partial_\mu A_\nu - \partial_\nu A_\mu - ig[A_\mu, A_\nu]. \quad (6.47)$$

In this model, the effective equation of motion (6.32) that determines the asymptons reads as follows;

$$\text{Im}[(\partial_\nu F_{\mu\nu} + ig_- [F_{\mu\nu}, A_\nu])e^{i\sigma}] = 0. \quad (6.48)$$

We solve this equation (6.48) under the following ansatz;

$$A_\mu(x) = \frac{-i}{\sqrt{48\pi^2}} \frac{(\bar{\sigma}_\mu \sigma_\nu - \delta_{\mu\nu})x_\nu}{x^2} s(\tau) \quad (6.49)$$

where $\tau = \log x^2$ ($x^2 = \sum_{i=1}^4 x_i^2$) and using the Pauli matrices σ_μ ,

$$\bar{\sigma}_\mu = (-i, \sigma^a), \quad \sigma_\mu = (i, \sigma^a). \quad (6.50)$$

This ansatz is motivated by the fact that the instanton, anti-instanton, and instanton-anti-instanton pairs (valley) that shares a common center $x_\mu = 0$, can be described using this ansatz. The existence of interplay between perturbative and non-perturbative effects implies

*) Actually, there is another cause of the non-summability in field theories, called renormalons. It is most plausible that renormalons are not isolated configurations, but a sum of contribution from the path-integration over a wide region of the functional space, unlike the asymptons. This is still an open question.

that they share similar structure. We will see that it is evident from the analysis of the asymptons.

By substituting (6.49) in (6.48), we find that (6.48) reduces to the following single equation;

$$\text{Im} \left[\left(\left(\frac{d^2 s}{d\tau^2} \right) - 2\tilde{g}_-^2 s^3 + 3\tilde{g}_- s^2 - s \right) e^{i\sigma} \right] = 0, \quad (6.51)$$

where $\tilde{g}_- = g_-/\sqrt{48\pi^2}$. It is important to stress here that this is obtained not by narrowing our search for the asympton down to the subspace described by the ansatz Eq. (6.49); as long as Eq. (6.49) is satisfied, the full asympton equation Eq. (6.48) is satisfied. Therefore if we find a solution to Eq. (6.49), it is a peak of the perturbative functional $F_n[\phi]$ in the full functional space. This equation can be written as follows by using the scaled variable $\tilde{s}(\tau) \equiv |\tilde{g}_-|s(\tau)$:

$$-\frac{\partial^2 \tilde{s}}{\partial \tau^2} + \frac{\partial V_{\text{eff}}(\tilde{s})}{\partial \tilde{s}} = 0, \quad (6.52)$$

where the effective potential $V_{\text{eff}}(\tilde{s})$ is defined by

$$V_{\text{eff}}(\tilde{s}) = \frac{1}{2}\tilde{s}^2 - \kappa_3\tilde{s}^3 + \frac{1}{2}\kappa_4\tilde{s}^4. \quad (6.53)$$

This effective equation of \tilde{s} equals to that of the quantum mechanics (6.34). Therefore we can use the result of the quantum mechanics. This way the asymptons are identified in the SU(2) gauge field theory. Just as the asymptons in the quantum mechanical model were quite different from instantons or instanton pairs, and rather like the bounces, the asymptons in the SU(2) gauge field theory are not like instantons at all. It has non-zero field strength on a spherical shell, and look like a merged concentric instanton-anti-instanton pair.

6.2.4. Asympton on the Valley

From the above we have found that asymptons are quite unlike the instanton configurations in general. They are off the valley line studied extensively in the previous sections. On the other hand, we have seen in section 6.1 that the consideration of valley provides an insight into the summability properties of the perturbative series. Thus we will next study the behavior of the perturbative functional $F_n[\phi]$ on the valley.*⁾ In order to simplify the analysis, we adopt the following approximation for valley in the double-well quantum mechanical model;

$$s(\tau) = \frac{1}{\tilde{g}}(1 + e^{-\tau-d/2})(1 + e^{\tau-d/2}), \quad (6.54)$$

*⁾ Similar analysis were presented in Ref. 53). However, there was a mistake of factor two in one of the expression obtained in that paper. This changes the behavior of $F_n[\phi]$ drastically.

In (6.54), if we choose d large enough, we obtain instanton-anti-instanton pair. It gives a reasonable approximation of the valley line parametrized by d .

In the SU(2) gauge field theory, the valley has the tensor structure (6.49). If we substitute this expression into the action, we find that

$$S[A_\mu, g] = \int_{-\infty}^{\infty} d\tau \left[\frac{1}{2} \dot{s}^2 - \frac{1}{2} s^2 (1 - \tilde{g}s)^2 \right], \quad (6.55)$$

where the τ -integration comes from the integration over the four-dimensional radius from zero to infinity, and $\tilde{g} \equiv g/\sqrt{48\pi^2}$. Since the right hand side is equivalent to the double-well quantum mechanical model with (imaginary) time τ , and the coupling constant \tilde{g} , the following analysis is also valid for the SU(2) gauge field theory by rewriting g by \tilde{g} .

We first calculate the ratio of $F_n[A_\mu]g^n$ to e^{-S} on the valley. Using (6.27) for Eq. (6.30), we find it to be the following;

$$\frac{F_n[\phi]g^n}{e^{-S}} = e^\Delta \sin \sigma, \quad (6.56)$$

where

$$\Delta = \frac{c_1^2}{8c_2} + \frac{n}{2} - gc_1 + g^2c_2 - \frac{n}{2} \log \frac{n}{2g^2c_2} - \frac{1}{2} \log(\pi n \sin \theta). \quad (6.57)$$

The magnitude of the perturbation coefficient is determined by e^Δ . Therefore, we examine the behavior of e^Δ for large d . The coefficients $c_{1,2}$ are approximated as follows for large d ;

$$\begin{aligned} c_1 &= \frac{1}{g^3} (d - 3 + \dots), \\ c_2 &= \frac{1}{2g^4} \left(d - \frac{11}{3} + \dots \right). \end{aligned} \quad (6.58)$$

Using (6.58) for Δ in (6.57), we find that

$$\Delta \sim -\frac{d}{4g^2} + \frac{n}{2} + \frac{n}{2} \log \frac{d}{ng^2} - \frac{1}{2} \log \pi n + \frac{1}{4} \log \left(1 - \frac{d}{4ng^2} \right). \quad (6.59)$$

From (6.59), we find that e^Δ has the peak on $d = 2ng^2$ and that the magnitude of the peak is proportional to $2^{n/2}/\sqrt{n}$. We will call this peak “the valley asympton”, as it is the asympton solution when limited to the valley line. As n increases, the valley asympton moves to the region of large d and grows exponentially. The numerical analysis shows that the main contribution of the asympton is in the following region:

$$0.46ng^2 + \frac{11}{3} \lesssim d \lesssim 5.34ng^2 + \frac{11}{3}. \quad (6.60)$$

We can obtain this result by solving the equation $\Delta = 0$ numerically. The perturbative functional $F_n[\phi]$ on the valley is plotted in Fig. 33.

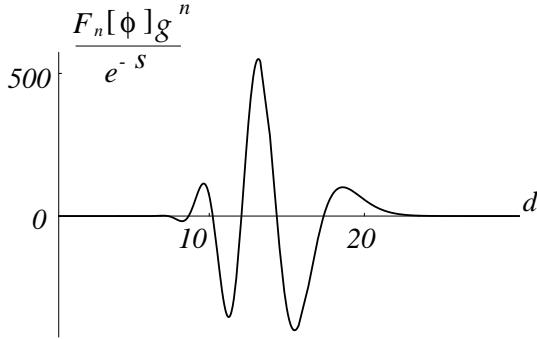


Fig. 33. The behavior of $F_n[\phi]g^n/e^{-S}$ for $n = 30$, $g = 0.4$.

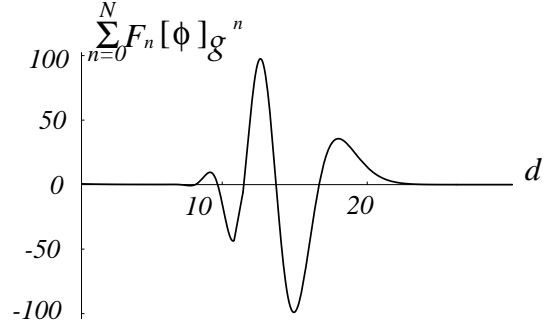


Fig. 34. The behavior of $\sum_{n=0}^N F_n[\phi]g^n$ for $N = 30$, $g = 0.4$.

The numerical comparison of the partial sum, $\sum_{n=0}^N F_n[\phi]g^n$ with e^{-S} is plotted in Figs. 34, 35 (for $N = 30$), and 36 (for $N = 50$). (Note the difference in the vertical scales between the first two and the latter.)

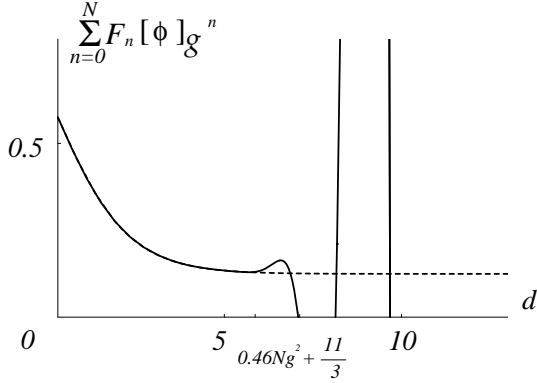


Fig. 35. The dashed line is e^{-S} . The solid line is $\sum_{n=0}^N F_n[\phi]g^n$ for $N = 30$, $g = 0.4$.

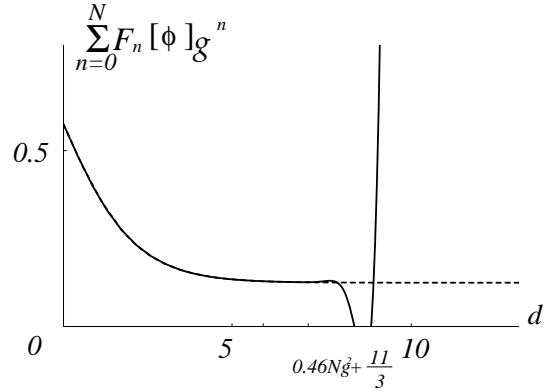


Fig. 36. The dashed line is e^{-S} . The solid line is $\sum_{n=0}^N F_n[\phi]g^n$ for $N = 50$, $g = 0.4$.

From Figs. 34, 35, we find that $\sum_{n=0}^N F_n[\phi]g^n$ deviates from e^{-S} where $F_n[\phi]$ has the large contribution. For $d \lesssim 0.46Ng^2 + \frac{11}{3}$, we find that $\sum_{n=0}^N F_n[\phi]g^n$ (the solid line) is very close to e^{-S} (the dashed line). This means that as far as the valley is concerned the n -th order perturbation is valid only in the region $d \lesssim 0.46Ng^2 + \frac{11}{3}$. The usual perturbation suffers from non-Borel summability due to the valley asymptote, even when limited to the valley line.

6.2.5. Discussion

We have so far identified the causes of the Borel non-summability as asymptons and valley asymptons. The next problem is to use this knowledge to look into the interplay of the perturbative series and the non-perturbative terms. In the double-well potential model, Aoyama and Tamra^{52), 53), 54)} proposed a modified perturbation theory, obtained by dividing the functional space into two fundamental regions of the symmetry $\phi \rightarrow 1/g - \phi$, and carrying out the functional integral in only one of them. The original path-integral is recovered by multiplying two on that integral, as the contribution from the fundamental regions are the same. As the order of the perturbation exceeds $O(1/g^2)$, the asympton moves out from a fundamental region into another. Thus the modified perturbation series is free from the asympton at higher orders. What remains is the anti-asympton, which has the property (6.45). This still renders the series non-convergent. But due to the disappearance of the asympton, the cancellation for $n = \text{odd}$ no longer holds, and the modified perturbative coefficient \tilde{z}_n behaves as,

$$\tilde{z}_n \sim (-1)^n n^{n/2}, \quad (6.61)$$

for $n \rightarrow \infty$. Thus this series is a Borel-summable series, which is quite desirable for many purposes.

This method, however, works only for the finite time-interval (or finite temperature). When the time-interval is infinity, the boundary of the fundamental region is at infinity and the asympton never moves out of the original region. Furthermore, we do not know how to make it work in the SU(2) gauge theory.

The valley asympton gives us a hope for possible resolution of the problem. It shows that (at least on the valley line) the perturbative series suffers from non-summability due to the configurations (valley asymptons) that live in $d > O(1) \times n/g^2$ region. This means that if we introduce a cutoff on d at $O(1)$, the perturbative coefficients begin to converge for $n < O(1)/g^2$. Since this is the order when the usual leading term, $n^{n/2}g^n$, is of $O(1)$, this perturbative series with the cutoff never suffers from any large terms. On the other hand, the region excluded by this cutoff is where the instanton and the anti-instanton are separated well. Thus the non-perturbative calculation (valley method) provides a quite effective evaluation of the path-integral.

What is to be done is to find a way to apply this kind of the cutoff method to the whole region with all the virtues seen on the valley. This is a fascinating possibility, but remains as an open question at this moment.

Acknowledgments

We would like to thank our colleagues at Kyoto University for encouragements and discussions at various stages of this work. H. Aoyama's work is supported in part by the Grant-in-Aid for Scientific Research (C)-07640391 and (C)-08240222. T. Harano and S. Wada's work is supported in part by the Grant-in-Aid for JSPS fellows. H. Kikuchi's work is supported in part by the Grant-in-Aid for Encouragement of Young Scientists, 08740215.

References

- [1] N. S. Manton, Phys. Rev. **D28** (1983), 2019; F. R. Klinkhamer and N. S. Manton, Phys. Rev. **D30** (1984), 2212.
- [2] G. 't Hooft, Phys. Rev. Lett. **37** (1976), 8; Phys. Rev. **D14** (1976), 3432.
- [3] V. A. Kuzmin, V. A. Rubakov, and M. E. Shaposhnikov, Phys. Lett. **B155** (1985), 36.
- [4] H. Aoyama and H. Goldberg, Phys. Rev. Lett. **188B** (1987), 506.
- [5] A. Ringwald, Nucl. Phys. **B330** (1990), 1.
- [6] O. Espinosa, Nucl. Phys. **B343** (1990), 310.
- [7] H. Aoyama and H. Kikuchi, Phys. Lett. **B247** (1990), 75; Phys. Rev. **D43** (1991), 1999; Int. J. Mod. Phys. **A7** (1992), 2741.
- [8] V. A. Rubakov and M. E. Shaposhnikov, hep-th/9603208.
- [9] S. Coleman, in *The Why's of Subnuclear Physics*, ed. A. Zichichi (Plenum, New York, 1979).
- [10] I. Affleck, Nucl. Phys. **B191** (1981), 429.
- [11] H. Aoyama and H. Kikuchi, Nucl. Phys. **B369** (1992), 219.
- [12] P. G. Silvestrov, Sov. J. Nucl. Phys. **51** (1990), 1121.
- [13] D. J. Rowe and A. Ryman, J. Math. Phys. **23** (1982), 732.
- [14] C. A. Cayley, Philos. Mag. **18** (1859), 264; J. C. Maxwell, Philos. Mag. **40** (1870), 421.
- [15] W. Quapp, Chemical Physics Letters **253** (1996), 286.
- [16] I. I. Balitzky and A. V. Yung, Phys. Lett. **B168** (1986), 113; Nucl. Phys. **B274** (1986), 475.
- [17] D. Boyanovsky, R. Willey and R. Holman, Nucl. Phys. **B376** (1992), 599.
- [18] S. Coleman, Phys. Rev. **D15** (1977), 2929.
- [19] C. Callan and S. Coleman, Phys. Rev. **D16** (1977), 1762.
- [20] D. E. Brahm and C. L. Y. Lee, Phys. Rev. **D49** (1994), 4094.
- [21] H. Aoyama, T. Harano, M. Sato and S. Wada, Mod. Phys. Lett. **A11** (1995), 43; Nucl. Phys. **B466** (1996), 127.
- [22] H. Aoyama and H. R. Quinn, Phys. Rev. **D31** (1985), 885; **D34** (1986), 662.
- [23] H. Aoyama and S. Wada, Phys. Lett. **B349** (1995), 279
- [24] P. B. Arnold and M. P. Mattis, Phys. Rev. Lett. **66** (1991), 13.
- [25] A. V. Yung, Nucl. Phys. **B191** (1981), 47.
- [26] V. V. Khoze and A. Ringwald, Phys. Lett. **B259** (1991), 106.
- [27] L. N. Lipatov, JETP Lett. **25** (1977), 104; Sov. Phys. JETP **45** (1977), 216.

- [28] E. Brézin, J. C. Le Guillou and J. Zinn-Justin, Phys. Rev. **D15** (1977), 1544,1558.
- [29] G. Parisi, Phys. Lett. **B66** (1977), 167.
- [30] Y. Frishman and S. Yankielowicz, Phys. Rev. **D19** (1979), 540.
- [31] T. Harano and M. Sato, *Kyoto University preprint*, KUNS-1391 HE(TH)96/04.
- [32] A. Hosoya and K. Kikkawa, Nucl. Phys. **B101** (1975), 271.
- [33] D. W. McLaughlin, J. Math. Phys. **13** (1972), 1099.
- [34] I. Bender, D. Gomez, H. Rothe and K. Rothe, Nucl. Phys. **B136** (1978), 259.
- [35] S. Levit, J. W. Negele and Z. Paltiel, Phys. Rev. **C22** (1980), 1979.
- [36] A. Patrascioiu, Phys. Rev. **D24** (1981), 496.
- [37] A. Lapedes and E. Mottola, Nucl. Phys. **B203** (1982), 58.
- [38] U. Weiss and W. Haeffner, Phys. Rev. **D27** (1983), 2916.
- [39] R. D. Carlitz and D. A. Nicole, Ann. Phys. **164** (1985), 411.
- [40] S. Y. Khlebnikov, V. A. Rubakov and P. G. Tinyakov, Nucl. Phys. **B367** (1991), 334.
- [41] V. A. Rubakov, D. T. Son and P. G. Tinyakov, Phys. Lett. **B287** (1992), 342.
- [42] D. T. Son and V. A. Rubakov, Nucl. Phys. **B424** (1994), 55
- [43] H. Aoyama and T. Harano, Mod. Phys. Lett. **A10** (1995),1136; Nucl. Phys. **B446** (1995), 315.
- [44] H. Aoyama and M. Kobayashi, Prog. Theor. Phys. **64** (1980), 1045.
- [45] F.J. Dyson, Phys. Rev. **85** (1952), 631.
- [46] J.C. Le Guillou and J. Zinn-Justin, ed. *Large-order behavior of perturbation theory* (North Holland, Amsterdam, 1990) and references contained therein.
- [47] H. Kikuchi, Phys. Rev. **D45** (1992), 1240.
- [48] C. Bender and T. Wu, Phys. Rev. **D7** (1973), 1620.
- [49] E. Brézin, G. Parisi, and J. Zinn-Justin, Phys. Rev. **D16** (1977), 408.
- [50] G. 't Hooft, in *The Whys of Subnuclear Physics* ed. A. Zichichi (Plenum, New York, 1979).
- [51] H. Aoyama, Mod. Phys. Lett. **A7** (1992), 1337.
- [52] H. Aoyama and A. M. Tamra, Nucl. Phys. **B384** (1992), 229.
- [53] H. Aoyama, Phys. Lett. **B329** (1994), 285.
- [54] H. Suzuki, Mod. Phys. Lett. **A11** (1996), 19.